The Fire Performance of Post-Tensioned Timber Beams

By

Phillip Michael Spellman

Supervisory committee

Professor Andrew H. Buchanan

Dr. David M. Carradine

Dr. Anthony K. Abu

Professor Peter J. Moss

This thesis is submitted in partial fulfilment of the requirements for the degree of Masters of Engineering in Fire Engineering.

Department of Civil and Natural Resources Engineering

University of Canterbury

Private Bag 4800

Christchurch, New Zealand

March 2012

Abstract

Post-tensioned timber frames have recently been undergoing heavy research and development at the University of Canterbury. The recently developed post-tensioned timber system utilises engineering wood products such as Laminated Veneer Lumber (LVL) and glue laminated timber (Glulam), which are formed into box sections and post-tensioned with high strength steel tendons made from stranded steel wire or solid steel bars. The post-tensioning serves to counteract some of the bending actions imposed on the timber beam from loading through a variety of mechanisms. Previous research has focused on the seismic performance and gravity frame performance of post-tensioned timber, both of which yielded promising results. There is however a commonly perceived increase in fire risk with timber building, particularly multi-storey timber buildings, and the fire performance of post-tensioned timber had not previously been investigated.

Therefore, the focus of this research was to investigate the fire performance of post-tensioned timber beams. This was completed through a series of full-scale furnace tests, and the development of a fire resistance design method. Three 4.36m span post-tensioned timber beams were exposed to the ISO 834 standard fire. Each of the test beams were glued box beams made from 63mm LVL and were of varying external dimensions. Each beam was intended to demonstrate a specific failure mechanism at approximately 60 minutes of fire exposure. The failure mechanisms demonstrated were a shear failure in the lower corner of due to corner rounding, and a combined bending and compression failure at the end of the beam. These failure mechanisms are unique to post-tensioned timber in fire. The results of the experimental testing were used to validate and refine the proposed fire resistance calculation. Also tested during the full-scale testing were five different forms of anchorage fire protection. These were tested as a secondary objective, but useful thermal data was collected.

Through the full-scale testing and the calculation method development it was found that it is important to consider shear during fire design. The post-tensioning increases the bending capacity of a beam but doesn't affect its shear capacity, therefore when more loading is applied to utilise the increased bending capacity the shear action is increased which leads to shear governing the design in many cases. It is also important to consider shear not only in the webs at the centroid where the shear flow is greatest but also in the lower corners, which can become much thinner than the webs. Without calculation it is not possible to determine where the shear stress will be greatest and therefore both the web and the lower corners need to be checked. It was also found that as the timber section chars on three sides the post-tensioning eccentricity increases which can lead to the moment at the end of the beam becoming critical. Other failure mechanisms which need to be checked include, combined bending and compression at mid span, and tension in the bottom most fibre at mid span. It was found that the proposed calculation method, when used with a char rate of 0.72mm/min and an additional allowance of 7mm for temperature-affected timber beneath the char layer, provided good predictions of the failure times for the full-scale experiments.

Acknowledgements

Thank you to my supervisors Professor Andy Buchanan, Dr Tony Abu, Dr David Carradine, and Professor Peter Moss for their guidance and support during the writing of this thesis. Dr Tony Abu and Professor Peter Moss provided excellent support during numerical modelling and with structural analysis and Dr David Carradine's expertise in full- scale testing was invaluable. Professor Andy Buchanan helped immeasurably to keep this research focused and on-track.

I would also like to thank the Structural Concrete Innovation Company (STIC) for the expertise they provided and the funding they provided, for full-scale testing, and which allowed me to focus on this research.

Also thank you to the New Zealand Fire Service for their support of the Masters Engineering in Fire Engineering (MEFE) programme.

I would like to express my gratitude to the University of Canterbury technical staff Grant Dunlop and Bob Wilsea-Smith for helping me prepare for the full-scale tests. Some times at the last minute and with unique issues and constraints imposed by recent earthquakes.

I would like to recognise the support, criticism, and feedback from my fellow students during our weekly meetings and other discussions. I would like to individually thank Norman Werther and Jacob Studhalter our European visitors who had a particular interest in timber and fire. Also thanks to James O'Neil my timber in fire student colleague.

Thanks to Mark Gannon and the technical staff at BRANZ in Wellington for their help in organising the sometimes daunting logistics of full-scale testing and for helping in the construction and testing of our specimens.

Thank you to McIntosh Timber Laminates in Auckland for fabricating our timber specimens and allowing for our unusual request for me to come up and drill holes in the beam during construction.

Thank you to Professor Dr Andrea Frangi and Peter Collier for their comments and suggestions for my thesis.

Also thank you to my parents for their support and thank you to my mother in particular for her help and reading many parts of the thesis that she may not have had any interest in reading.

Lastly I am grateful and appreciative to my partner Ruby Langdon for her support and company during this sometimes stressful research.

Table of Contents

List of Figures

List of Tables

Nomenclature

a	Distance from vertical support to point load (for 4 point loading)
a_{heated}	Thickness of temperature effected timber beneath the char layer
A	Area of the object denoted in subscript
b	Breadth of the timber member
C_{top}	Distance of the timber member centroid from the top of the
$C_{top}\ X$	Distance from a shape X from the top of the section
$C_{centroid}\ X$	Distance from a shape X to the cross section centroid
d	Depth of the timber member
D_{Load}	Vertical flexural deflection of the timber member due to the external loading
D_{PT}	Vertical deflection of the timber member due to the post-tensioning end moment
D_{Shear}	Vertical shear deflection of the timber member due to the external loading
D_{Bowing}	Additional vertical deflection due to the axial post-tensioning loading
e	Eccentricity of the post-tensioning group from the centre of the group to the centroid of the remaining timber section.
e_0	Initial eccentricity of the
E_T	Modulus of Elasticity for the timber member
E_{PT}	Modulus of Elasticity for the tendons, fire subscript denotes the temperature reduced value
f_c	Characteristic compressive stress for timber
f_b	Characteristic bending strength for timber
F_{PT}	Force applied by post-tensioning group
I	Second moment of area, subscript can denote axis or shape depending on context
I_{zz}	Second moment of area of a shape around the axis Z
I_{local}	Second moment of area of a single shape being used to calculate I_{global}
I_{global}	Second moment of area of a complex shape made up of simple geometric shapes
I_{cm}	Second moment of area of a shape around the shapes centre of mass
I_{cold}	Second moment of area of the timber member at ambient conditions or fire conditions at time 0

k_1	Duration of load factor for timber strength as stated in NZS3603
k_{24}	Size factor for timber members as stated in NZS3603
L	Length of the simply supported beam
L_o	Original length of tendon required to elongate to length L when loaded
M^*	Bending moment action
M^*_{fire}	Total bending moment action after the specified fire duration
M^*_{load}	Bending moment action due to loading
M^*_{PT}	Bending moment action due to post-tensioning eccentricity
M^*_{bow}	Bending moment action due to post-tensioning axial load
N^*_{fire}	Axial load action at specified fire duration
P	Point Load
q	Shear flow kN/m
Q	First moment of area about the shapes centroid
r	Radius or distance between two axes
t	Thickness
t_f	Thickness of single timber flange
t_w	Thickness of single timber web
t_c	Thickness of the char rounded corner of the timber section
$T(x)$	Temperature of timber at depth x below the char layer
T_i	Ambient (initial) temperature
T_p	Timber Pyrolysis temperature (300°C)
V^*	Maximum shear action
y	Distance from the centroid to the extreme fibre
Z_{cold}	Section modulus for timber member
α	Angle of the line the thinnest part of the timber corner rounding
Δx	Linear elongation

Δx_{total}	Total elongation
$\Delta x_{mechanical}$	Elongation due to axial loads
$\Delta x_{thermal}$	Elongation due to thermal expansion
Δ_{Total}	Total vertical mid span deflection
$\varepsilon_{mech\,0}$	Initial mechanical strain on the tendon at ambient conditions after loading
$\varepsilon_{mechanical}$	Axial strain due to the applied axial force,
$\varepsilon_{thermal}$	Thermal strain,
$\varepsilon_{rotation}$	Effective strain due to the rotation of the anchorages
$\varepsilon_{compression}$	Effective strain due to the increased axial deflections of the timber beam
θ	Tendon temperature
ϕM_n	Nominal bending capacity
ϕq_n	Nominal shear flow capacity
$\phi N_{crushing}$	Nominal compressive capacity due to crushing
$\phi N_{buckling}$	Nominal compressive capacity due to buckling
$\sigma_{Top,Mid}$	The stress developed in the top chord of the beam at mid span
$\sigma_{Bottom,Mid}$	The stress developed in the bottom chord of the beam at mid span
ϕ	Material reduction factor
$\phi\sigma_{Cn}$	Nominal compressive stress capacity
$\phi\sigma_{Tn}$	Nominal tensile stress capacity

Subscripts

$Fire$	depicts a value relevant after the specified fire duration
$Cold$	depicts a value relevant to ambient design
PT	depicts a value relevant to the post tensioning steel
T	depicts a value relevant to the timber section
mid	depicts a value relevant to the mid-span of the member
end	depicts a value relevant to the end of the member
top	depicts a value relevant to the top most extreme fibre of the cross section
$bottom$	depicts a value relevant to the bottom most extreme fibre of the cross section

1. Introduction and background

Timber is the material of choice for residential construction in New Zealand, Australia and many other parts of the world. However, commercial and industrial construction are dominated by steel and concrete. New Zealand has large renewable forest plantations and timber is the third largest export commodity behind dairy and meat products. New Zealand contributes 1.1% of the world's timber, but New Zealand contributes nearly 9% of Asia Pacific timber products by volume and approximately 20% by value. Timber and forest products export contributes approximately 3% of the New Zealand GDP. (Ministry of Agriculture and Forestry, 2011)

New Zealand's plantation forests consist of sustainable exotic timber species. 90% of the New Zealand plantation consists of Radiata Pine, and 6% Douglas Fir, the remaining 4% is made up from other softwood and hardwood species including eucalyptus. Sustainable plantations cover 7% of New Zealand's land area. (Ministry of Agriculture and Forestry, 2011)

The reliable or characteristic strength and stiffness of timber is governed by defects in the wood. The values used in design are commonly the lowest fifth percentile strength and mean stiffness. Engineered wood products such as LVL and glue laminated timber allow for an increase in the strength and stiffness of the timber material used. These products distribute defects evenly throughout the composite products, which means the effect of a defect is small and doesn't affect the entire timber cross section. The lower fifth percentile strength of these products approaches the average values of the timber. The increased properties of engineered timber products allow for new technologies such as post-tensioned timber to become more practical.

For many years the University of Canterbury in New Zealand has been researching the use of timber in structures using a variety of methods. The research has included construction costs, sustainability, seismic design, and fire design. In 2008 the Structural Timber Innovation Company (STIC) was founded which promotes timber research and new construction techniques. One of the techniques STIC has been supporting is post-tensioned timber construction, which has become viable with the high strength and low variability of engineered wood products.

There are substantial benefits to post-tensioned timber construction over steel and concrete construction. Timber is very light and easy to work with, meaning smaller lifting equipment can be used and construction can proceed much faster. The post-tensioning system can be used to make the main beam column connections and can make many connections at once, again speeding up construction. Timber is a "green" and sustainable building material. Timber as a building material stores carbon and its components can be recycled, or when it reaches the end of its useful life it can be a clean source of energy.(John, 2008, John et al., 2010)

Post-tensioned timber is an adaptation of the mature technology of post-tensioned or pre-stressed concrete (Priestley et al., 1999). It is made from engineered wood products such as LVL and Glulam which allow for the most efficient use of materials. The timber is then post-tensioned with a high strength steel wire tendon or bar which is run through a cavity within the member and through multiple bays of a frame. This forms the main moment resisting connections of the frame. Under seismic conditions this type of connection is self-centring which eliminates residual displacements after a seismic event. The tendon applies a compressive force, clamping the beams into place

between the columns. Additionally if the tendon profile is deviated it can provide uplift forces within the beam span further reducing the deflections of the beam.

Because timber is combustible there is a commonly perceived increase in risk during a fire. The fire performance of heavy timber is well understood and shows that a properly designed timber member can provide excellent fire resistance. When exposed to fire timber reacts predictably, a layer of charcoal forms as it burns which progresses through the timber at an approximately constant rate. This can be used in design to ensure that the timber remaining after chosen fire duration is capable of withstanding the loads it is required to resist.(Buchanan, 2001)

Post-tensioned timber has a number of factors which complicate fire performance and may lead to failure mechanisms unique to this system. These complications include cavities within the timber members which house the tendons and the use of highly stressed steel tendons which provide some additional capacity to the member. The cavities may result in decreased shear capacity due to the char rounding in the corners of the section. The pre stressing forces applied to the tendons may be sensitive to relatively small increases in temperature as their stiffness decreases with an increase of temperature and thermal strain can decrease the mechanical strain which is responsible for the original force. This research is an investigation into the performance of post-tensioned timber members in fire and seeks to provide advice on the fire design of post-tensioned timber members to achieve this, the following objectives were set.

1.1. Objectives

The objectives of this research were the following:

- Investigate the fire resistance of post-tensioned timber beams and develop a calculation method for determining the Fire Resistance Rating (FRR) of post-tensioned timber beams. Sub objectives include:
    - The determination of the potential failure mechanisms of a box configuration timber beam under fire conditions.
    - Understanding the effects of heating on unbonded post-tensioning tendons.
- Provide recommendations for future designs of post-tensioned timber members for fire conditions.
- Perform a full-scale furnace test of a post-tensioned timber beam to demonstrate the fire resistance characteristics of post-tensioned timber and provide verification data for the proposed calculation method.

1.2. STIC

The Structural Timber Innovation Company or STIC is a timber industry driven research consortium with the vision of promoting “The construction of large numbers of innovative and sustainable commercial and industrial multi-storey and long-span timber buildings in Australia and New Zealand”. The company is developing a portfolio of timber structural systems, one of which is EXPAN a pre-stressed post-tensioned timber construction system (STIC Ltd., 2009).

1.3. Timber Design

The New Zealand Timber Structures Standard NZS3603:1993 (Standards New Zealand, 1993) sets out the requirements for the design of timber elements in buildings to achieve New Zealand Building Code compliance. The Standard covers sawn timber, glue laminated timber, natural round timber,

and construction plywood. LVL can be used with characteristic properties supplied by the manufacturer; however no LVL specific advice is given within the code. Fire design information is presented in Section 9 of the standard.

Eurocode 5 (British Standard Institute, 2004b) is the corresponding European standard for the design of timber structures. In addition to the sawn timber design guidance in NZS3603, the Eurocode also specifically covers LVL. Eurocode 5 is split into two parts; part 1 covers ambient design with a substantial sub-part on fire design, while part 2 covers the design of timber bridges.

Both codes are based on "limit state" design principles, where various limit states are defined, commonly the ultimate limit state (ULS) and the serviceability limit state (SLS), and the beam is designed to maintain integrity and resist applied loads to satisfy these limit states. The ultimate limit state deals with the strength of the member in that the beam is designed so that the design strength is greater than the actions applied, while the serviceability limit state deals with the deflections and vibrations the member may experience during its working life. The design actions for Eurocode are found in Eurocode 1: Actions on structures (British Standard Institute, 2002a). For NZS3603 the design actions are found in the Structural Design Actions standard AS/NZS:1170 (Standards New Zealand, 2002). Both codes also use modification factors to incorporate the effect of various phenomena, such as duration, bearing, lamination, and size factors (Buchanan, 2007).

The codes differ slightly in how some calculations are presented and in the level of detail given. Eurocode provides more information in annexes which can be used for advanced calculation techniques. It also provides calculations for techniques which are more common in Europe and the United Kingdom than in New Zealand, such as doweled connections or notched members. The Eurocode also does not use the section modulus as NZS3603 does. Instead structural checks are done based on stresses, as shown in the combined stress index from Eurocode 5 presented in Eq. 1-1. The comparable bending check for NZS3603 is presented in Eq. 1-2.

$$\frac{\sigma_{m,y,d}}{f_{m,y,d}} + k_m \frac{\sigma_{m,z,d}}{f_{m,z,d}} \leq 1 \qquad \textbf{Eq. 1-1}$$

$$M^* \leq \Phi M_n, \quad M_n = k_m f_b Z \qquad \textbf{Eq. 1-2}$$

Where:

$\sigma_{m,y,d}$ and $\sigma_{m,z,d}$ are the design bending stresses about the principal axes for a beam designed with Eurocode 5.

$f_{m,y,d}\ and\ f_{m,z,d}$ are the corresponding design bending strengths for a beam design with Eurocode 5. These values are comparable to Φf_b.

M^* is the design bending moment produced by the ultimate limit state design loads for a beam designed to NZS3603.

M_n is the bending design strength for a beam designed to NZS3603.

Φ is the strength reduction factor for new Zealand structural design. The Eurocode has similar strength reduction factors. They are however applied at a difference stage of the calculation.

f_b is the characteristic bending strength for a beam designed with NZS3603.

Z is the elastic section modulus for a beam designed to NZS3603.

k_m is the combined modification factors which make allowances for re-distribution of stresses and the effect of inhomogeneities of the material in a cross section.

1.4. Post-tensioning

1.4.1. Post-tensioning vs. pre-stressing

The terms pre-stressed and post-tensioned are sometimes used almost interchangeably; however, these terms do have some distinctions. Pre-stressing describes the overall principle and post-tensioning is a type of system which incorporates pre-stressing.

Principle:

Pre-stressed members are members (traditionally concrete) which have an initial compression stress applied to them via tensioned tendons. There are two common types of pre-stressed members, pre-tensioned and post-tensioned.

Types:

Pre-tensioned members have tendons which are stressed prior to the casting of the concrete. The tendons may be anchored at either end or may rely on the bonding of the concrete to remain in place. These members are currently only made from concrete as they require the material to be cast around them. Pre-tensioned members are fabricated in a factory and then shipped to site. Whilst this means the building can be constructed quickly, the concrete members are very heavy and expensive to transport.

Post-tensioned members have tendons which are stressed after the member has been constructed (e.g. the concrete has been cast). The tendons must be anchored at either end to transfer the initial stress from the tendon into the main material. As the tendons do not require the main material to be cast around them, this form of pre-stressing is most appropriate for materials other than concrete. Post-tensioned members can also be prefabricated.

1.4.2. Pre-stressing benefits

Pre-stressed members have several advantages over comparable non pre-stressed members. These benefits include the following (Precast New Zealand Limited - Stresscrete, 2003):

- Pre-stressing allows for smaller members to resist the same load as a similar non pre-stressed member. This is because pre-stressing utilizes materials more efficiently.
- Pre-stressing allows for members to be smaller and lighter, increasing the member strength to weight ratio.
- Pre-stressing allows for increased prefabrication of structural elements. This is particularly evident with concrete post-tensioning.
- Pre-stressing a member allows for deflections to be reduced and controlled.

1.4.3. Pre-stressing fundamentals

Pre-stressing can provide gains to a member in two main ways. The initial compressive force can cause some benefits depending on the material being pre-stressed. Pre-stressing can also provide a moment which counteracts the moment due to loading. It can do this through applied end moments or uplift forces along the member.

Many materials are stronger in compression than they are in tension, or their compressive failure mechanism is more ductile than their tensile failure mechanism. With pure bending the tensile and compressive stresses developed would be similar, for a symmetrical cross section. With an initial compressive stress applied to the member the bending stress distribution shifts, increasing the compressive stress and decreasing the tensile stress as shown in Figure 1-1. With concrete, which is much stronger in compression than it is in tension, the high compressive strength can be utilised more effectively than if it was normally reinforced. With other materials such as timber which have similar compressive and tensile strength, the tensile failure mechanism can be brittle and therefore dangerous, requiring a larger factor of safety, which is often built into the published characteristic stresses. With the compressive stresses now larger than the tensile stresses the failure mechanism is compressive and more ductile. The stress distributions on a beam with axial post-tensioning are demonstrated in Figure 1-1 (right) which can be compared to the bending distribution developed in a simply supported beam, shown in Figure 1-1 (left).

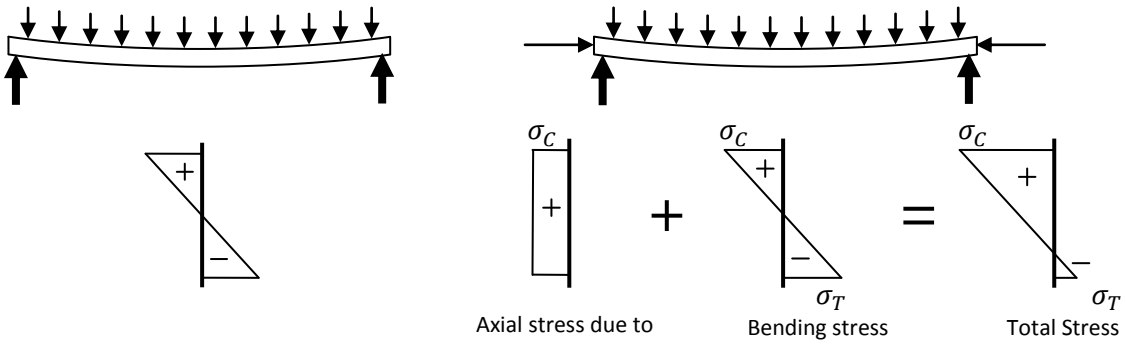

Figure 1-1: Bending stress distribution for simply supported members (Left) and with an initial axial stress applied (Right)

A bending moment can be applied to a beam or member with post-tensioning in two ways. Firstly the post-tensioning can apply an end moment by loading the member eccentrically. Secondly the use of a deviated or curved tendon can provide uplift forces within the member. The tendon can be placed below the beam's centroid which causes an eccentricity between the tendon force and the reaction force, which acts through the beam centroid. This produces a negative moment throughout the beam which reduces moments and deflections due to loading. Stress distributions developed in a beam with eccentric axial post-tensioning are shown in Figure 1-2.

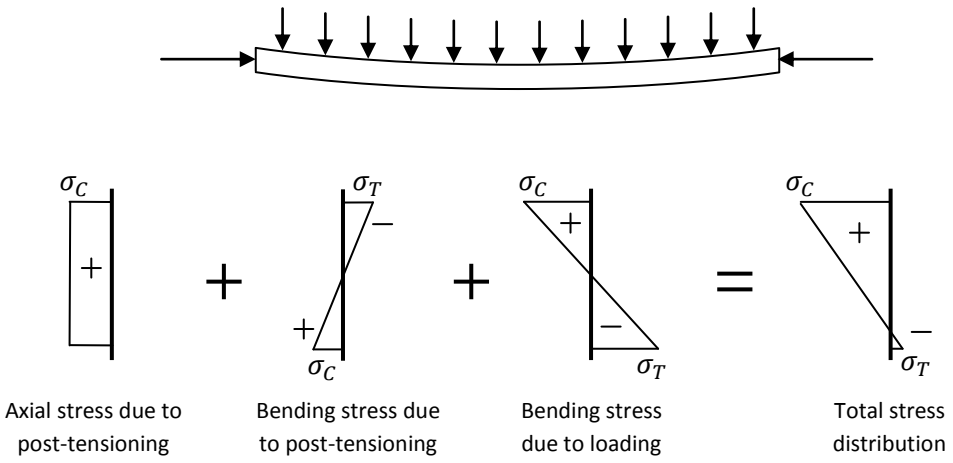

Figure 1-2: Bending stress distribution with an initial compression stress and opposing bending stress distribution

If a straight eccentric tendon group cannot provide the required load resistance without overstressing the primary material, a deviated tendon profile can be used. Because the direction of the force changes as the angle of the tendon changes, a reaction force is formed as demonstrated in Figure 1-3. This reaction force can be used to provide uplift forces at multiple positions along the beam. With concrete a curved tendon can be cast into the member which instead of providing uplift at discrete points would provide a distributed uplift force along the beam.

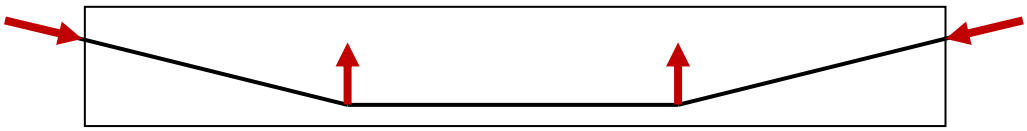

Figure 1-3: Beam with deviated tendon demonstrating forces acting on the beam from post-tensioning.

1.4.4. Concrete Post-tensioning Historical Overview

Post-Tensioned concrete was first explored by P. Jackson and C. W. Doehring in the late 1800's. P. Jackson, an American engineer, in 1872 patented a post-tensioning system using tie rods to build beams or arches from discrete blocks. C .W. Doehring, a German engineer, in 1888 patented a system for post-tensioning concrete slabs with metal wires. Neither of these attempts were particularly effectual due to the low yield stress of early steel. Further problems such as low initial jacking stress, high creep, and concrete shrinkage meant that much of the pre-stressing force applied to the steel tendons was lost. This meant that the steel was largely ineffectual. (Aalami, 2007, Nawy, 2003)

In the late 1920's French engineer Eugene Freyssinet acknowledged the impact of long-term stress losses in pre-stressing. Freyssinet used a new high strength steel to successfully use post-tensioned members in the foundations of a marine terminal in France (Gales, 2009). Freyssinet also introduced

the well-known “Freyssinet system” which used a conical wedge to anchor the wound wires used in post-tensioning.

Post-tensioning started to see wider applicability in the 1950’s.This was due to the development of higher strength steels, reduced cracking, and smaller deflections than in similar non pre-stressed members. During the 1960’s T.Y. Lin introduced the concept of load balancing. This is a simplified method of designing pre-stressed concrete which allows the designer to visualise the effect of the pre-stressing or post-tensioning as a reduction of the permanent loads applied to the member. The simplicity of the load balancing allowed pre-stressing and post-tensioning to be applied in building construction (Aalami, 2007).

1.4.5. Post-tensioned pre-stressed concrete fire performance

The performance of post-tensioned concrete is still not fully understood and is undergoing research around the world (Ellobody and Bailey, 2009, Min et al., 2012). Due to the comparatively thin members and high compressive forces in comparison to reinforced concrete, post-tensioned or pre-stressed concrete can heat faster and experience higher levels of spalling than with normally reinforced concrete. However, Eurocode 2 part 1-2 (British Standard Institute, 2004a) provides design advice on the fire performance of post-tensioned and pre-stressed concrete. This includes the thermal characteristics of the tendons used in post-tensioning.

1.5. Timber post-tensioning

1.5.1. Post-tensioned timber Overview

Transversely post-tensioned timber bridges

Post-tensioned timber technology was born in 1976 in Ontario, Canada with the invention of transversely post-tensioned bridges. This new technology was applied as an upgrade to the existing, aging, nail-laminated timber decking system of some bridges. The idea behind this system was to squeeze the deck back together using transverse post-tensioning tendons. The success of this rehabilitation technique prompted further research and development at the Ministry of Transportation Ontario (MTO) and Queens University. The goal was to introduce this technology into new constructions as well as the rehabilitation program (Crews, 2002).

This system utilises high strength post-tensioning bars (shown as red in Figure 1-4) and steel anchorage plates to clamp the timber members together effectively laminating them and creating a monolithic plate. This is also referred to as Stress Laminated Timber (SLT). The compression in the timber allows shear forces to be transferred between the members through friction, which allows all of the members to help resist a given load, not just the members the load is applied to. The steel also helps resist transverse bending caused by loads on the deck. The post-tensioning does not directly provide any bending resistance along the bridge.

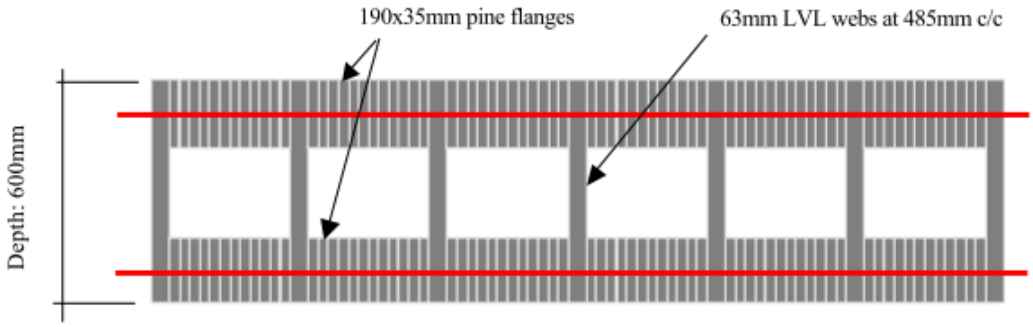

Figure 1-4: Cross sectional Detail of an example transversely post-tensioned timber deck. (Crews, 2002)

Post-tensioned timber frames

Post-tensioned timber frames have recently been the topic of substantial research at the University of Canterbury. Many applications of post-tensioned timber have been explored including shear walls, columns, beams, and beam-column joints. In 2005 a seismic resisting timber frame was developed, based on the PRESSS (PREcast Structural Seismic System). PRESSS is an American based research program looking at improving the seismic performance of precast and pre-stressed concrete buildings (Palermo et al., 2005a, Priestley et al., 1999). The frame was developed to investigate the seismic behaviour of a post-tensioned beam-column joint in an LVL frame This then led to further research into post-tensioned timber frame members (Newcombe et al., 2011). Currently there is ongoing research in to the gravity frame design of these members which will provide methods to optimise the use of timber material, allowing timber members to span further with cross section depths similar to that of comparable steel or concrete members (van Beerschoten et al., 2011).

The feasibility of post-tensioned timber framed buildings has also been explored. It was found that for a case study building the post-tensioned LVL frame had only a 6% increase in total cost compared to the steel and concrete options (Smith, 2008). As the technology matures and contractors become more familiar with the system it is believed this cost will reduce making it a very competitive alternative to steel and concrete structures.

1.5.2. Post-tensioned timber in application

Existing post-tensioned timber buildings

There have been a number of post-tensioned timber buildings constructed in New Zealand including; a recent addition to the Nelson Marlborough Institute of Technology is the Arts and Media Building which is a 3 storey post-tensioned timber framed building, shown in (NZWOOD, 2011b); The Diocesan School Aquatic Centre which utilised a post-tensioned timber roof, shown in Figure 1-6 (Kylek, 2010); The STIC office which was previously a 2/3rd scale seismic test specimen for research at the University of Canterbury, shown in Figure 1-7 (NZWOOD, 2011a); and the Nikau office at Wellington BRANZ campus which used post-tensioned columns, shown in Figure 1-8 (McGechie, 2011).

Whilst uncommon there are some older post-tensioned timber framed buildings. Information on these buildings is scarce. The building shown in Figure 1-9 has exposed tendons supporting a truncated column suspended beneath a timber beam.

Figure 1-5: Nelson Marlborough Institute of Technology (NMIT)

Figure 1-6: Diocesan school for Girls, Aquatic Centre, Auckland.

Figure 1-7: STIC office building, Christchurch, previous test specimen. (Carter Holt Harvey Woodproducts New Zealand, 2011)

Figure 1-8: BRANZ Nikau office, Wellington. (Carter Holt Harvey Woodproducts New Zealand, 2011)

Figure 1-9: An example of older post-tensioned timber construction, Virginia US. Taken by Jason Coleman.

1.5.3. Tendon configurations for post-tensioned timber

Researchers have investigated the benefits of post-tensioning timber members at the University of Canterbury (Palermo et al., 2010). They looked at the serviceability performance of long span LVL box beams which were post-tensioned using 12.5 mm diameter seven strand tendons. The research looked at multiple tendon configurations including straight tendons, internally deviated tendons and externally deviated tendons.

Straight tendons

A straight or undeviated tendon configuration is most suitable for simply supported members. An example of a straight tendon profile is presented in Figure 1-10. For a box beam the tendons can be placed near the bottom of the cavity below the timber section's centroid. The post-tensioning benefit is gained from the eccentricity of the tendon group which applies a moment opposing the loads applied. In addition to this there is also some benefit in applying a pre-compression to the cross section as timber is slightly stronger in compression than in tension. This means that any tensile stresses induced by bending first need to overcome this pre-compression.

This configuration can still be used in a continuous beam across multiple bays of a frame; however the post-tensioning moment no longer comes from the beams eccentricity but from the clamping force on the columns.

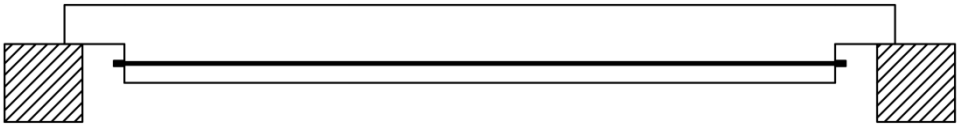

Figure 1-10: Simply supported post-tensioned beam with straight tendon

Internally deviated tendons

Employing a draped tendon profile has added benefits in comparison to a straight tendon. Instead of only gaining pre-camber through end moments due to eccentricity, tendon deviators are placed within the timber cross section. When the tendon is stressed it causes upward reaction forces in the beams at the location of the deviators. This effectively provides some level of mid-span support at each deviator. The internally deviated tendon profile is demonstrated in Figure 1-11.

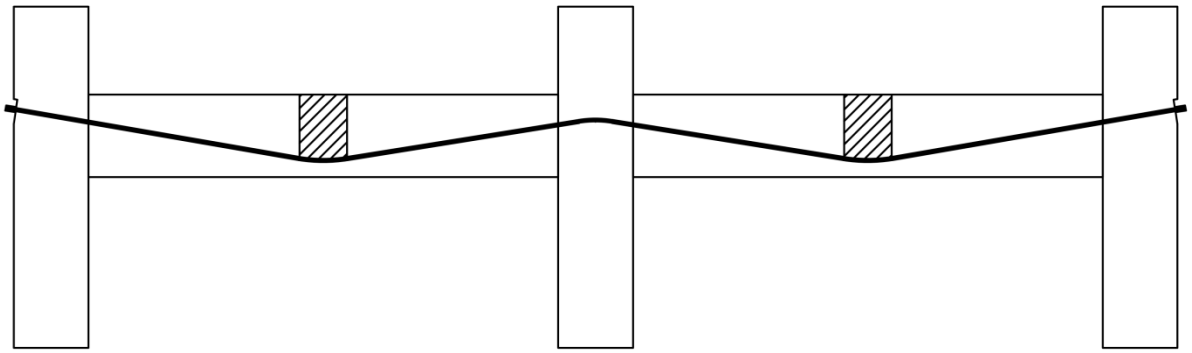

Figure 1-11: Post-tensioned Frame with internally deviated tendon

This tendon configuration is most appropriate for beams continuous over multiple spans or tendons which are continuous over multiple bays of a frame. However due to the tendon having to bend

around the deviator, the deviated tendon configuration is limited to flexible tendons such as 7-wire strand and is unsuitable for solid high strength steel bars.

Externally deviated tendons

Externally deviated tendons provide capacity in the same was as internally deviated tendons. The external deviation takes advantage of being able to provide the same upward support at the deviator locations requiring less tension in each tendon. This reduction in required tension is due to the increased angle of deviation. This solution can result in a smaller timber cross section in comparison to the other configurations; however, the tendons do sit below the beam and could affect the architectural or fire design. The externally deviated tendon profile is presented in Figure 1-12.

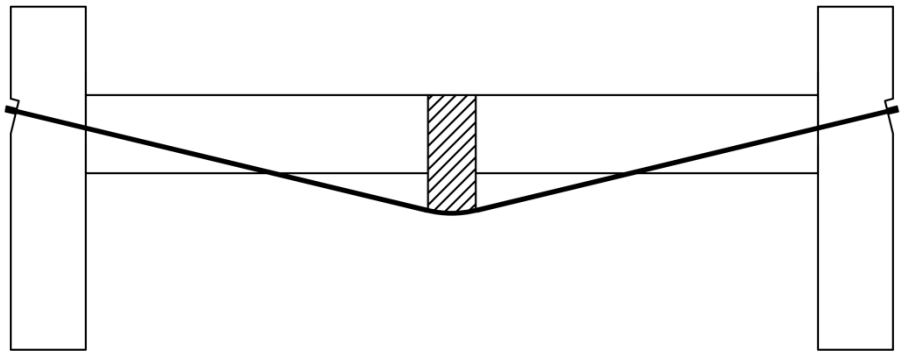

Figure 1-12: Post-tensioned Frame with Externally deviated tendon

Geometric non-linearity

Palermo et al. (2010) also discussed the geometric nonlinearity of the beam stiffness. This effect is more pronounced as the deviation of the tendons increases. This nonlinearity arises due to the length of the tendon being forced to change. The length of the tendon is forced to increase as the beam deflects downwards, which causes more strain and therefore more stress to develop in the tendon. This mechanism increases the beam's stiffness with deflection. Also the rotation at the end of the beams causes the length of the tendon to change. If the beam is deflecting downwards the end rotation will decrease the stiffness of the beam if the tendon anchorages are above the neutral axis, and will increase the stiffness with deflection if the anchorages are below the neutral axis.

For a simply supported beam with a straight tendon only the nonlinearity due to end rotation is applicable. For a continuous beam both mechanisms apply. However it was found that the nonlinearity was negligible for ambient design if the tendons remained within the beam cross section and were not deviated below the beam.

1.5.4. Seismic Performance of post-tensioned timber

Post-tensioned timber frames and wall systems perform well under seismic conditions (Iqbal et al., 2010, Newcombe, 2007, Newcombe et al., 2011, Palermo et al., 2005b). Recent design philosophies stress the importance of energy dissipation by including ductility in the structural system. This is commonly done by including "sacrificial" elements which undergo plastic deformation during a seismic event. With steel and concrete frames this can lead to residual displacements and cracking in concrete. The repair and reinstatement of this damage can be very costly for a region which is most likely already experiencing severe socio-economic losses due to the seismic event.

Post-tensioning can provide damage control for seismic events regardless of the material used. The post-tensioning connections are able to provide a centring moment when displaced which pulls the structure back to centre. This is however is in the elastic range only, the added damping or ductility can be added with additional mild steel dissipaters which undergo plastic deformations while absorbing energy. This allows large levels of ductility to be achieved without damaging the structural members or having residual displacements after a seismic event. These dissipaters can then be easily and cheaply replaced. If a timber frame is being used the mass of the timber is small compared to a comparable reinforced concrete frame. This means the forces experienced by certain ground accelerations will be lower. If the timber member is correctly designed only negligible crushing will occur due to the rocking motion of the connections (Palermo et al., 2005b).

1.5.5. Gravity performance of post-tensioned timber

A draped profile tendon can be used for gravity design as it provides uplift within the span of the beam. The deviator blocks change the angle of the force in the tendon which applies a reaction force on the deviator block and the beam. These uplift forces which help to limit deflections also increase the ultimate capacity of the beam. This system is similar to the concrete post-tensioning technology named the Brooklyn system which has been used in several buildings in Italy (Pampanin et al., 2004).

The beam column connection also provides a moment which further resists gravity deflections. Post-tensioning serves to clamp the columns together, holding the beam in place between them. As the beam deflects and its ends rotate, it pushes against the column near the bottom of the beam, which creates a moment between the clamping force and the beam's centroid. The clamping force is spread over an area due to the slight elastomeric nature of timber. The pressure distribution can be estimated with empirical formulas presented by van Beerschoten which can be used to calculate the lever arm for the moment calculation (van Beerschoten et al., 2011).

The shear connection between the column and beam is either obtained from a steel or timber corbel, the friction between the beam and the column, or a combination of both these methods. A corbel is often required to hold the beam in place during construction before the post-tensioning is applied. This corbel may only be adequate to hold the weight of the beam and would rely on the friction caused by the post-tensioning force to resist further loads.

In both gravity and seismic design the post-tensioning of beams applies a substantial force to the columns perpendicular to the grain of the timber. As the perpendicular to grain bearing strength is comparatively low compared to the parallel to grain bearing strength, this can cause problems. Possible methods of reinforcing the column include bearing against the steel corbel which is reinforced with screws into the column, or using cross banded LVL which allows some veneers to be oriented parallel to the bearing force (Iqbal et al., 2010).

1.5.6. Post-tensioned timber design methodology

The design of a post-tensioned beam follows the following basic steps. The different styles of post-tensioned timber change the technical details in some of the steps, such as how deflections are calculated, and what actions are considered. For the following steps consider that a trial beam size has been assumed and the calculation will be reiterated until a solution is found.

Post-tensioning design

The post-tensioning is designed first, and is designed to balance the deflections of some proportion of the ultimate limit state load, usually the dead load, and 40% of the live load. Deflections of the beam due to this load case are then calculated. Then the post-tensioning is designed by calculating what post-tensioning force is required to create the equal and opposite pre-camber deflection. This pre-camber deflection calculation will vary for different styles of post-tensioned timber. For example if there is a deviated tendon the deflections will be calculated from the uplift forces and the end moments.

Ultimate limit state design

Once the post-tensioning is designed the strength check can be done on the timber member. This can be done in two ways. The first being a conventional combined bending and compression check similar to what is presented in NZS3603. The second method being to calculate the stress distributions developed due to the axial loading, the bending due to the external loads, and the bending due to the post-tensioning, and to then check the developed stresses against the characteristic bending strength of the LVL.

The calculation is then iterated until a solution is found. For long term deflections and the ultimate limit state design it can be important to estimate the pre-stressing losses over time. This occurs as both the tendons and the timber experience creep. The tendon over time elongates and the timber compresses reducing the post-tensioning force.

1.6. Timber fire performance and design

As timber is flammable there is a common perception that it performs poorly in fire. However, structural timber can be designed to have excellent fire resistance. Structural timber often only adds a very small amount to compartment fire loads in comparison to the room contents. There is a risk associated with timber linings as in some cases they can govern the fire growth. Threats to occupants are usually in the early stages of fire development when there may be a risk of becoming trapped or becoming incapacitated due to smoke inhalation. During these early stages the structure is usually unaffected. Structural fire performance only becomes important in the later stages of fire development, often when the compartment has flashed-over. Timber, when exposed to fire, chars at a predictable rate. The char rate is slightly increased in the first 20 minutes of the fire as the char layer develops. Then the char layer acts to insulate the rest of the timber from the fire, slowing further char layer propagation to a slow and predictable rate. The member can then be designed based on this char rate to ensure the remaining timber has enough capacity to resist the expected load (Buchanan, 2001, Buchanan, 2007).

Both Eurocode and New Zealand Standards provide information on the expected loads for the fire limit state and the char rates to consider. NZS3603 specifies a char rate of 0.65mm/min for radiata pine and for timber of approximately the same density, but allows for charring rates to be determined from tests or calculations if the timber is of a higher density than radiata pine. It also requires corner rounding to be included in the calculations and specifies a minimum of 90mm for any beam or column dimension, it only refers to rectangular cross sections and doesn't provide any advice for other configurations . Eurocode 5 specifies two char rates for a number of types of timber. For LVL with a density greater than 480kg/m^3, it states a one-dimensional charring rate of 0.65mm/min, and a two-dimensional charring rate of 0.7mm/min. The two-dimensional charring

rate or notional charring rate is used in rectangular sections and includes effects of corner rounding. AS/NZS1170 specifies that a member should resist the un-factored dead load applied and the long-term live load, which is usually 40% of the specified live load. Eurocode 1 has similar requirements where the member must resist the un-factored dead load and a proportion of the characteristic live load. The proportion of live load is dictated by factors which may vary from country to country and are detailed in National Annexes for Eurocode 0 (British Standard Institute, 2002c).

1.6.1. Eurocode 5 advanced fire design

Eurocode 5, part 1-2 (Annex B) provides simplified calculation methods and advice on advanced calculation methods for determining the fire resistance of timber members. The advanced calculation methods allow for realistic analysis of the structure and can involve thermal and structural modelling. Eurocode 5 provides thermal properties including thermal conductivity, specific heat, and a density ratio which can be used in a numerical heat conduction model. These properties are effective properties which take into account the complex nature of charring without having to model the complexities of char shrinkage, cracking, decomposition, and timber pyrolysis. As the properties are only effective, they are only valid for ISO834 fire exposure, and if used in the cooling phase the model would re-grow timber as it does not capture the one-way nature of charring. The thermal properties of Eurocode 5 are presented in Figure 1-13 and in more detail in Chapter 4 of this thesis.

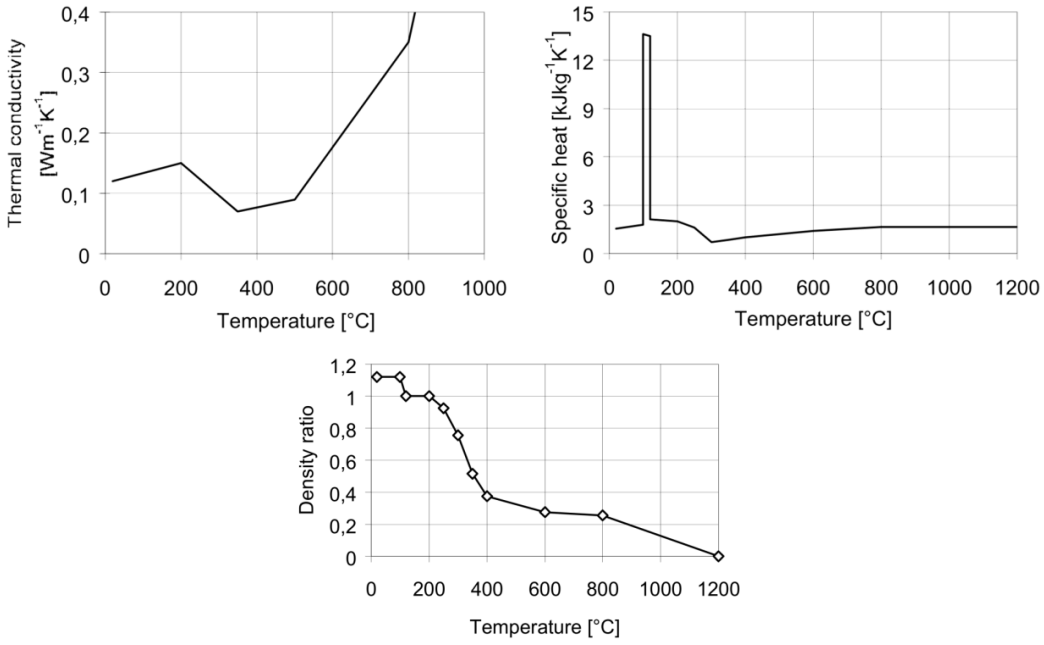

Figure 1-13: Eurocode 5 timber thermal properties

Eurocode 5 presents two simplified calculation methods, the reduced cross section method, and the reduced properties method. The *reduced cross section method* is a similar method to that in NZS3603 where a char rate is assumed and the size of the beam is reduced, however a 7mm zero strength layer is also assumed to account for reductions in strength and stiffness in the heat-affected portion of the timber. The remaining timber cross section is then used to calculate the strength of the member. The *reduced properties method* applies a strength reduction factor, based on the area and perimeter of the charred member, which represents the loss of strength due to temperature

effected timber. The reduced properties method is used instead of taking an extra 7mm zero strength layer (König, 2005, British Standard Institute, 2004b).

1.6.2. Full-scale fire testing

Full-scale furnace testing is done most commonly for two reasons; to demonstrate a particular system's fire resistance so a Fire Resistance Rating (FRR) can be assigned to it, or to provide data for research purposes. Often these objectives are not mutually exclusive.

Full-scale timber- concrete composite floors have been tested by the University of Canterbury to expand on the work of Frangi and Fontana (Frangi and Fontana, 1998). The experiments were conducted at the Wellington based Building Research Association of New Zealand (BRANZ) testing facility. These tests looked at the shear connection between the timber beams and the concrete slabs of the floor systems. It was found that the reduction of timber section size governed the failure of the floor systems. The test data was used to develop a spreadsheet model capable of predicting the fire resistance of these floor systems (O'Neil, 2009).

Often fire tests demonstrate phenomenon which are not able to be captured by simple numerical modelling. The timber-concrete composite floor tests described above contained double beams made from two 63mm thick beams nailed or screwed together to form a 126mm wide beam. When exposed to fire these beams curled away from each other and opened the centre of the beams, exposing more surface area to the furnace; the resulting cross section is presented in Figure 1-14. This was investigated in more detail with further testing and thermal modelling in subsequent research (Tsai, 2010).

Figure 1-14: Opening of screwed double LVL beam (O'Neil, 2009)

This work was later expanded on further by James O'Neill (O'Neil et al., 2012). Two fully timber floor systems were tested in a similar manner to above. Both systems had a 35mm cross-banded LVL deck supported on either a single 90mm wide 400mm deep LVL joist or an LVL box beam formed by the deck two 45mm thick 400mm deep webs and a 45mm thick 300mm wide flange. The single joist floor system did not run to failure due to an integrity failure due to the floors support condition. Whilst not immediately clear due to an issue during testing it is believed that the box-joist floor systems failed in bending and compression.

1.6.3. Fire performance of New Zealand LVL

A detailed investigation into the ignition properties and the char rates of New Zealand LVL was performed by Lane (Lane, 2005). This investigation utilised small-scale tests of LVL in a cone

calorimeter, two pilot-scale tests at BRANZ, and one full-scale load-bearing test at BRANZ. The small scale testing investigated LVL in a variety of orientations with varying radiant heat fluxes which was used to determine ignition properties of LVL and to measure the charring rate. The pilot-scale and full-scale tests were exposed to the ISO 834 standard fire.

This research recommended that a char rate of 0.72 mm/min, or 0.65mm/min with an allowance for an additional 7mm to 9 mm zero-strength layer, be adopted for New Zealand manufactured LVL. These char rates were representative of fire exposure in both grain orientations, and were appropriate to use with simple design methods which assume that material below the char layer (or below the zero-strength layer) is at ambient temperature and is at full strength, such as in NZS3603 or Eurocode 5.

1.6.4. Numerical modelling of LVL

Timber beams in fire can be modelled numerically using finite element analysis. The benefit of finite element analysis is that a model is less limited by geometry and cost than full-scale experiments. There are two analyses required to model a loaded member in fire; the thermal analysis and the mechanical analysis. The thermal analysis looks at temperature development within the cross section which could include the effects of; thermal conduction radiation and convection, moisture migration, and charring. However, for simplicity the models are often simplified to thermal conduction with radiative and convective boundary conditions. The other effects are incorporated in effective thermal properties. The most commonly used thermal properties are those presented by Eurocode 5 (British Standard Institute, 2004b).

The second analysis required is of the timber's mechanical response. This requires mechanical properties which are temperature dependent. Eurocode 5 provides mechanical properties which were developed to work with the thermal properties it provides. There are two main methods which can be used to link the thermal and mechanical models, which are, sequentially coupled modelling, and fully-coupled modelling. Sequential modelling is where the thermal model is run prior to the mechanical model and the temperature results are imported into the mechanical model. This is appropriate if the mechanical response is unlikely to affect the thermal analysis. If the thermal analysis is likely to be affected by the deflections of the beam a coupled analysis is more appropriate, where the thermal and structural analyses happen in parallel and results are passed between the analyses at each iteration. This form of analysis is still developing for timber and requires careful attention to detail to achieve realistic results (Werther et al., 2012).

1.7. Summary

In this review it was determined that the fire performance of rectangular timber members is well established, the fire performance of New Zealand LVL has been thoroughly investigated, and post-tensioned timber is an emerging technology which is currently undergoing research into its seismic and gravity performance. There is however a lack of research on the fire performance of box configuration timber beams and post-tensioned timber beams. This lack of research is due to the emerging nature of post-tensioned timber technology. It was also found that the post-tensioned concrete industry has thermal-mechanical properties for post-tensioning tendons which are applicable for post-tensioned timber. This research seeks to investigate the fire performance of post-tensioned timber and provide fire design advice for its future commercial use.

2. Full-scale furnace testing

2.1. Introduction

In order to validate the post-tensioned timber design method described in Chapter 3 of this thesis and to demonstrate the fire performance of post-tensioned timber beams, a series of full-scale tests were performed. These tests were developed to demonstrate a number of predicted failure mechanisms and to observe any unexpected and unpredicted behaviour which may affect the safety of this system. The tests were undertaken at the Building Research Association of New Zealand (BRANZ). BRANZ is an independent research and testing company servicing the New Zealand Building Industry (Building Research Association of New Zealand, 2011) and have two large furnaces for fire testing various building systems. These tests have been designed for the 4m by 3m full-scale furnace.

Whilst there are multiple implementations of post-tensioned timber, these experiments were designed based on 63mm thick LVL box beams with 12.5mm diameter strength steel wire tendons. This style of post-tensioned timber was chosen as it would be able to demonstrate the most failure mechanisms and challenges which other styles may not. The results of these tests whilst specific to this type of post-tensioned beam also provided useful insight into the design of other similar types of post-tensioned timber members.

Some of the defining features of a box beam are the large cavity and comparatively thin webs and flanges. This means that when much of the timber has charred away the beam may still be able to resist applied loading, however the remaining thickness would be much thinner in comparison to a solid rectangular cross section. Likewise, due to the thin section the air in the cavity will heat up and affect the tendons within it. Further, when a thin section is exposed to a fire the corner charring can cause failure due to the geometry of the material. This is discussed further in Section 2.3.9 and in Chapter 3.

The choice of tendons instead of Macalloy bars had two benefits. Firstly tendons are easier to manipulate during construction, as they can be bent and coiled easily. Secondly they are slightly better suited for demonstrating possible issues that could arise when a tendon is heated. This is due to the higher level of strain placed on a tendon and less thermal mass allowing it to heat faster.

2.2. Objectives

The objectives for these tests were:

- To perform full-scale tests on post-tensioned timber members to demonstrate the potential fire performance, and fire safety, of post-tensioned timber beams for use in commercial markets.
- To investigate potential failure mechanisms for post-tensioned timber beams exposed to fire.
- To investigate the performance of post-tensioning anchorages in fire. In particular, the suitability of traditional steel fire protection methods for this application

Originally two tests were planned, one to investigate a potential shear failure mechanism and one to investigate a potential bending failure mechanism. Due to premature failure in the latter test a third test was designed. The objectives for this third failure test were the following:

- To ensure that a combined bending and compression failure was demonstrated.
- To ensure that the premature failure was abnormal and not indicative of an unexpected failure mechanism.
- To allow the anchorage tests intended for the original test to be run to completion.

2.3. Experimental Procedure

2.3.1. Full-scale Furnace (BRANZ)

The full-scale furnace is 4m long by 3m wide and approximately 1m deep and powered by diesel injection burners as shown in Figure 2-1. Instead of test specimens hanging within the furnace they are constructed on test frames which sit above the furnace. This allows large systems to be tested. The furnace must then be enclosed with a material that will remain intact for the duration of the test in order to maintain temperature and pressure in the furnace.

Figure 2-1: BRANZ 4x3m furnace

The furnace is equipped with twelve permanent thermocouples which are used to monitor the temperature. This allows the fuel and air intakes to be adjusted to maintain the correct fire exposure throughout the test. Each diesel injection burner can be controlled and adjusted independently in order to provide an even temperature distribution within the furnace.

2.3.2. Furnace Test Frame

The furnace utilises interchangeable test frames upon which a specific test is assembled and then lifted onto the furnace. A 20mm layer of Kaowool blanket is laid between the frame and the furnace to ensure an adequate seal.

The test frame consists of a steel perimeter with a concrete ring cast within it, as shown in Figure 2-2. The steel provides structural rigidity and the concrete provides thermal mass and insulation from the heat within the furnace. The clear area within the concrete area is approximately 4m by 3m. The concrete ring adds approximately 150mm thickness and the steel an extra 200mm per side. In order to avoid damage to the concrete the test specimens must rest on the steel frame. Therefore the useable span is slightly more than 4.3 meters. There are also additional mounts on the loading frame used to support the test frame in a horizontal configuration for testing wall systems which were not used during this series of tests.

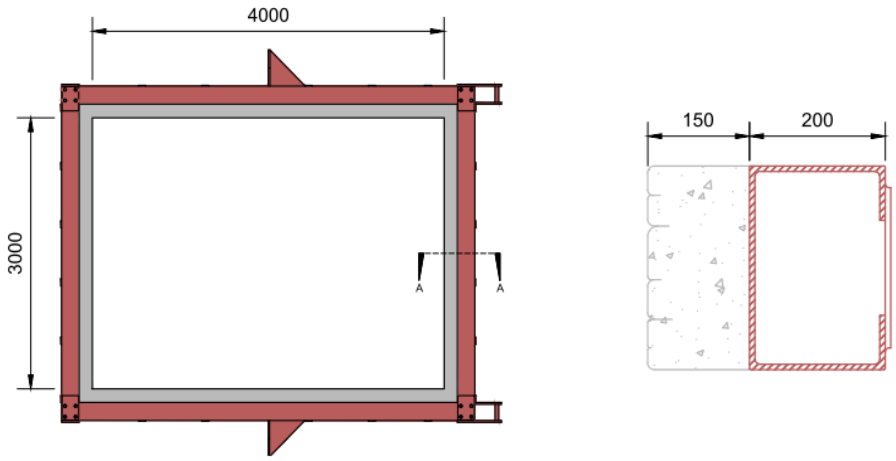

Figure 2-2: Test frame plan (left), Loading frame cross section A-A (right). Grey: Concrete, Red: Steel

2.3.3. Exposed Temperature Profile

The tests were all exposed to an ISO834 standard cellulosic fire (The International Organization for Standardization ISO, 1999). This type of fire exposure is used to compare the relative performance of different structural systems. It only roughly emulates the possible exposure of a real fire. There are other design fires which could be used such as the Eurocode parametric fire (British Standard Institute, 2002b); however, as they are specific to the compartment they are used in, they are of little use in comparing two systems for generic fire resistance.

The time-temperature profile of the ISO834 fire can be calculated as:

$$T_{ISO834} = 345\ log_{10}(8t + 1) + 20$$

Eq. 2-1

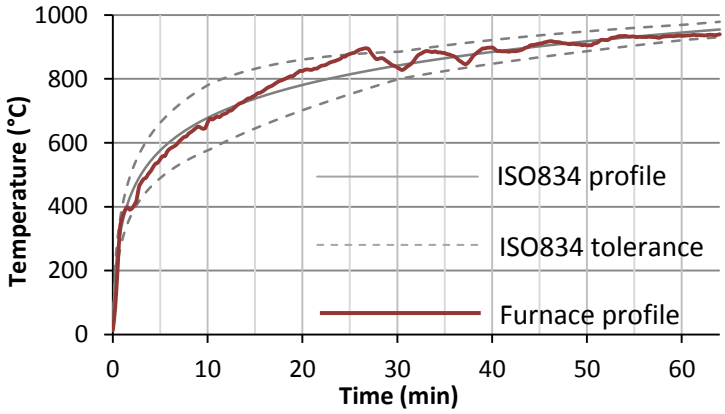

Figure 2-3: ISO834 temperature profile compared to the furnace temperature exposed to Beam A.

2.3.4. Internal Pressure

The ISO 834 standard specifies a pressure differential of 20 Pa 100mm below the underside of the test specimen. This is of little influence to this series of tests as charring is dominated by the gas temperature. However in order to attempt to match the standard as closely as practical the 20 Pa pressure difference was incorporated.

2.3.5. Steel plate design for post-tensioning anchorages

The anchorage systems for post-tensioned timber are currently under development. Currently systems utilising generic barrels and wedges and a steel bearing plate are common (van Beerschoten

et al., 2011). As the system matures the anchorages will become better suited/customized for timber and will become more efficient. The anchorage designs are likely to change in the near future. Due to this fast pace of evolution of post-tensioned timber systems, the anchorages are a secondary part of this investigation. As such the design of the anchorage plates has been done in a conservative manner to ensure that they do not have a large influence on the test results for the main beams. This has been done by using a conservative mechanical analysis and then checking the expected deflections and ensuring they are negligible in comparison to the strain in the tendons.

The tests on anchorage protection details are focused on temperatures reached rather than the mechanical performance of the anchorages. An understanding of temperatures reached by the anchorages will provide data for modelling and analysis of future research.

The smaller plates used for the anchorage protection tests were designed using hand calculations. The calculations assumed the plate was bending in a single direction. The post-tensioning load was applied as a point load and a tri-linear load distribution was assumed for the reaction against the timber (van Beerschoten, 2011). The tri-linear load distribution assumed zero load at either end of the plate which linearly increases to the maximum stress loading (σ_{max}) in the centre third of the plate as shown in Figure 2-4. The timber was assumed to act in a similar manner to an elastic foundation; the assumed load distribution was chosen to reflect this, but was very simplified. The bending moment due to this loading distribution was calculated using traditional analysis methods. The deflections were also able to be calculated using traditional methods however for ease the deflections where calculated using finite element analysis.

The plates for the main beam were designed in a very similar manner, but due to the size of the cavity and the span of steel plate a 3-point load distribution was assumed (right in Figure 2-4). This method of design was very conservative.

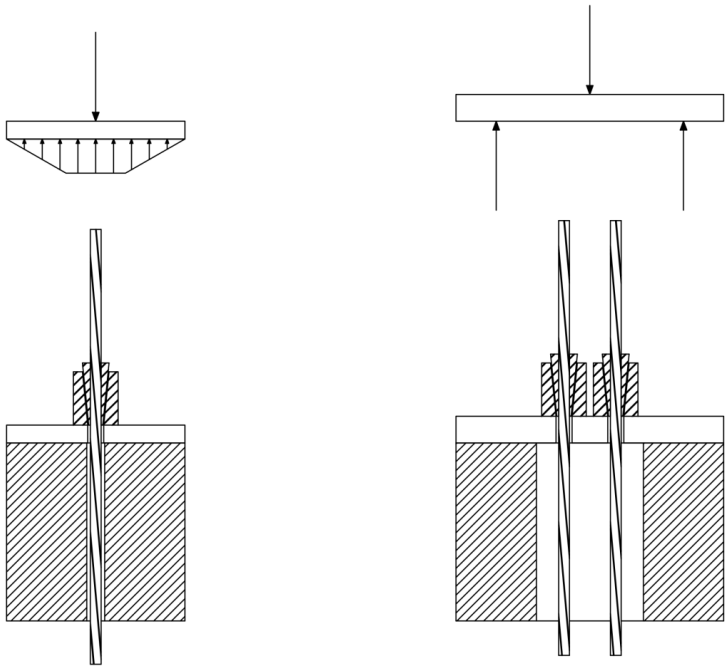

Figure 2-4: Stress distributions assumed for the design of the anchorage plates. Anchorage members (left), beam A (right)

2.3.6. Measurement tools

Two main tools were used for data measurement during these tests. Thermocouples were used to measure temperatures and load cells were used to measure tendon loads. Further to these a separate load cell and potentiometer were used to measure the load and deflections experienced by the test specimens.

There were two data acquisition systems required for these experiments due to the limitations of the BRANZ data loggers. BRANZ equipment recorded all temperature, deflections, and applied load measurements, where as a separate University of Canterbury data logger was used to record the post-tensioning forces. The time difference of the systems was recorded so that the data could be synchronised.

Load cells

Load cells measure the force applied to them. The majority of load cells use a series of strain gauges as the sensing elements. A force is applied to the structure of the load cell, usually made from a metal, which is deformed by that load. This deformation is then measured by the strain gauges. Because the metal structure of the load cell deforms elastically, the load can be accurately estimated from the deformation or strain.

In order to measure the force in tendons a load cell with a specially designed structure is used. The structure is a solid metal tube which the tendon is passed through. The tendon barrel and wedge then compresses the load cell against the steel plate.

It is important to calibrate load cells with the equipment they are to be used with during testing. A signal from a load cell can be interpreted slightly differently with different acquisition hardware. In order to calibrate the load cells a known load is applied to them. The load cell reading can then be adjusted to read the same as the applied load. Figure 2-5 shows the load cells used being calibrated. The loading frame on the right of the picture has a properly calibrated load cell which was used to measure the force applied.

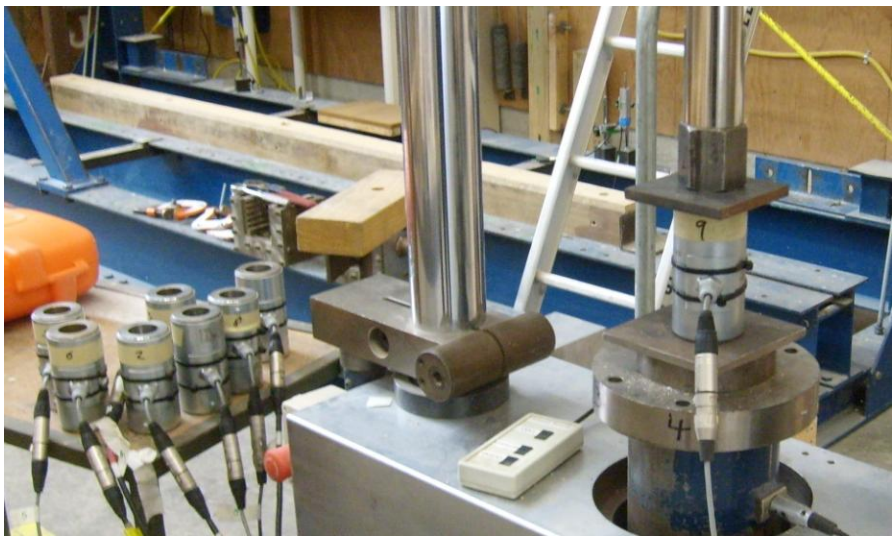

Figure 2-5: Tendon load cells undergoing calibration at BRANZ

Thermocouples

Thermocouples measure their own temperature using the Seebeck effect. The Seebeck effect occurs where electrically dissimilar metals produce a voltage proportional to their junction temperature (Rowe, 2006). This is utilized in thermocouples to measure temperatures. K type thermocouples consist of chromel and alumel wires. The two wires are welded into a small junction. This junction then produces a voltage proportional to its temperature.

A thermocouple needs time to heat up to the temperature of that which it is measuring and may be cooler than what it is measuring. Also if the wires of the thermocouple touch anywhere they will form another junction and will affect the reading. K type thermocouples have a sensitivity of approximately 41 uV/K. Figure 2-6 shows one of the thermocouples used in the testing.

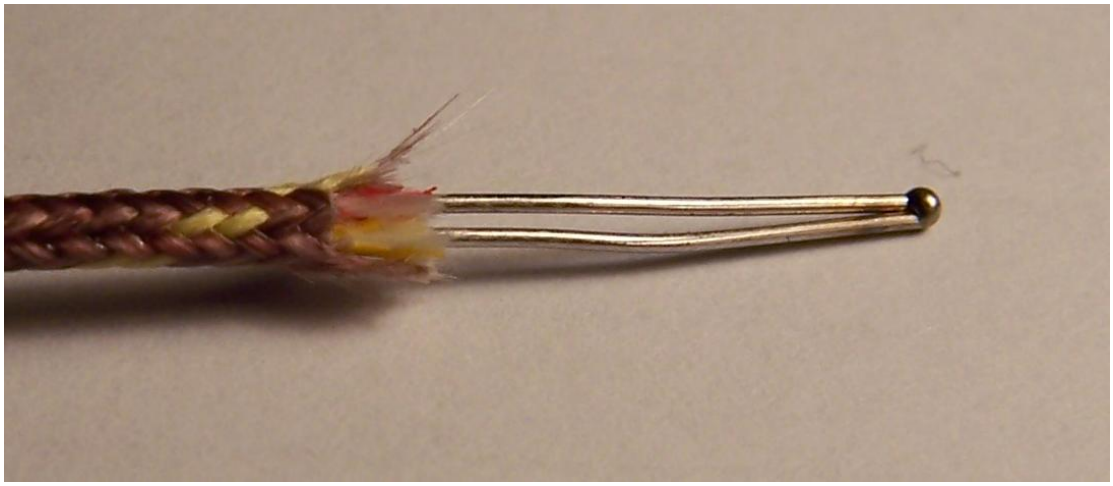

Figure 2-6: K type thermocouple as used in testing. (Picture scale approximately 40mm wide)

2.3.7. Data Acquisition

Thermocouple scheme

Temperatures were measured with K type thermocouples. Within the timber a series of thermocouple "plugs" were used to measure temperatures through the thickness of the timber. Each plug consisted of a 40mm diameter cylinder that was cut from 63mm LVL and shaved down to 58mm. 6 holes were drilled into the plug for thermocouples to be placed in. A channel was also cut down the side of the plug to allow for the thermocouple wires. An orthographic drawing of a thermocouple plug can be seen in Figure 2-7.

These plugs were then glued into the specially drilled holes in the webs and bottom flanges of each main test beam using the same resorcinol glue used to glue the beams together. The holes were drilled with a 41mm forstner bit which created a flat-bottomed hole. These holes needed to be drilled at the time of construction (Figure 2-8) as there would be no access to areas inside the member after the box beams had been glued together.

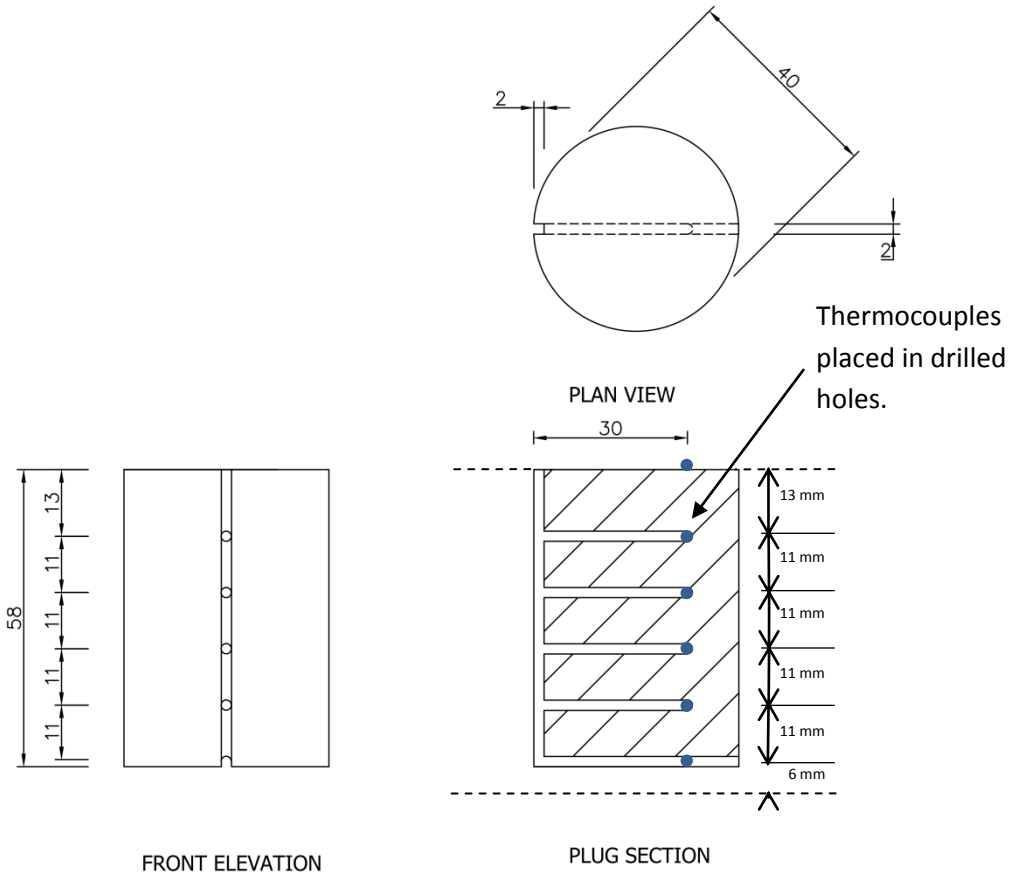

Figure 2-7: Orthographic drawing of a thermocouple plug.

Figure 2-8: Thermocouple plug and associated hole

All thermocouple placements in the main test beam were done at three main positions along the beam; Positions A, B and C. Position B is in the centre of the beam, Position A is 1 meter to the left of Position B and Position C is one meter to the right of Position B as shown in Figure 2-9

For each 5m long beams thermocouple plugs were placed at Positions A, B and C in the centre of the bottom flange of each beam, in one web at Positions A and C, and in the centre of the opposite web at Position B (Figure 2-10). A thermocouple was also placed in one of the lower corners of the beam cavity and on each of the tendons at Position A, B and C.

In order to investigate the effect of tendon placement on the heating of the tendons two 40cm lengths of tendon were placed inside Beam A with two thermocouples attached to each of them. The first was placed at Position D, fixed to the centre of one web inside the cavity. The second was suspended near the centre of the cavity at Position E. These lengths of tendon were only included in Beam A due to its larger size.

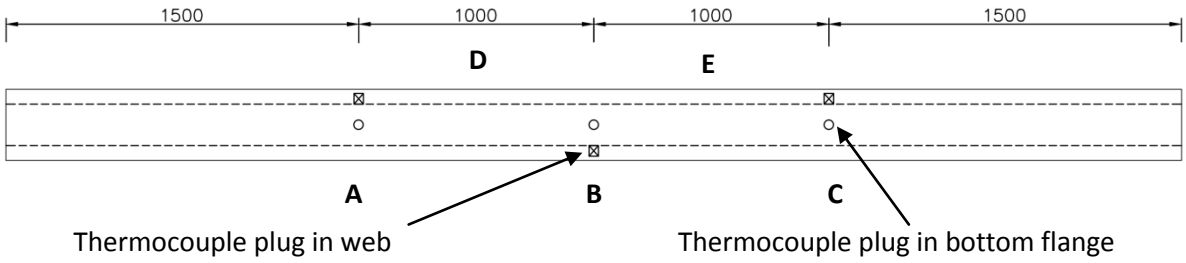

Figure 2-9: Plan view of typical test beam showing thermocouple plug locations (O: thermocouple plug in bottom flange X: thermocouple plug in beam web).

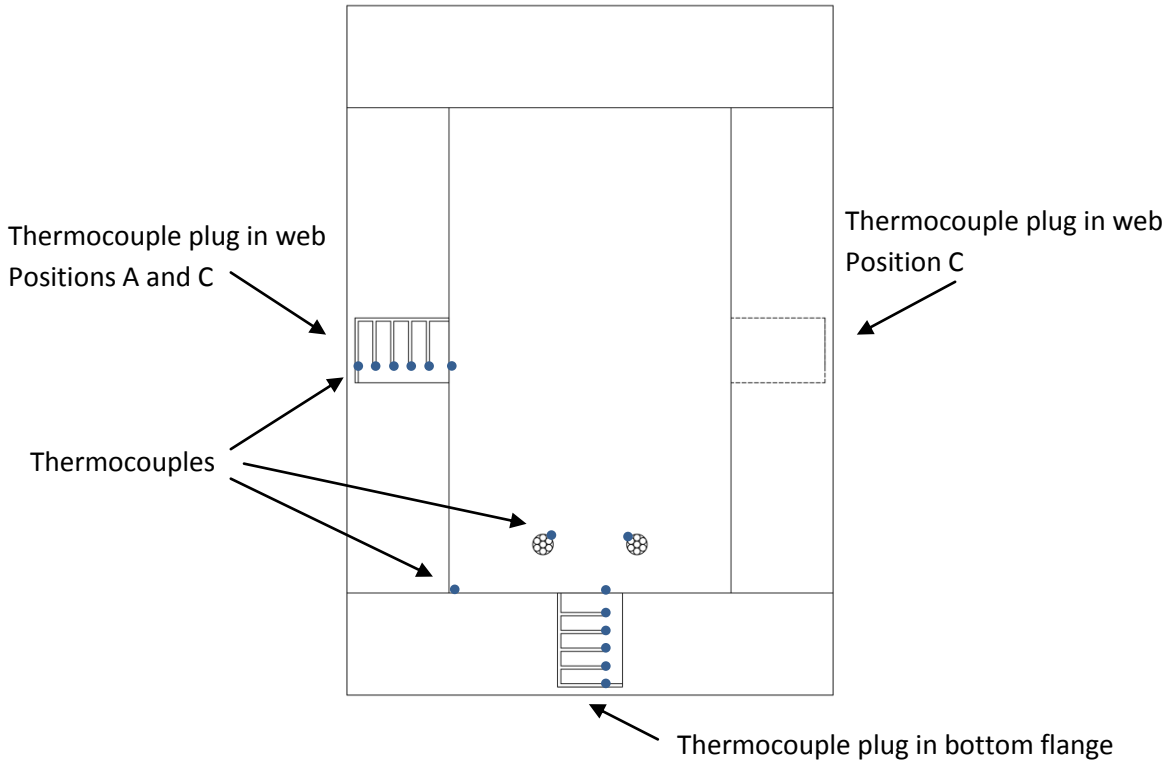

Figure 2-10: Thermocouple locations within a typical test beam cross section at Positions A and C

Six thermocouples were used to measure temperatures of the steel anchorages and were place in the positions shown in Figure 2-11. At positions X and Y a thermocouple was placed on top of the plate underneath the fire protection. At positions X, Y and Z a thermocouple was placed between the steel plate and the timber member. The sixth thermocouple was attached to the tendon 50mm into the beam.

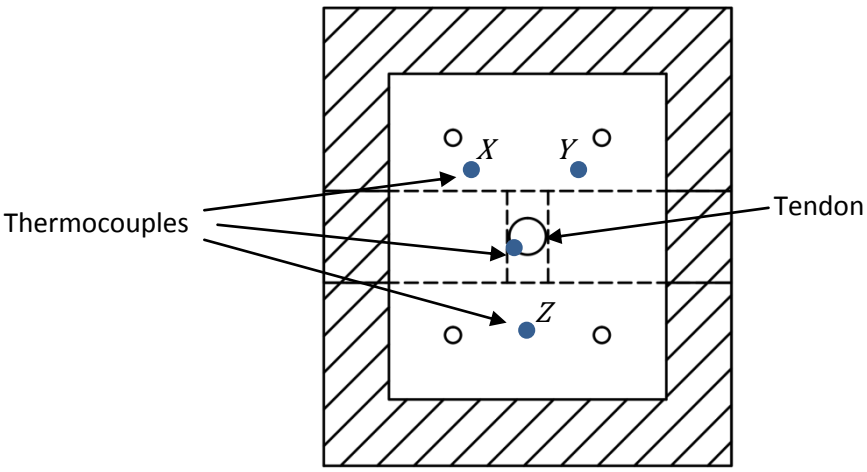

Figure 2-11: Anchorage thermocouple placement

Post-tensioning tendon load cell scheme

Eight load cells were used during testing to measure load in the post-tensioning tendons. The load cell scheme is shown in Figure 2-12. Two load cells were used on the main beam of each test, one for each tendon. In the test beams the load cells were staggered, one on either end, due to geometric constraints making it difficult to have both load cells at one anchorage. Each of the smaller beams had a load cell on the end of the beam not exposed to the furnace.

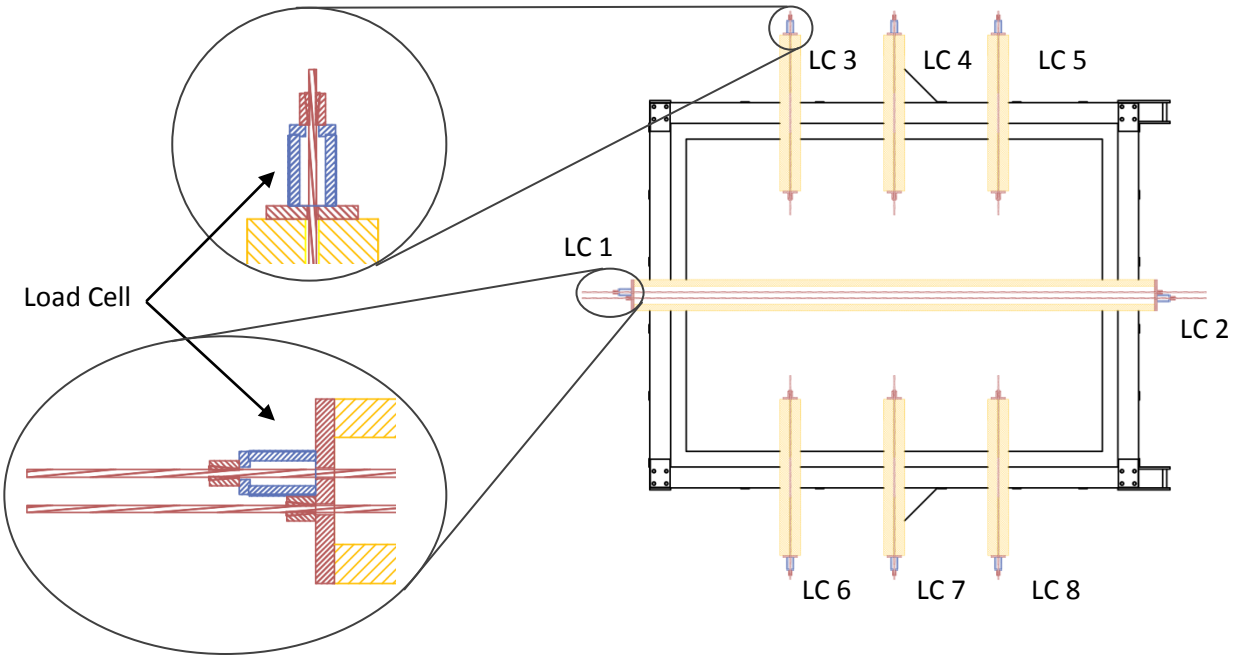

Figure 2-12: Load cell scheme for the Beam A test. Diagram shows load cells LC1 to LC8. (Typical)

Loading and deflections measurement

A single load cell and potentiometer were used to measure the load applied to the beam and the subsequent deflections. The potentiometer and load cell were placed above the load-spreading bar. This positioning meant that the values recorded for deflection were the average of the deflections of the beam at each load point and the loading force recorded was the sum of the loads at each load point. This affects the comparison of recorded deflections and calculated deflections as the calculated deflections were for the mid-span.

Figure 2-13: Spreader bar, load cell, and deflection potentiometer used during testing.

2.3.8. Test process

Each test was conducted in three main stages; construction and setup, testing, and post-testing. In the first phase the test specimen was constructed on the test frame. This involved the main test beam having post-tensioning applied and tuned to the required post-tensioning force. Then the anchorage members had post-tensioning applied. A GIB board enclosure was constructed around the main beam, and the anchorage members were put in place afterwards. Once everything was in place any potential gaps found were filled with a fire rated mastic compound or Kaowool blanket.

The entire test frame was then lifted by overhead crane into position on top of the furnace. A layer of Kaowool was placed between the furnace and the frame to stop any gaps forming. Then the loading A-frame was lifted into place around the test frame. The A-frame held the hydraulic jack used for loading, the deflection measuring potentiometer, and the large spreader bar used to split the force from the jack to two point loads on the beam. Holes were cut from the GIB board roof on top of the beam and steel plates were placed within them. These allowed the force from the spreader bar to be applied directly to the beam, avoiding any issues that might arise from the GIB board crushing. Just preceding the start of the furnace test the load was applied to the beam. The hydraulic pump was computer controlled to provide a constant load throughout the test.

Once the tests had started, temperature measurement recording, on BRANZ equipment, was started automatically whilst the post-tensioning load measurement recording, on University of Canterbury equipment, was started manually before the initiation of each test. The time at which the tests started was recorded to allow the data from both systems to be synchronized later. The furnace temperature was controlled by BRANZ technicians; each burner was controlled individually to maintain an even temperature throughout the furnace. During testing any gaps which form were evident as smoke was forced out of them due to the increased pressure inside the furnace. These gaps were able to be somewhat sealed from the outside with fire rated mastic. During testing the deflections and temperatures measured were able to be monitored on screens near the furnace.

When failure occurred, as indicated by runaway deflections or other obvious problems, the furnace burners were stopped. The loading A-frame was unbolted and lifted off the furnace using the overhead crane while all load cells were unplugged and thermocouple wires were cut. Once the A-frame was clear and the crane was available the test frame and specimen were lifted off the furnace and suspended above the workshop floor where it could be hosed down to cool the members and stop the charring and any continued burning. It took about 5-10 minutes from the end of each test until the test specimens could be hosed down. The removal of the loading frame and then test frame is shown in Figure 2-14.

Once the specimens where adequately cooled, the GIB enclosure was broken, exposing the specimen and allowing pictures to be taken. Once the specimens were cool enough to handle samples were cut from the beams for later analysis. Some anchorage members still had much of their post-tensioning stress remaining and required careful de-stressing.

Figure 2-14: Top left - Beam A test 30s before failure. Top right – Beam A after failure, thermocouples being cut, and the loading frame being lifted from furnace. Bottom – Test frame and specimen being lifted from furnace

2.3.9. Expected Failure Mechanisms

There were four potential failure mechanisms considered; combined bending and compression, longitudinal shear in a corner, longitudinal shear in a web, and the loss of post-tensioning. For this series of tests the failure mechanisms of combined bending and compression and longitudinal shear failure in the bottom corner were chosen to be demonstrated.

Combined bending and compression was expected to be seen as crushing near the top of the section in the central portion of the beam where the bending moment would be maximum. The failure was expected either in the top flange or in the web where the web meets the top flange and as it is a crushing failure it was expected to be comparatively slow and ductile. It was expected to occur in long slender beams and was chosen to be demonstrated as it was expected that it may affect a large number of beams in practice.

Longitudinal shear failure in the corner of the cross section was expected to be seen as a reasonably sudden or brittle loss of strength. It was expected to manifest as a split at the corner of the cross section near either end of the beam between the load points and the supports, where the shear stress was maximum. Also as the shear in the web and the corner were closely related, it was expected that as the corner failed it would "dump" the shear stress that it was resisting into the web and cause a crack to form in the web.

A longitudinal shear failure in the web was expected to manifest in a similar manner to a shear failure in the corner. For this reason only the shear failure in the corner was chosen to be demonstrated.

Loss of post-tensioning due to fire was not specifically investigated during these tests as it is very dependent on the beam and its application. This makes it ideally suited for simple mechanical modelling during design or further research.

2.3.10. Supporting assembly details

In-order to maintain the temperature and pressure inside the furnace the test needed to be enclosed. For this series of tests this enclosure was made from a timber frame lined with GIB Fyreline™ for Beams A and B, and a Hebel block wall with precast concrete lid for Beam C. The GIB enclosure was made using a 45mm square, rough sawn, H1.2 treated, radiata pine frame with studs at 450mm centres lined with 2 x 13mm layers of GIB Fyreline, which provides a 60/60/60 minute fire rating for a one way wall according to the GIB fire rated systems manual (GIB, 2006). A lid was also made from the same timber and GIB boards. The lid rested on the beam in the centre and the stud wall around the perimeter of the test frame. The enclosure had penetrations cut into it to allow the anchorage members to be inserted into the furnace whilst keeping the outer anchorages and load cells out of the furnace. The enclosure is presented in Figure 2-15.

Figure 2-15: GIB Fyreline™ furnace enclosure

Hebel Blocks are a brand of aerated cement blocks made by Supercrete New Zealand. The block wall made the test setup substantially shorter and less intensive. The cement blocks were able to be easily cut with a hand saw to create penetrations for the anchorage members. Two large precast concrete slabs were available to be used as a lid for the Hebel Block enclosure. These slabs left a 1.2m space in the centre where the main test specimen was. This space was able to be covered with two layers of GIB Fyreline™. A timber lip was made into the lid to ensure a tight seal against the concrete slabs as shown in Figure 2-16.

Figure 2-16: Hebel block furnace enclosure

2.3.11. Test Layouts

Three full-scale tests were carried out. They are referred to here by the main beam for each test; therefore, the Beam A B and C tests, as shown in Figure 2-17. The Beam A test included Beam A, two Kaowool protected anchorages, two GIB board protected anchorages and two timber (LVL) protected anchorages. The Beam B test included Beam B, and two intumescent protected anchorages. The Beam C test included Beam C, two intumescent protected anchorages, and two unprotected anchorages.

The main beam for each test spanned 4.36m across the long dimension of the loading frame. Each of the anchorage test members were placed around the periphery of the loading frame with the anchorage to be tested placed approximately 1m within the furnace.

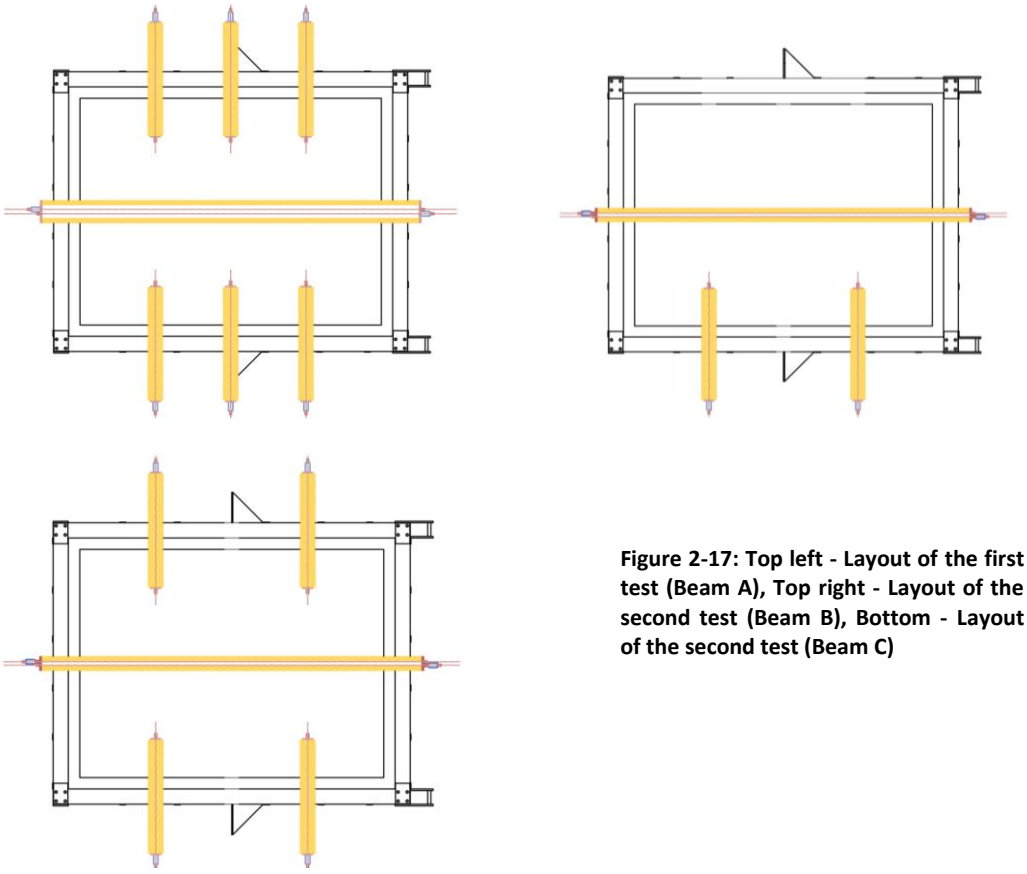

Figure 2-17: Top left - Layout of the first test (Beam A), Top right - Layout of the second test (Beam B), Bottom - Layout of the second test (Beam C)

2.3.12. Test Loading

The Hydraulic jack was used to apply 40 kN of force onto the test specimens. This force was limited by the loading frame. This force was applied to the beam specimens at two points 1.5 m apart through a spreader bar. The 4 point loading arrangement applied pure bending moment in the centre of the beam with very little shear, and constant shear at either end of the beam.

Because the test setup was limited to applying 40 kN of force the maximum bending moment applied was 28.6 kNm and the maximum shear applied was 20 kN. These values were used to back calculate the following effective load cases:

- 2.185m Tributary width
- 3.0 kN/m^2 Dead load (G)
- 3.0 kN/m^2 Live load (Q)
- 8.1 kN/m ULS (1.2G+1.5Q)
- 4.2 kN/m FLS (1.0G+0.4Q)

The ULD loading was converted to point loading by multiplying by the tributary area of each load point. This shows that applying 40 kN to the beam is approximately equivalent to 52% of the beams ULS design loading. Through ambient calculations this also shows that the beams are loaded to approximately 49% of their ambient capacity.

2.4. Materials

Presented below are descriptions of the materials used during testing and the relevant material properties.

2.4.1. Laminated Veneer Lumber (LVL)

Laminated veneer lumber or LVL is an engineered timber product consisting of a number of 3-4mm thick layers (veneers) of timber which have been peeled from logs and glued together (laminated) as shown in Figure 2-18. The lamination of a number of layers causes defects to be spread throughout the member, which means the timber, in any one area, is stronger than a single piece of solid sawn timber with a knot or other defect present. Also through manipulation of which veneers are used through the depth of the LVL the overall stiffness can be manipulated. Often the outer laminates have a higher stiffness and strength than the inner laminates. The veneers in LVL are oriented so that the grain is parallel, unlike plywood where the veneer orientation is perpendicular between layers. Plywood utilises the alternating orientation of veneers to provide bending resistance in two directions. LVL is usually used in applications where it only bends in one direction which makes it more efficient to orient all the veneers in one direction. There is however cross-banded LVL where some veneers are oriented at 90° to the others, which are used to provide greater bearing or shear resistance and increased dimensional stability. The LVL used in the manufacturing of these test specimens was Carter Holt Harvey LVL13. The material properties in Table 2-1 are as presented by the manufacturer. (Carter Holt Harvey Woodproducts New Zealand, 2009)

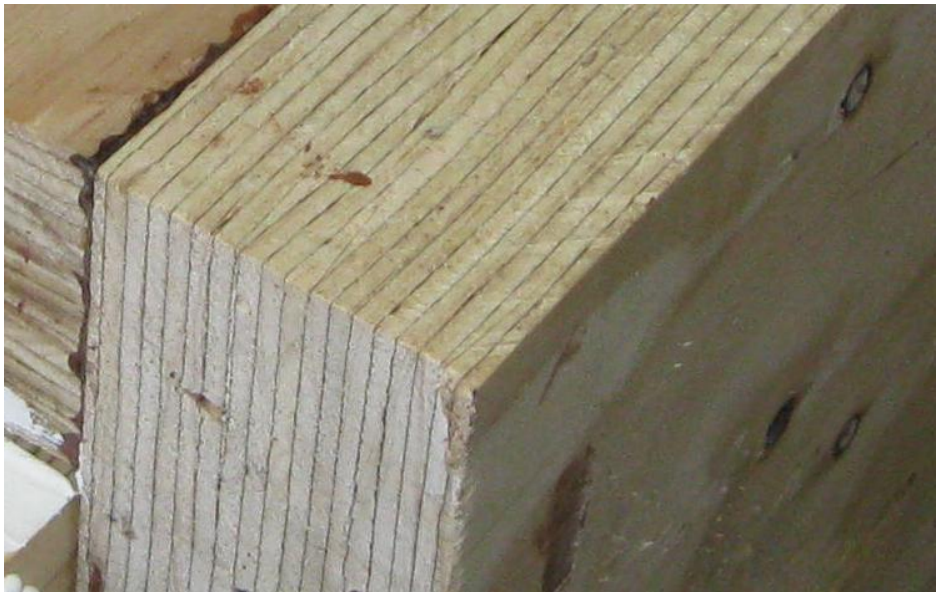

Figure 2-18: Example of LVL demonstrating veneer thickness and orientation.

Table 2-1: LVL Material Properties. (Carter Holt Harvey Woodproducts New Zealand, 2009)

Modulus of Elasticity	**E**	13.2	GPa
Bending Strength	$\mathbf{f_b'}$	48	MPa
Tension Strength Parallel to grain	$\mathbf{f_t'}$	33	MPa
Compression Strength Parallel to grain	$\mathbf{f_c'}$	45	MPa
Shear in beams	$\mathbf{f_s'}$	5.3	MPa
Density	**ρ**	620	kg/m^3

Veneer thickness		3-4	mm
Adhesive type		Type A (phenolic)	

Char rate	**β**		
including zero-strength layer		0.72	mm/min
with additional 7mm zero-strength layer		0.65	mm/min

2.4.2. Steel

There were two steel components used in these tests. First the steel plates used as bearing plates for the anchorages and secondly the steel post tensioning system.

2.4.3. Anchorage plates

As the anchorages for post-tensioned timber are still undergoing substantial development the anchorage system was not a main subject of these tests. As such the plates were conservatively designed from grade 250 steel. Little emphasis was placed on the plate performance and therefore the material and mechanical properties were not closely scrutinized.

2.4.4. Post-tensioning system

The tendons used for these tests were 12.7mm nominal diameter 7 wire strand. The same tendons are used in unbonded post-tensioned concrete systems and the properties are provided in Table 2-2.

Likewise the barrel and wedge anchorage system used (Figure 2-19) were developed for application in post-tensioned concrete. The anchors and tendons were supplied by Construction Techniques group limited (BBR Contech). Little information on the properties of the post-tensioning barrel and wedge anchorage system was available as it was the tendon performance that governed the post-tensioning design.

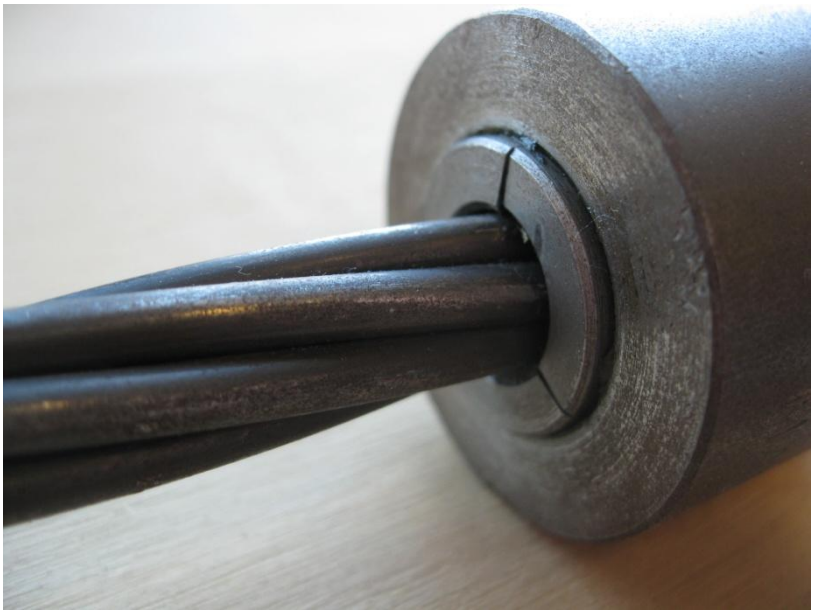

Figure 2-19: Post-tensioning tendon, barrel, and wedge system used for full scale testing

Table 2-2: Tendon Properties provided by BBR Contech– Post Tensioning Design Data (Construction Techniques Ltd, 2007)

Post-tensioning Tendon Properties			
Modulus of Elasticity	**E**	180-205	GPa
Steel Area	**A_s**	100.1	mm^2
Nominal Diameter	**Ɵ**	12.7	mm
Linear Mass	**m_L**	0.768	kg/m
Maximum Breaking Force	**MBF**	184	kN
Maximum Jacking Force	**MJF**	80	%MBF

2.4.5. Post-tensioning Anchorage Fire Protection Methods

The following materials and methods were used as thermal protection for the post-tensioning anchorages consisting of the steel plate, exposed tendon, and barrels and wedges used to secure the tendons in place. Discussed below are the thermal properties of protection materials, the relative advantages, and disadvantages of the protection methods (ignoring performance) and some discussion on their practical implementation.

GIB Fyreline ™

GIB plasterboard is a brand of plasterboard manufactured by Winstone Wallboards Ltd. in New Zealand. The sheets of plasterboard are made from gypsum based plaster slurry rolled flat and lined with paper on the faces and the edges. The Fyreline™ product line uses glass fibres and chemical

additives within the gypsum to give some additional fire resistance. The manufacturer recommends 2 layers of 13mm GIB Fyreline™ board for a one way wall system to achieve a 60 minute fire rating (GIB, 2006).

As the GIB heats the crystals which form the gypsum break down due to the loss of the water of crystallization. This causes the gypsum to become powdery. The fibres added to the Fyreline gypsum serve to increase the thermal insulation and to hold the powdery gypsum in place longer than it would otherwise remain.

GIB board is a cheap and readily available building material. It can be used to form a box around the post-tensioning anchorage using normal construction tools and methods. It can be plastered and painted to match the surrounding features. If the anchorage is recessed into a column GIB board can very easily be used to cap the cavity. However if the anchorage is recessed it may be preferable to use timber to enclose the cavity.

Kaowool

Kaowool is a brand of ceramic fibre insulation material that comes in rolls of various thicknesses and it often 600mm wide. The fibres are made from blown alumino-silicate. The material provides good temperature insulation and remains continuously stable up to temperatures of 1200°C. It is also chemically inert and has a good resistance to chemical attack. The manufacturer provides the thermal properties for Kaowool blanket presented in Table 2-3 and Figure 2-20. (FORMAN building systems, 2002)

Table 2-3: Kaowool Thermal Properties. (FORMAN building systems, 2002)

Specific Heat	c_p	1.13	kJ/kgK
Bulk Density	ρ	128	kg/m^3

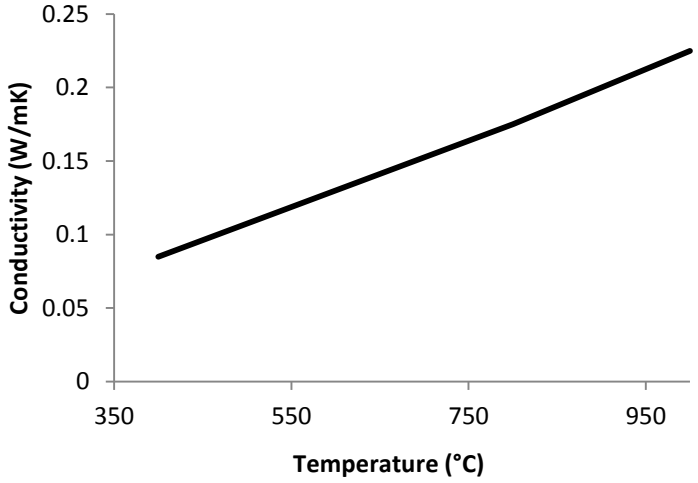

Figure 2-20: Kaowool Thermal Conductivity. (FORMAN building systems, 2002)

Kaowool blankets can easily be wrapped around anchorages and stapled to timber. However, using Kaowool blankets or boards does not provide a good architectural finish and would only be suited for non-visible areas. Due to its malleability and its ease to work with, Kaowool blankets may be ideal for retrofit fire protection.

Intumescent

The intumescent paint used in these tests was Firepro PST-100, which is a water-based intumescent paint used for the fire protection of steel members. The intumescent system requires a primer coat and an acrylic top coat for durability and a good standard of finish. Due to the intumescent market being very proprietary the actual material properties are unknown. The manufacturer recommended a dry film thickness of 1mm which can be achieved with three brushed coats. It should be noted that this recommendation is based on a critical temperature of 550°C which is unlikely to be appropriate for a post-tensioning anchorage.

Intumescent paints protect by foaming up at their activation temperature, usually near 200 °C, and then insulating the member from the fire. Due to the activation temperature being approximately 200 °C the steel surface will get close to this temperature before the intumescent expands and slows down the heat transfer.

Intumescent paint is very specialized and difficult to work with. In order to provide and ensure the correct thickness it needs to be applied by specialist contractors. Even with professional application it can be difficult to achieve a good architectural finish. If the anchorages are to be visible and require fire protection, professionally applied intumescent paint might be used to achieve this.

Due to how intumescent paint works it may not be suitable for every post-tensioning system. The paint does not activate below a certain temperature (approximately 200°C). If the post-tensioning system is unable to perform up to this temperature then intumescent paints may not be able to provide any protection against post-tensioning force losses.

Timber fire protection

The LVL timber used in construction of the beams was also used as a protection material for anchorages. As stated previously the char rate is given as 0.72mm per min. There is also an alternative char rate of 0.65mm per min which should be used with an allowance for an additional 7 mm layer of zero strength material (Carter Holt Harvey Woodproducts New Zealand, 2009). These char rates assume that beneath the char surface timber is still at ambient conditions. This can make the calculation of LVL fire protection for post-tensioning anchorages very easy.

Timber can be used to create a box around an anchorage. As the timber matches the columns and beams it is easy to incorporate the anchorage protection into architectural designs. Also if the post-tensioning anchorage is recessed within a cavity inside the columns it is very easy to cap these cavities using a certain thickness of LVL or glue-laminated (Glulam) timber. This would completely hide the post-tensioning anchorage and provide fire protection, which may be useful for certain architectural designs.

Timber is a relatively inexpensive material and only small additional volumes would be required compared to the entire frame. Timber allows architects to invisibly hide the connections if desired. Timber is easy to work with and no specialist skills are required to install it.

2.5. Specimen details

Each of the three main beams had the common attributes shown in Table 2-4: Typical beam test specimen attributes.

Table 2-4: Typical beam test specimen attributes

Length	5m
Span	4.36m
Configuration	Box beam
Web and flange thickness	63mm
Anchorage Plate	30mm thick
Tendons	2

The beams were supported at either end on steel sections approximately 100mm wide. This approximates a pined-roller support condition. There is some friction between the beams and the supports holding it in place. However the steel section can rock to allow movement. The beams were assumed to be simply supported.

2.5.1. Beam A

Beam A was a 426mm deep and 300mm wide box beam with 63mm thick webs and flanges. A drawing of the beam's cross-section and a photo of the completed beam are presented in Figure 2-21. The tendons were stressed with 104 and 109 kN respectively, providing a total post-tensioning force of 213kN.

Beam A was designed using the proposed design method presented in Chapter 3, and predicted to fail in longitudinal shear near one of the bottom corners of the section after 61 minutes. However, a web shear failure was predicted to occur 2 minutes after this. Due to random fluctuations in char rates and strengths it was possible that a shear failure in the web may occur before a shear failure in the corner. The corner shear failure was expected to occur somewhere between the load points and the beam supports either side of the beam, where the shear force in the beam is maximum. At 61 minutes the rounded corner charring was expected to cause the thickness of the timber at the corner to become less than required to resist the shear flow around the section. A diagram showing the expected corner geometry is presented in Figure 2-72 on page 59.

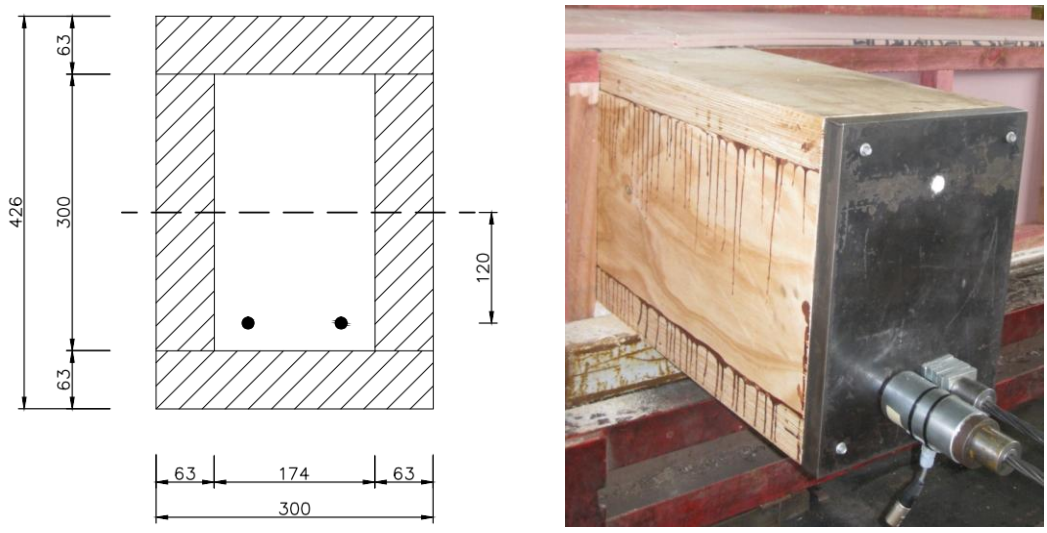

Figure 2-21: Beam A – LVL cross section (left). Photo of completed beam showing post-tensioning anchorage (right)

2.5.2. Beam B

Beam B was initially designed to fail in mid-span combined bending and compression at approximately 43 minutes. However, this estimate was later revised to 37 minutes. The combined

bending and compression failure was expected to result in crushing near the top of the cross section. Due to the post-tensioning a tensile bending failure was not expected. The cross section and a photo of the beam are presented in Figure 2-22.The tendons where stressed with 106kN and 107kN, resulting in an overall post-tensioning force of 213kN.

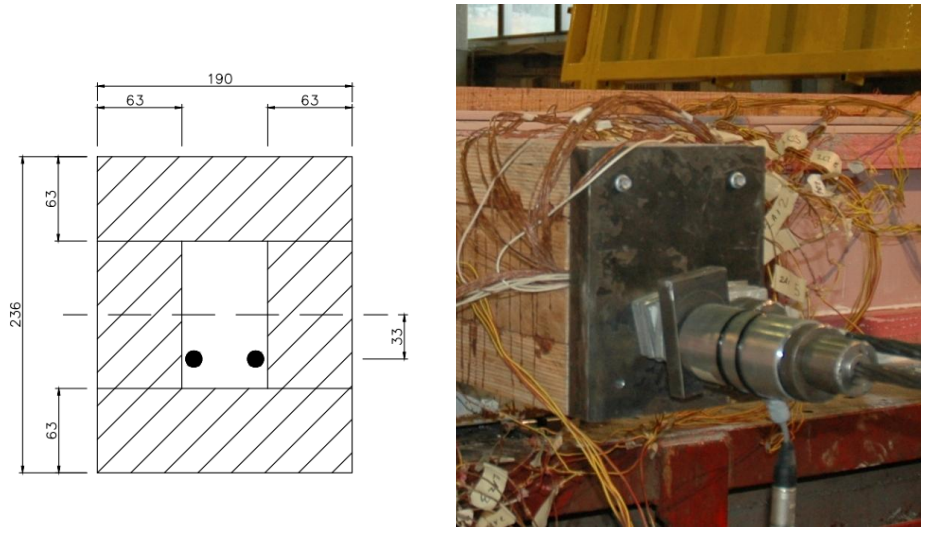

Figure 2-22: Beam B - LVL cross section (left). Photo of completed beam showing post-tensioning anchorage (right)

2.5.3. Beam C: Bending and compression failure

Beam C was initially designed to fail in combined bending and compression mid-span at approximately 58 minutes. However, after revisions to the design method the beam was predicted to fail at 53 minutes in combined bending and compression at the end of the beam due to the axial force and moment applied by the post-tensioning. The tendons were stressed with 115 and 117 kN, giving an overall post-tensioning force of 232 kN. The timber cross section and a photo of the completed beam are presented in Figure 2-23.

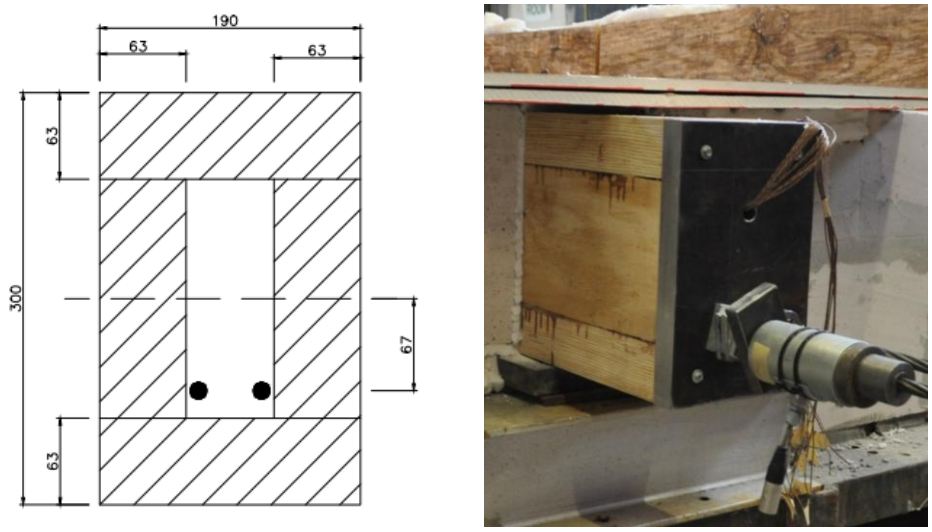

Figure 2-23: Beam C - LVL cross-section (left). Photo of completed beam showing post-tensioning anchorage (right)

2.5.4. Failure Predictions

Predicted failure modes and times to failure for each beam are provided in Table 2-5.

Table 2-5: Failure prediction for full-scale specimens

	Predicted Failure Mechanism	Predicted Time of Failure
Beam A	Shear failure in bottom corner	61 Minutes
Beam B	Mid-span combined bending and compression Failure	37 Minutes
Beam C	End of beam combined bending and compression Failure	53 Minutes

2.5.5. Anchorages protection tests

Anchorage protection methods were tested on 1.5m centrally post-tensioned members which were placed in the furnace surrounding the main test beams. These beams resisted no loads other than the compression due to post-tensioning.

Anchorage members were 200mm by 225mm as shown in Figure 2-24. The timber beams used 90mm thick LVL flanges and webs. This allowed for a 20mm by 45mm cavity in the centre to allow the post-tensioning tendon to pass through.

The anchorages consisted of 20mm thick steel plates of 150mm by 160mm. The plates are held on by friction after the post-tensioning, but for ease of construction the plates were held in place with four 40mm long, 16 gauge, Type 17, screws.

It should be noted that the anchorage protection details were not specifically designed to perform for a specific time when exposed to the standard fire. The protections used were in most cases the requirements to achieve a 60-minute generic rating based on the manufacturer's recommendations. As such the protection was not specifically designed for this application and the design level of each protection method will be different and should not be compared to one another, but rather only to the unprotected anchorages. These tests were a demonstration of the protection methods and not an in-depth investigation into their performance. Figure 2-24 presents an unprotected anchorage.

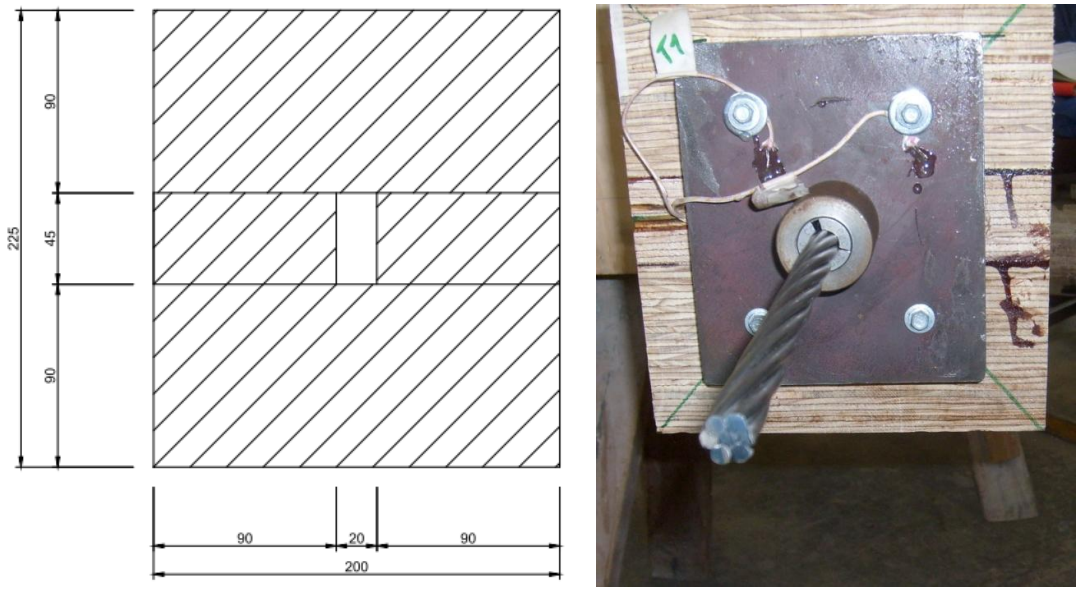

Figure 2-24: Anchorage member cross-section (left), unprotected anchorage (right)

Unprotected

The unprotected anchorage was fully exposed to the furnace to provide a control for the other protection methods. The thermal mass of the steel plate is what slows the temperature rise in the tendon. A photograph of the unprotected anchorage is shown in the right of Figure 2-24. A section elevation of the anchorage member is shown in Figure 2-25.

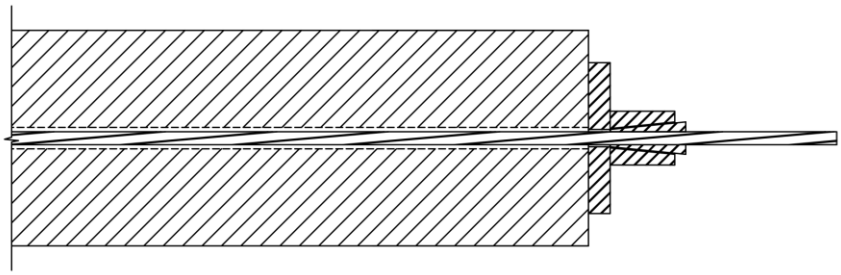

Figure 2-25: Unprotected post-tensioning anchorage longitudinal section drawing.

GIB Fyreline™

The GIB protected anchorage used two layers of 13mm thick Fyreline GIB board. The GIB board was constructed as a box around the anchorage and protruding tendon. Small lengths of timber were used to provide structural support at the end of the GIB box and small amounts of fire resistant mastic were used to close gaps along the edges of the GIB board. A cross-section drawing is shown in Figure 2-26, and the anchorage in shown in place is presented in Figure 2-27.

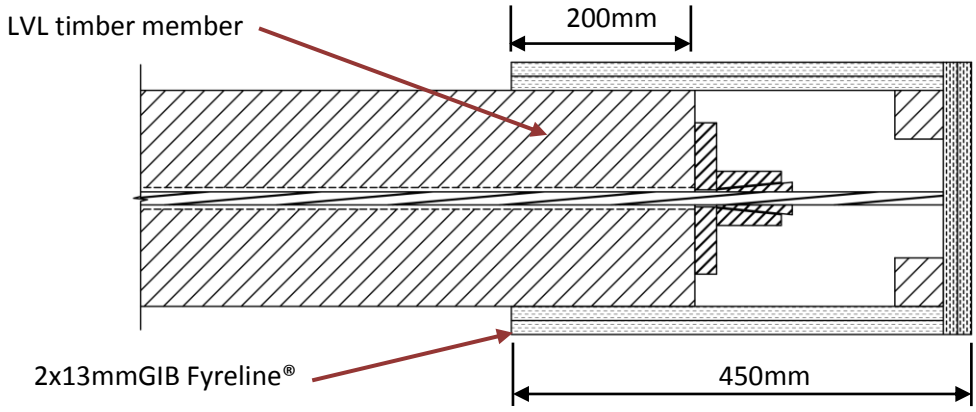

Figure 2-26: GIB board protection for post-tensioning anchorage longitudinal section drawing.

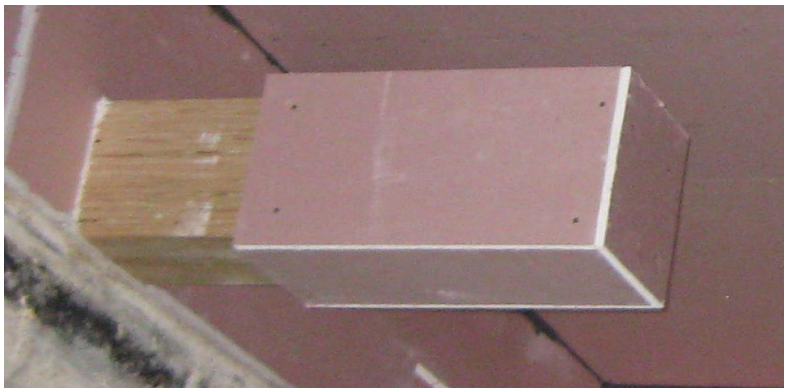

Figure 2-27: Photograph of GIB protected and timber protected post-tensioning anchorages.

Kaowool

The Kaowool protected anchorage utilised one 20mm thick layer of Kaowool held in place with steel wire. Masking tape was used to hold the blanket in place while the wire was positioned. It was expected that the masking tape would burn away quickly and not affect the Kaowool or the anchorage. The Kaowool was stapled onto the timber around the steel plate. This was to ensure that the steel plate was well protected. A section drawing of the Kaowool protected anchorage is shown in Figure 2-28 and a photograph of one of the Kaowool protected anchorages tested is shown in Figure 2-29.

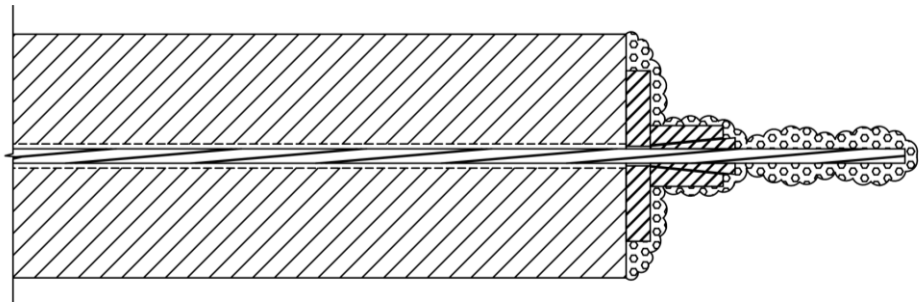

Figure 2-28: Kaowool protected post-tensioning anchorage longitudinal section drawing.

Figure 2-29: Kaowool protected post-tensioning anchorage.

Intumescent

The intumescent paint protected anchorage used a 1mm layer of intumescent paint (Figure 2-30), which was a generic manufacturer recommendation for 60 minutes of fire resistance. It was not expected that the intumescent paint would protect the anchorage for 60 minutes due to the expectation of the anchorage to lose its post-tensioning force at relatively low temperatures. The steel work had a primer under coat applied to it before the intumescent. Three brushed layers of intumescent paint were applied to reach the desired thickness of 1mm. The intumescent paint was then sealed with a coat of clear acrylic paint. This process was recommended by the manufacturer for best results.

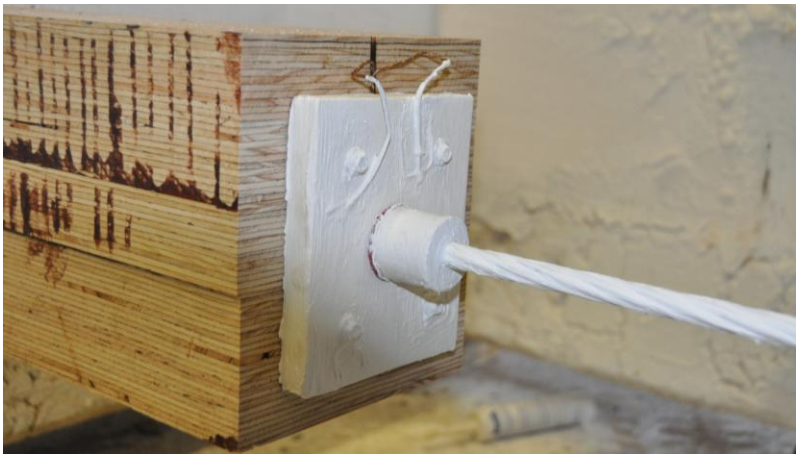

Figure 2-30: Intumescent paint protected post-tensioning anchorage.

Timber

The timber protected anchorage was encased in a cap made from 63mm thick LVL as shown in Figure 2-31 and Figure 2-32. The cap was professionally manufactured using resorcinol glue and 63mm LVL and secured to the beam using fire resistant mastic to seal gaps and timber screws to provide a mechanical connection.

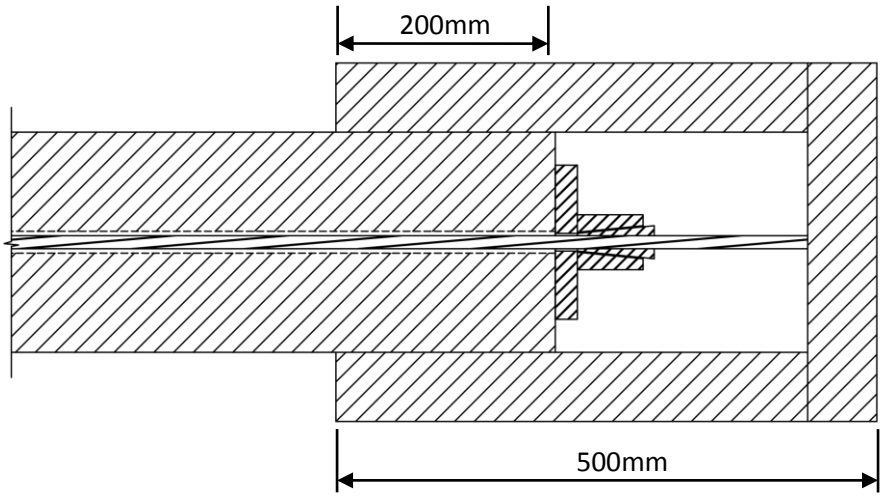

Figure 2-31: LVL timber protected post-tensioning anchorage, longitudinal section.

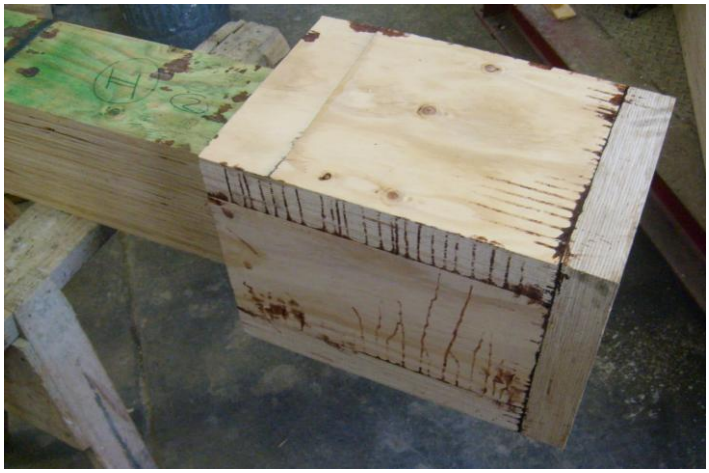

Figure 2-32: LVL timber protected post-tensioning anchorage.

2.6. Full-Scale furnace test results

2.6.1. Furnace Temperatures and Loading

Each beam was exposed to a standard ISO834 fire (The International Organization for Standardization ISO, 1999). The furnace temperature stayed within the tolerances set in the ISO standard, straying above the upper bound briefly at 27 minutes during the Beam A test and straying just outside the bounds during the first 2 minutes of each test. The Furnace temperatures and the ISO834 temperatures are presented in Figure 2-33 to Figure 2-35.

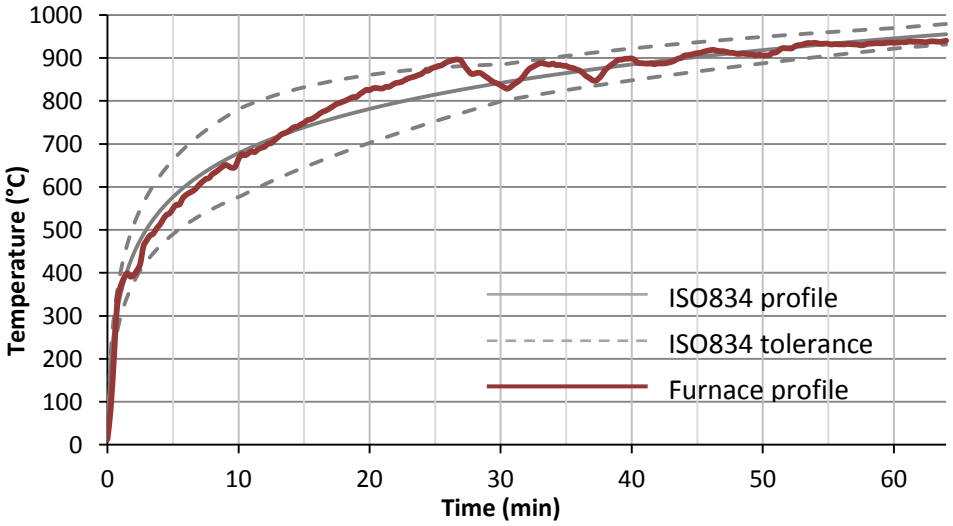

Figure 2-33: Exposed temperatures for Beam A, compared to the ISO834 fire curve, and prescribed tolerances.

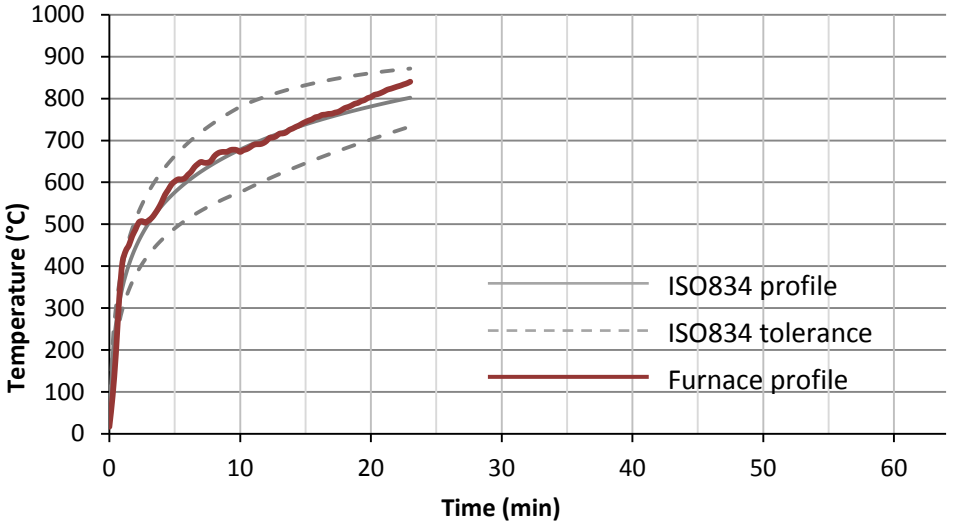

Figure 2-34: Exposed temperature for Beam B, compared to ISO834 fire curve, and prescribed tolerances

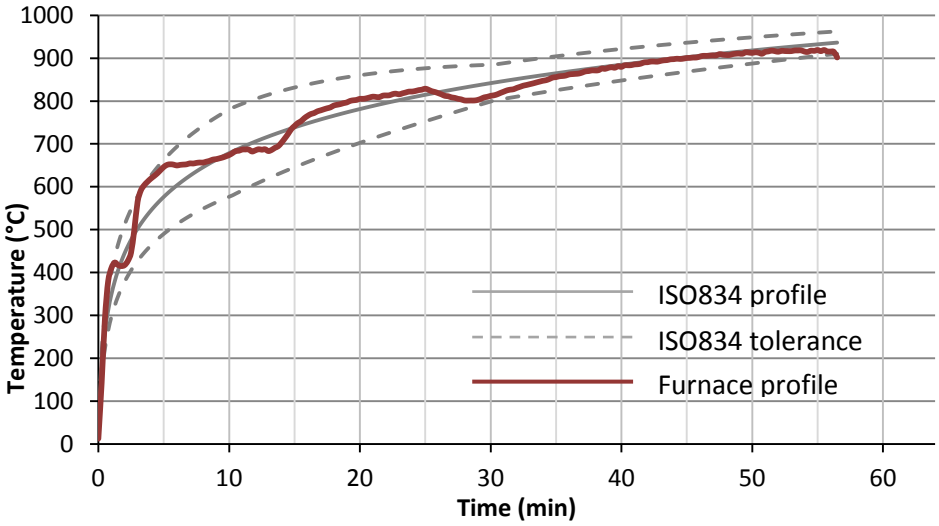

Figure 2-35: Exposed temperatures for Beam C, compared to the ISO834 fire curve, and prescribed tolerances.

The load applied to each beam was set at 40kN, while the actual loading varied between 36 kN and 39 kN. Early during the Beam A test the load remained relatively constant near 38kN. Towards the end of the Beam A test the rate of deflection started to increase noticeably, during this time the applied loading varied more than earlier in the test. During the Beam B test the load was comparatively more variable; this was likely due to the comparatively higher deflections during this test. During the Beam C test again the load remained relatively constant during the first 35 minutes of the test and became more variable as deflections increased approaching failure.

2.6.2. Displacements

During the Beam A test the deflections remained in the order of 0.5mm-1mm for the first 45 minutes of the test. Beyond this the deflections started to increase steadily until approximately 64 minutes where runaway deflections occurred. The deflections measured during each test are presented in Figure 2-36.

During the Beam B test deflections increased at an approximately constant rate for 15 minutes. After this the rate increased slightly until failure. The failure mechanism which occurred during this test was different and much earlier than predicted. The top flange suddenly became disconnected from the rest of the beam. The deflection profile reflects the flexible nature of this beam showing deflections increasing quickly, early in the test.

The deflection profile during the Beam C test was similar to the Beam A test. However because of the beam being more flexible due to its geometry, deflections were greater. The deflections increased approximately linearly for the first 40 minutes of the test. The rate of deflection then increased over the last 16 minutes of the test. At 56 minutes and approximately 30mm of deflection the beam failed.

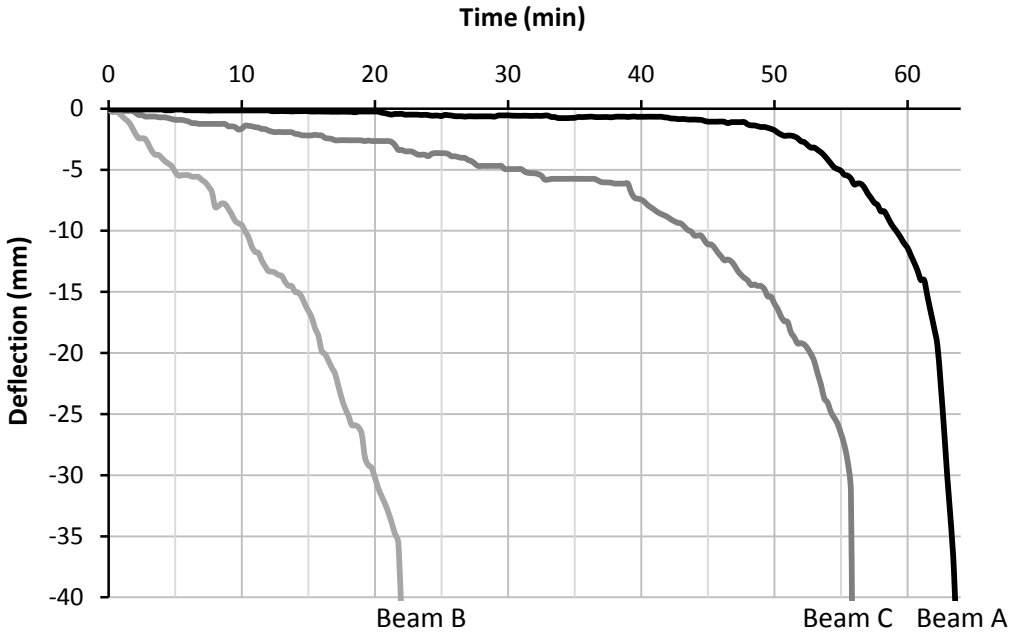

Figure 2-36: Vertical deflections of the main test beams during standard fire exposure.

2.6.3. Temperatures

Beam A: timber temperature- time distribution

During exposure to the ISO834 fire the temperature profiles of the timber close to the surface followed the random variations in the furnace temperature. Further into the section these fluctuations became less evident and the curves became smoother.

Deeper than 17mm into the section the temperatures approached 100 °C slowly, and once 100°C was reached, heated more quickly. This effect was less evident near the surface where the rate of temperature rise was comparatively higher. This effect was most likely due to moisture evaporation and migration in the timber.

There were small differences in temperature distribution between the flanges of the beam and the web of the beam. The flange heated slightly more quickly than the web. Two possible explanations for this effect are that the flange partially shielded the webs from some of the furnace and therefore received more radiation, or possibly the width of the beam was small enough that two dimensional heat transfer served to increase the temperature more quickly.

The temperature of the inside faces of the LVL did not appreciably rise beyond 100°C whilst the beam was still intact. Temperature distributions for the web and the flange of Beam A are presented in Figure 2-37 and Figure 2-38 respectively.

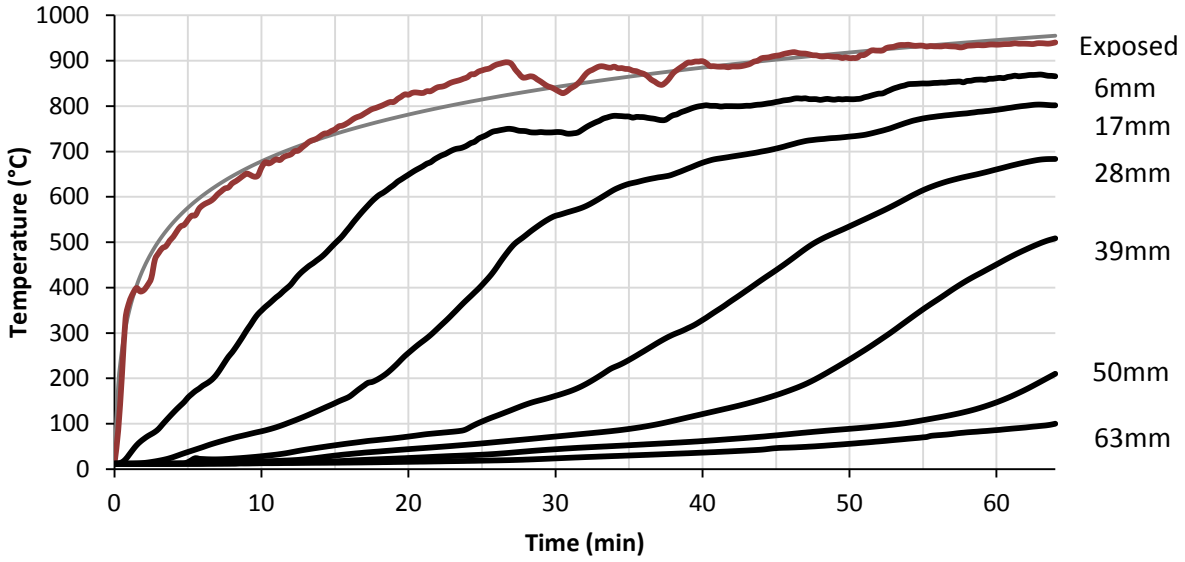

Figure 2-37: LVL temperature distribution in web of Beam A. Temperatures are presented for various depths below the LVL original outer surface.

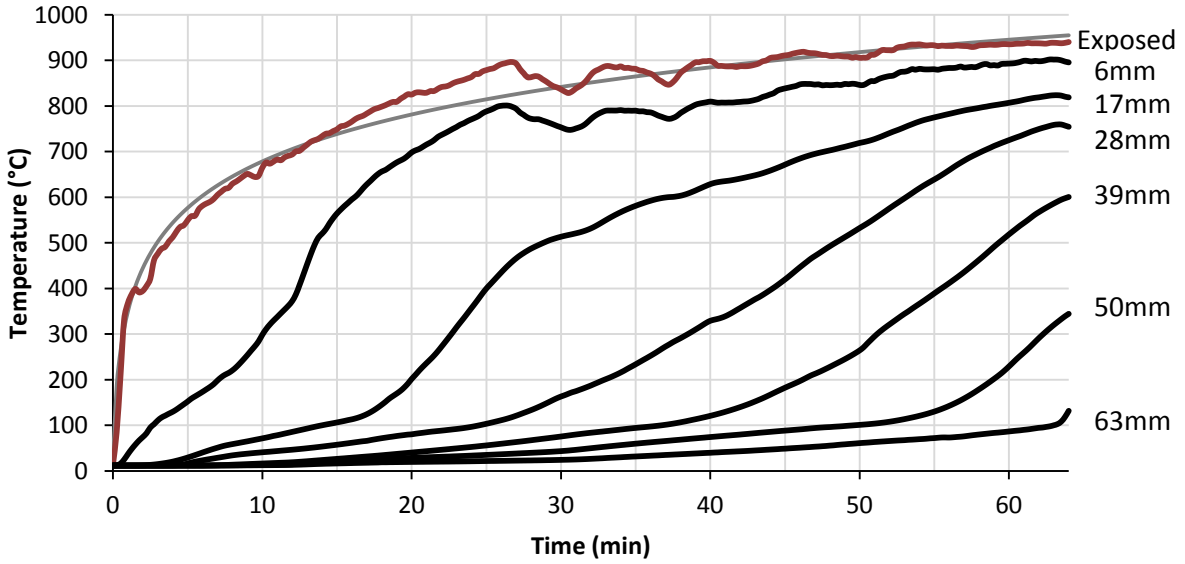

Figure 2-38: LVL temperature distribution in bottom flange of Beam A

Beam B: timber temperature- time distribution

The LVL in beam B heated in a similar manner to beam A. Due to the short duration of the test less data was obtained. Again the measurements close to the surface of the timber exhibit fluctuations similar to the furnace temperature. Deeper in the section much of the timber did not reach temperatures above 80°C. The two measurement points that did reach above 80°C grew slowly in temperature until 100°C where the rate of temperature rise increased. At approximately 600 °C the rate of temperature rise decreased again. The difference in temperature profiles between the flange and the web was almost indistinguishable. This diminished effect could be due to the shallow depth of penetration achieved by the short test duration.

During this test the internal timber surface temperatures did not reach above 25°C, until there was an integrity failure in the timber enclosing the cavity. When this happened hot gasses were forced

into the cavity heating up the internal surfaces. Temperature distributions for the web and bottom flange of Beam B are presented in Figure 2-39 and Figure 2-40 respectively.

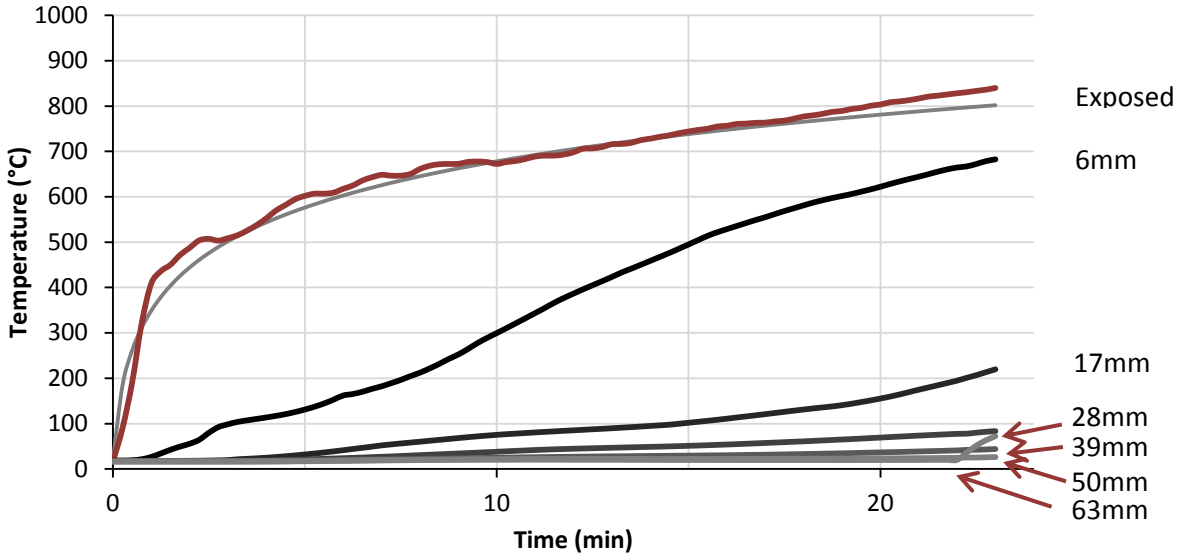

Figure 2-39: LVL temperature distribution in web of Beam B. (24 minute duration only)

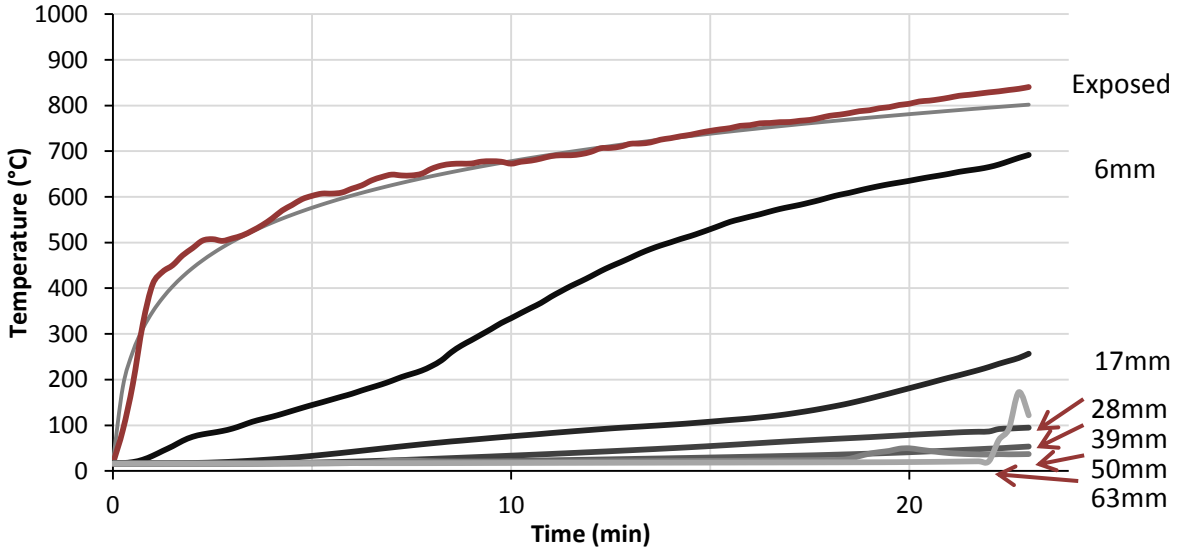

Figure 2-40: LVL temperature distribution in bottom flange of Beam B. (24 minute duration only)

Beam C: timber temperature- time distribution

The thermal wave through the timber for the Beam C test shows very similar features to that of the Beam A test, although temperatures reached within the section were not as hot compared to the Beam A test. At 50 minutes the thermocouple at 39mm depth reached only 100°C where as in the Beam A test that thermocouple reached approximately 250 °C at 50 minutes. This is likely due to random variations in timber density, moisture content, and furnace temperature; however, the size of the beam cavity and overall size of the beam may also have had an effect.

Again, at thermocouples deeper than 17mm, temperature slowly grew until 100 °C and then the rate of temperature rise increased. The 6mm deep thermocouple did not show this effect. The rate of temperature rise at all depths started to decrease at approximately 600 °C.

Near the surface there was some difference between the flange and the web heating profile. The 6mm thermocouple at 20 minutes reached 480°C in the web where as it reached 600°C in the bottom flange. Again this was likely due to the bottom flange receiving more radiation than the webs. The bottom flange was exposed to the entire furnace while the webs were only exposed to the half of the furnace they were facing towards.

The inside surfaces of the timber did not rise appreciably above 50°C. This value was slightly lower than observed during the Beam A test. However as noted above the timber did heat more slowly overall during the Beam C test. Temperature distributions for the web and the flange of Beam C are presented in Figure 2-41 and Figure 2-42 respectively.

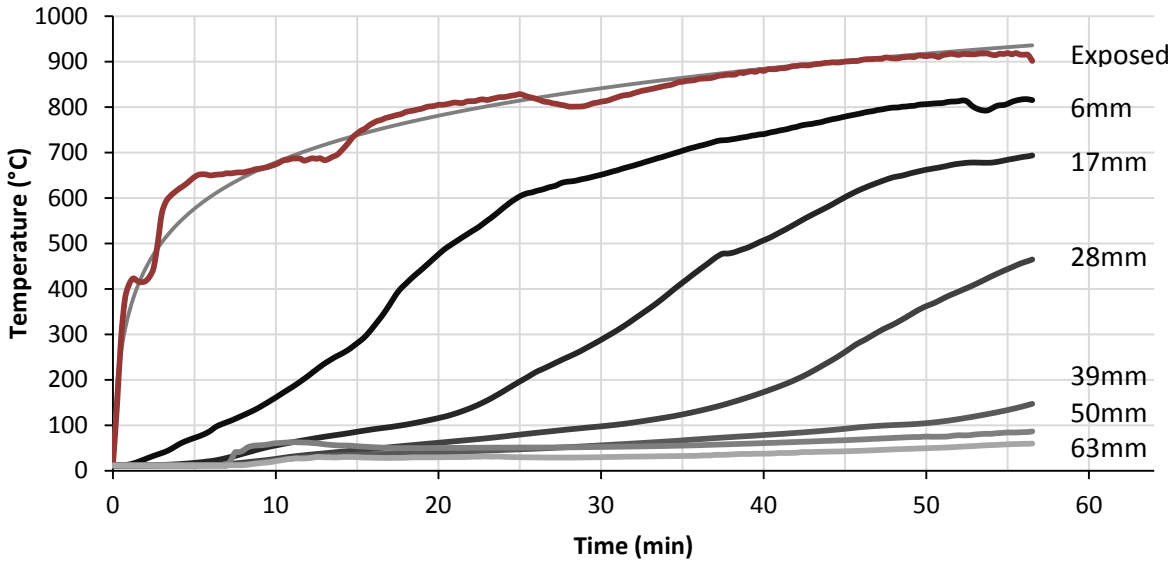

Figure 2-41: LVL temperature distribution in web of Beam C.

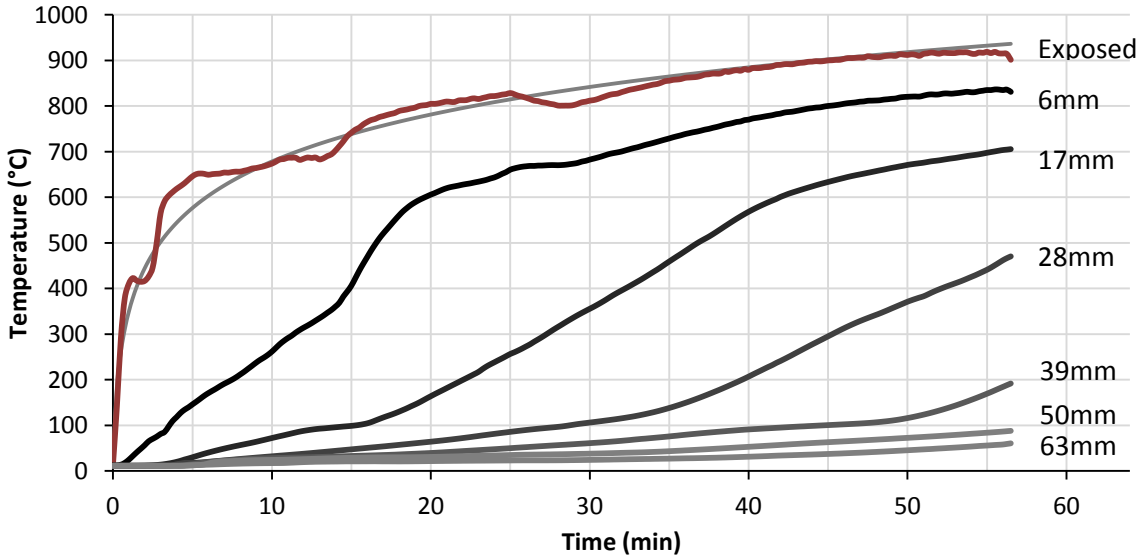

Figure 2-42: LVL temperature distribution in bottom flange of Beam C.

2.6.4. Tendon temperatures compared to internal timber surface temperatures.

As the timber sections were burnt the inside faces of the section became warmer. The tendon within the cavity also rose in temperature. In the Beam A experiment neither the tendon nor the interior

timber surfaces became hotter than 100°C during most of the test. The timber surfaces reached 100°C at 64 minutes just before failure where the tendon only reached 75°C.

The tendon temperature lagged behind the timber temperature as expected. After 45 minutes the timber was approximately 25-30 °C hotter than the tendon. However the tendon temperature may have slowly caught up with the timber temperature if the test progressed longer than 64 minutes. The temperature of the internal surface and the tendon are presented in Figure 2-43.

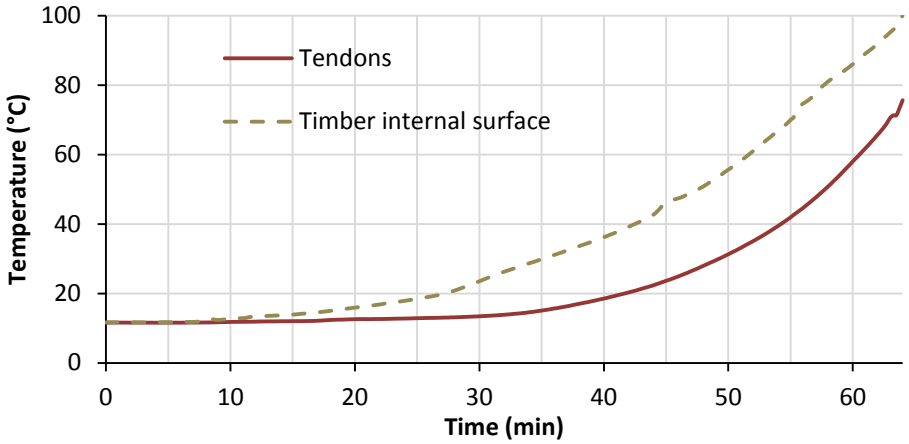

Figure 2-43: Average temperature of the post-tensioning tendon and the internal surface of the cavity in Beam A. Internal surface profile presented as recorded in the lower corner of the cavity.

During the Beam B experiment the temperature of both the inside surfaces and the tendon remained below 22 °C whilst the beam was intact. Once the beam's integrity failed the temperatures increased beyond 100°C very quickly. The temperatures of the tendon and the timber surfaces stayed within 5°C of one another. The temperatures of both the inside surfaces and the tendons are presented in Figure 2-44.

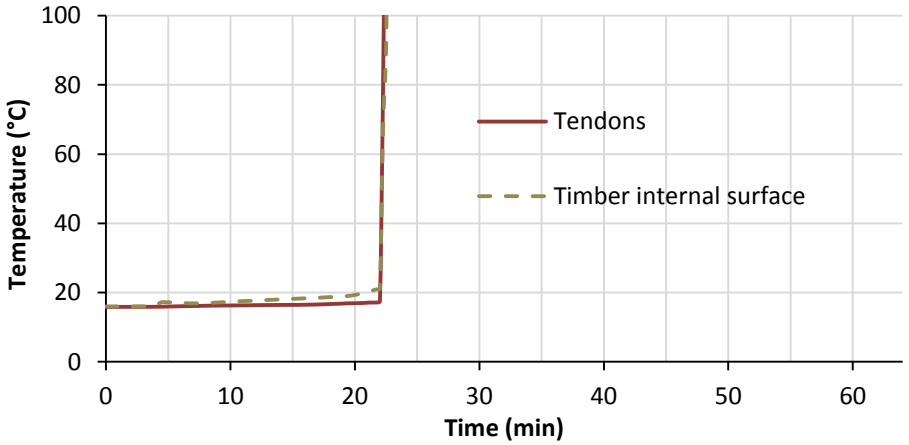

Figure 2-44: Average temperature of the post-tensioning tendon and the internal surface of the cavity in Beam B. Internal surface profile presented as recorded in the lower corner of the cavity.

During the Beam B test the internal surface temperature remained under 60°C and the tendon temperature remained under 45°C for the duration of testing. At 9 minutes the temperature of the thermocouple on the internal surface raised from ambient temperature of 12°C to approximately 30°C over 5 minutes. From then the temperature raised slowly in a similar manner to the Beam A

test. Again the tendon lagged behind the timber surface by approximately 20°C. The temperature profiles of both the inside surfaces and the tendon are presented in Figure 2-45.

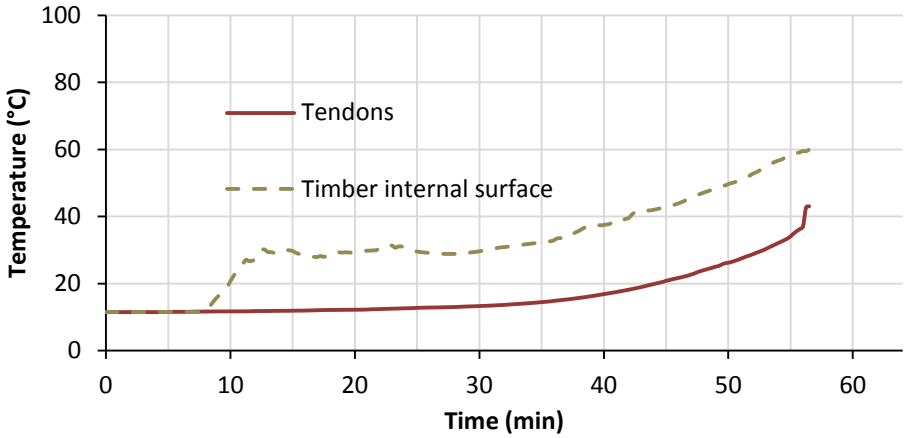

Figure 2-45: Average temperature of the post-tensioning tendon and the internal surface of the cavity in Beam C. Internal surface profile presented as recorded in the lower corner of the cavity.

The effect of tendon position within the cavity and tendon temperatures.

The position of the tendon within the cavity showed little effect on its temperature. The positions, near the bottom flange, near the web and near the centre of the cavity, showed a maximum temperature difference of 2 °C. The temperature profiles for the tendon at various positions are presented in Figure 2-46.

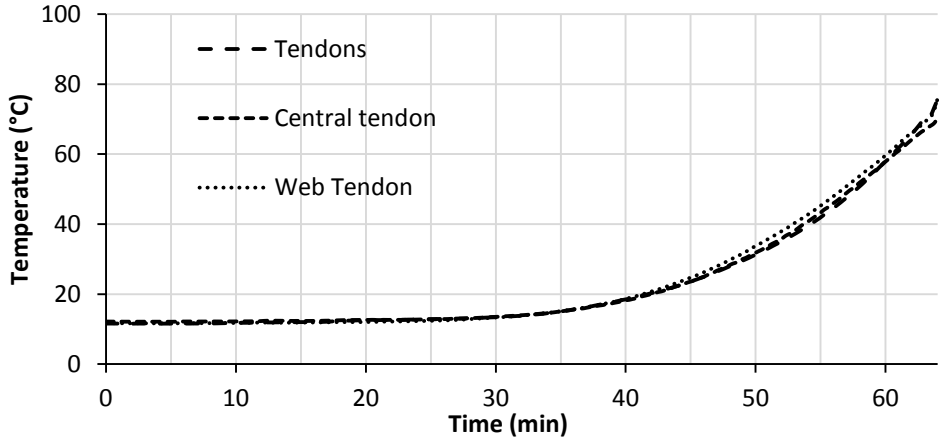

Figure 2-46: Temperature profiles for different tendon positions.

2.6.5. Tendon post-tension force and relaxation

Over the course of each test the post-tensioning force decreased with time. The causes of these decreases were most likely due to heating of the tendons and their subsequent thermal expansion and loss of stiffness, and also the loss of timber cross section resulting in less overall compressive stiffness of the LVL beam. Whilst the tendon forces decreased with increased tendon temperatures, there were other losses in stress which the increase in temperature alone does not account for; this is discussed further in Chapters 3 and 4.

During the Beam A test at 60 minutes the tendons had lost approximately 25% of the initial applied stress. At this time the tendon temperatures were approximately 58°C. Before 30 minutes of fire

exposure both the temperature and post-tensioning force were only negligibly affected by the fire, as shown in Figure 2-47.

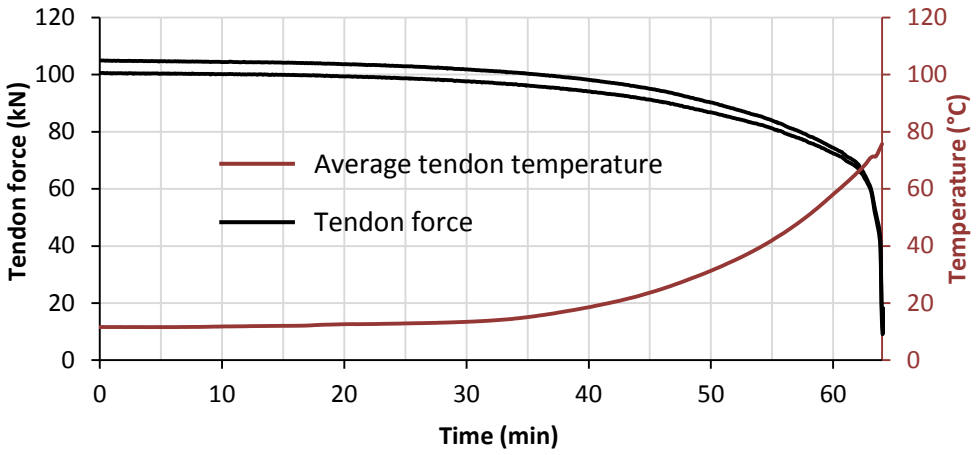

Figure 2-47: Tendon post-tensioning forces and tendon temperatures during standard fire exposure of Beam A.

During the Beam B test the post-tensioning lost most of their load suddenly at 21 minutes. Before this occurred the tendons had lost only 4.5% of their original load and had increased in temperature by 2.5°C. The post-tensioning force of each tendon and their average temperature is presented in Figure 2-48.

The post-tensioning load was lost one to two minutes before the tendon temperatures started to increase in temperature quickly. It is possible that this difference in time was due to a timing error in the two separate data acquisition systems. However the time difference may be due to the failure mechanism. All the data collected on the BRANZ data acquisition system showed a jump or sharp change in gradient at approximately the same time. As the BRANZ temperature data was being captured according to the same clock used to operate and control the experiment, those results reflect the failure time more accurately.

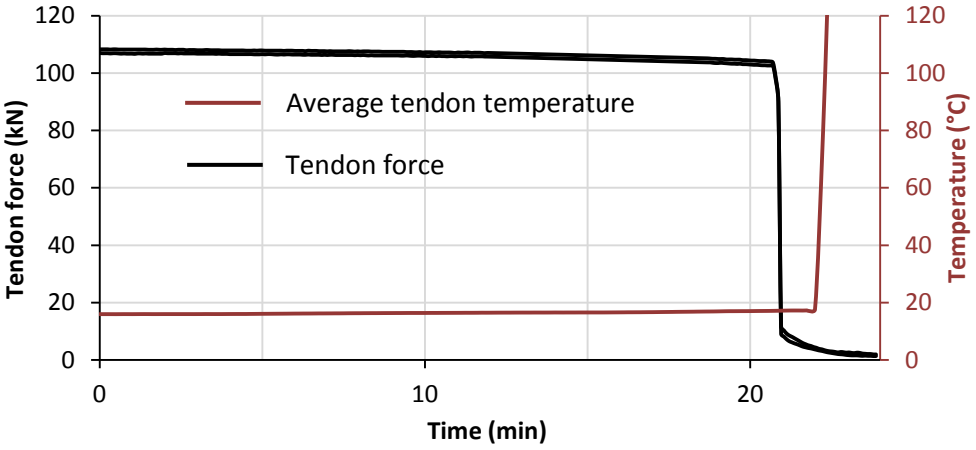

Figure 2-48: Tendon post-tensioning forces and tendon temperature during standard fire exposure of Beam B.

During the Beam C test the post-tensioning load slowly relaxed until a runaway loss of load occurred at approximately 56 minutes. At 40 minutes duration the tendons had only lost 6% of their initial load. Just before the runaway loss of load at 55 minutes the tendon temperatures had reached 33°C

and had lost 17% of their initial load. The post-tensioning force of each tendon and their average temperature are presented in Figure 2-49.

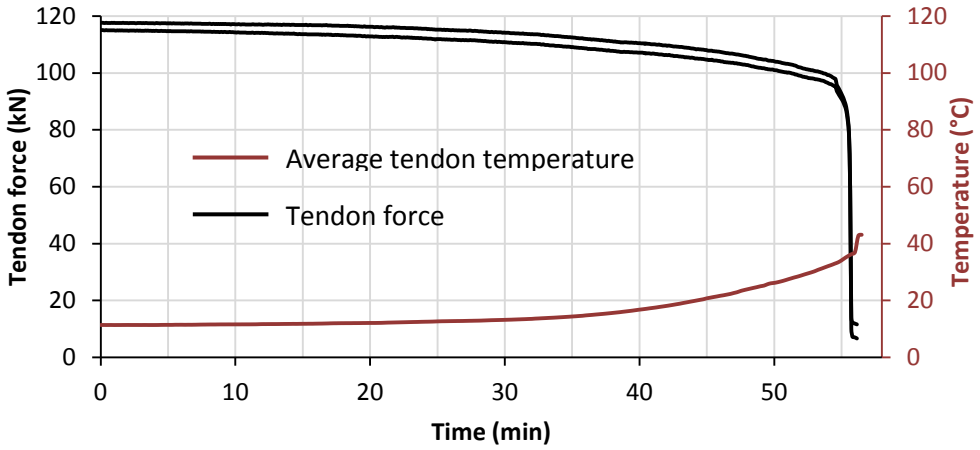

Figure 2-49: Tendon post-tensioning forces and tendon temperatures during standard fire exposure of Beam C.

2.6.6. Char rates and depths

Due to the time involved with removing the loading frame, the beams continued to burn in the furnace for approximately 5-10 minutes before they are able to be lifted off and cooled down. The furnace was turned off and no air or fuel flowed through the inlets, but the timber was still hot and continued to burn and char. However, the exposed temperature over the extra time was lower than the temperature in the furnace during the test, which means the charring may have progressed at a slower rate over this time. In order to estimate the effect of this extra time it has been assumed that the charring during that time was equivalent to 2 minutes at the assumed char rate. Therefore 2 minutes have been added to the char time which has been used to calculate the charring rates.

It would be useful to be able to continue measuring the timber temperatures during this end of test time. However this is difficult in reality as the thermocouple cables needed to be cut in order to lift the specimen of the furnace to a position where it can be cooled.

The calculated charring rates were very close to the manufacturer's stated char rate. It was expected that random temperature variations during the test and in the timber material used would lead to a final char rate that varied from the published rate more. These char rates are sensitive to the above assumption and arbitrary addition of 2 minutes to the charring time. It is possible to include a greater additional effective charring time however, 2 minutes is an estimate which produces conservative charring rates.

An estimated error can be calculated for the char rates. The depth measurements were accurate to ±1mm and the time is assumed to be accurate to approximately ±2 min. This inaccuracy in time was again due to the extra charring that occurred after the test had ended. The char depth measurement inaccuracy was due to both the lack of definition between charred and un-charred timber and the random variation in depth across the surface of the timber. The error in the char rates for the longer tests; Beam A, Beam C, and anchorage members, were between 5% and 6%. Whereas for the Beam B test, which was substantially shorter, the char rate error was between 13% and 14%.The overall error was calculated as the sum of the relative errors of the charring time and the char depth. Because the Beam B test was much shorter and the char depth much smaller, the percentage of the

error was much larger than for the longer tests. The char rates measured during the test are presented in Table 2-6 and char rates calculated from the 300°C isotherm are presented in Table 2-7. Also presented is the effective charring time and char depth measured which were used to calculate the charring rate.

Table 2-6: Char rate results as measured from test specimens.

	Char time (min)	Char Depth (mm)	Charring rate (mm/min)	Corner radius (mm)
Beam A	66	47.5	0.72	20-25
Beam B	25	18	0.72	20
Beam C	58	40	0.69	30
Anchorage members	58	42	0.72	30

Table 2-7: Char rates results as calculated from the 300°C isotherm.

	Char Depth (mm)	Char Rate (mm/min)	Error (mm/min)
Beam A	39	0.74	0.11
Beam B	6	0.61	0.20
Beam C	28	0.61	0.08

Corner rounding was also measured. This was difficult to measure because the rounding was not completely circular and its radii were open to interpretation based on where measurements are taken. It was simpler and more accurate to scale the corner radii from digital images by fitting a circle to the corner profile. An example of the circles fitted to the corner profile is presented in Figure 2-50.

Figure 2-50: Corner rounding radius fitting example

2.6.7. Failure Shapes and Mechanisms

Beam A

Due to the extra time Beam A was on the furnace before it could be cooled down, and the integrity failure of the beam, a large portion of one end of the beam burnt through. On the remaining half two cracks or splits were visible in one of the webs. One split ran along the bottom corner of the beam where a shear failure was predicted. The other crack was higher in the web approximately 30-50mm below the top flange. Figure 2-51 shows the failure shape of Beam A in an un-deflected state. Figure 2-51 to Figure 2-53 show Beam A following failure and removal from the furnace.

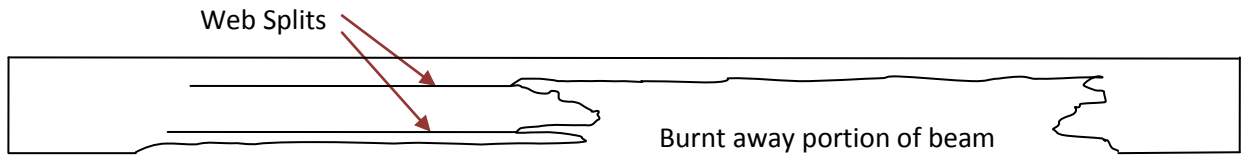

Figure 2-51: Failure shape of Beam A following removal from the furnace.

Figure 2-52: Residual timber of Beam A following removal from the furnace.

Figure 2-53: Beam A shortly after being lifted from furnace (left), Splits in web of Beam A (right)

Beam B

Beam B failed unexpectedly early. The top flange became detached from the webs along most of the beam. One end of the beam remained intact whereas, at the other end, the flange detached all the way to the anchorage. The bottom section of the beam formed a channel which crushed near the centre of the beam due to the post-tensioning compression and the compression due to bending. This formed a plastic hinge in the centre of the beam leaving only the flexible top flange intact which was unable to resist the applied load causing the beam to fail. This plastic hinge exhibited localized buckling in the web forcing the webs outward. Figure 2-54 to Figure 2-57 show Beam B after failure.

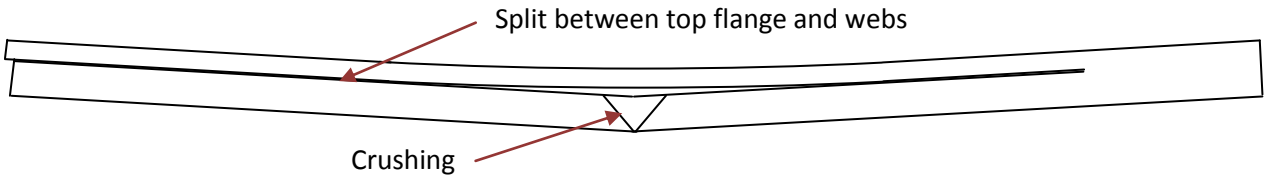

Figure 2-54: Failure shape for Beam B

Figure 2-55: Each end of Beam B shortly after failure. Top flange split from web (left) Intact beam end (right).

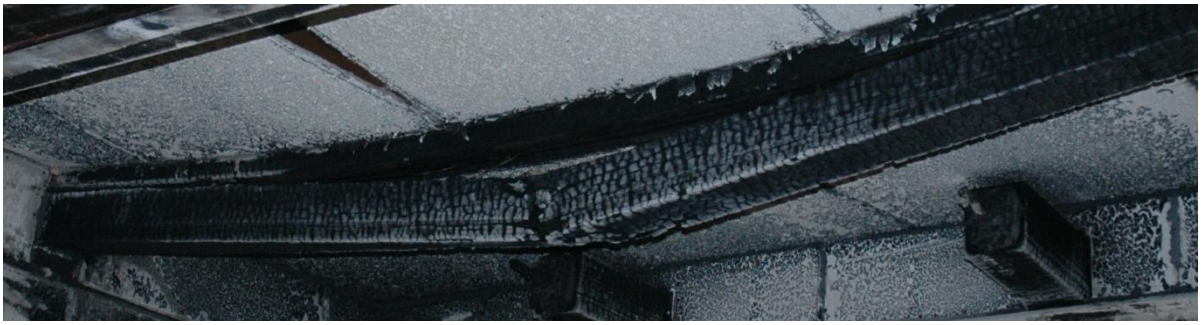

Figure 2-56: Beam B shortly after failure and removal from the furnace.

Figure 2-57: Crushed area in the centre of the Beam B looking down at the top of one of the webs at mid-span.

Beam C

Beam C failed in bending in a similar way to Beam B. Under one of the loading points a plastic hinge formed in the bottom channel of the section. This was again accompanied by a splitting of the web near the top flange, however during this test the split was far more localized and did not split down the entire length of the beam. This plastic hinge exhibited some localised buckling in the web.

A second plastic hinge formed near the vertical support closest to the bending failure. This point experienced no, or very low, bending moment due to the simply supported loading, however it did experience the maximum bending moment due to the post-tensioning. This plastic hinge formed upside down compared to the mid span failure. Figure 2-58 to Figure 2-61 shows Beam C following failure.

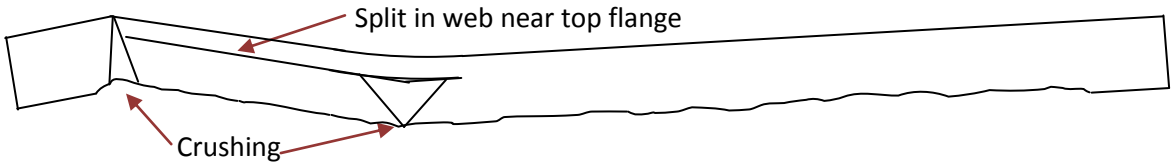

Figure 2-58: Failure shape of Beam C.

Figure 2-59: Beam C showing both plastic hinges and the resulting local buckling.

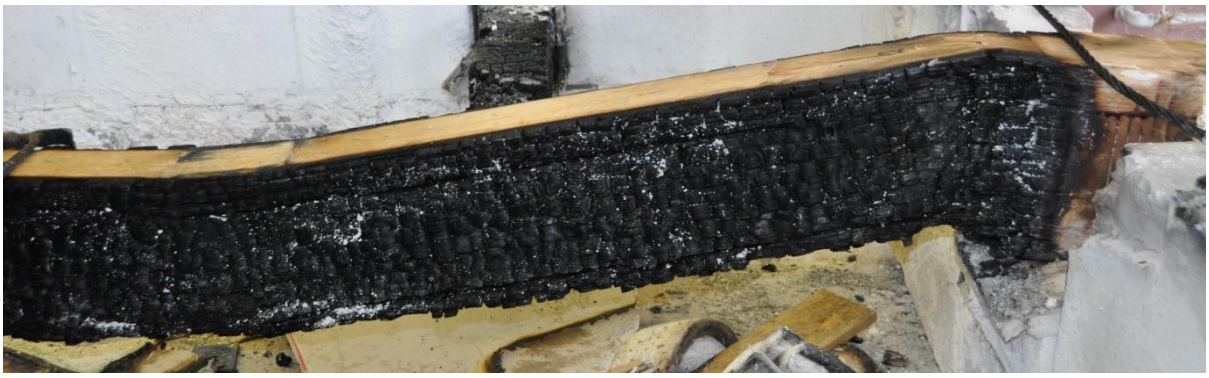

Figure 2-60: Beam C shown from the opposite side of the beam after failure.

Figure 2-61: Beam C: plastic hinge close to vertical support.

2.6.8. Anchorage beams

As previously mentioned these tests were a demonstration of the protection methods and not an in-depth investigation into their performance. The thicknesses and protection details were mostly based on manufacturer recommendations for generic fire resistance ratings and were not specifically designed for this application. As such, the levels of performance were not directly comparable between protection methods. Each method should only be compared to the unprotected anchorage.

Even if poor performance was exhibited here it does not mean that the specific protection method could not be made to work for this application. However it does imply that some care and further investigation should be taken when considering a particular method.

Unprotected anchorages

During the furnace tests the unprotected anchorages heated quickly. The exposed side of the steel plate followed the temperatures within the furnace quite closely. It took between 1 and 3 minutes for the average plate temperature to reach 200°C. The rear side of the plate warmed quickly but at a slower rate than the front of the plate. The tendon temperature near the plate lagged behind the steel plate but still heated quickly. The temperature profile for one of the two unprotected anchorage is shown in Figure 2-62.

The tendons lost 50% of their initial post-tensioning force at approximately 15 minutes. The post-tensioning tendon maintained more than 95% of its initial post-tensioning force for 10 minutes after which the post-tensioning force started to decrease almost linearly. This point corresponds roughly with a temperature of approximately 200°C in the tendon, measured at a point within 50mm of the anchorage plate. The tendon temperature near the anchorage and the remaining post-tensioning force are presented in Figure 2-63.

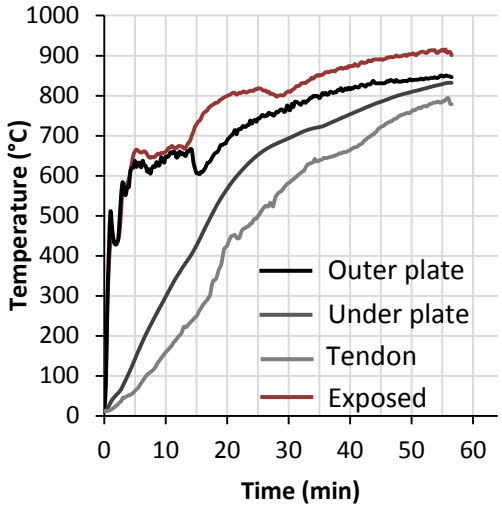

Figure 2-62: Unprotected anchorage temperatures

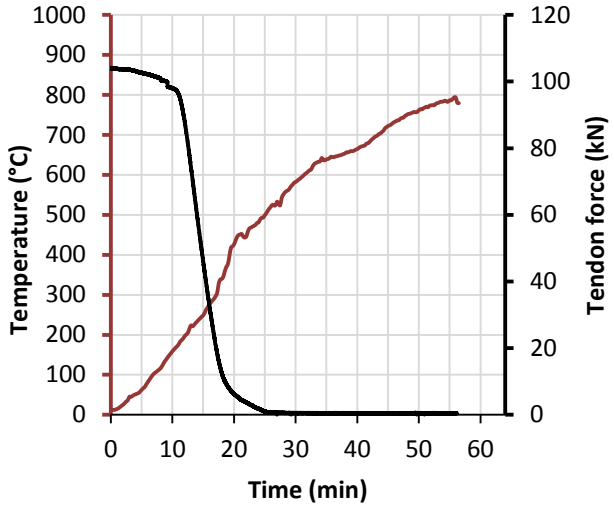

Figure 2-63: Unprotected anchorage, tendon temperature near anchorage and remaining tendon force

Intumescent Protection

The intumescent protected plates heated more slowly that the unprotected anchorages. It took approximately 5 minutes for the average plate temperature to reach 200°C. Again the rear of the plate heated more slowly than the front of the plate. However the temperature differences between front and rear were smaller. This was due to the slower heating rate which allowed more time for the temperature to conduct through the plate. The temperature profile for one of the two intumescent paint protected anchorages is shown in Figure 2-64. The intumescent was seen to activate at approximately 3 minutes which corresponds with a steel plate surface temperature of approximately 100°C to 150 °C.

The tendon again heated more slowly than the steel plate taking between 23 to 25 minutes to reach 200°C. The loss of 50% of the post-tensioning force occurred at approximately the same time as the tendon reached 200°C. The tendon temperature near the anchorage and the remaining post-tensioning force are presented in Figure 2-65.

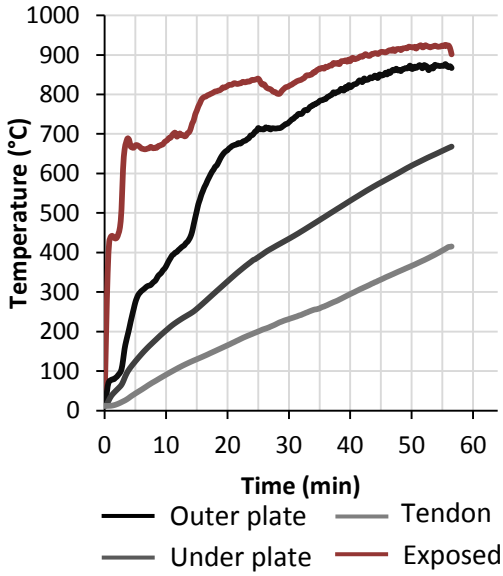

Figure 2-64: Intumescent paint protected anchorage temperatures

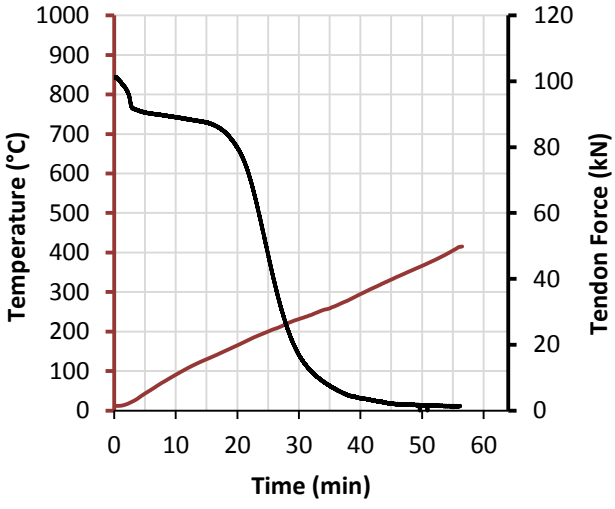

Figure 2-65: Intumescent paint protected anchorage, tendon temperature near anchorage and remaining tendon force

Kaowool blanket Protection

The anchorages protected with Kaowool blankets took between 32 and 37 minutes to reach an average plate temperature of 200°C. There was little difference between temperatures on either side of the plate or of the tendon. For most of the test the difference between temperatures measurements on the anchorage were less than 100°C. Again this was due to the slow rate of heating which allowed temperatures to distribute through the steel. The temperature profile for one of the two Kaowool protected anchorages is shown in Figure 2-66.

The tendon reached a temperature of 200°C between 36 and 40 minutes. However different to the other anchorages presented thus far, the tendon did not drop to 50% of its original force until 63 minutes just before the end of the test. This occurred at a tendon temperature of approximately 350 °C. The post-tensioning force remained above 95% of its original force for approximately 52 minutes. The tendon temperature near the anchorage and the remaining force are presented in Figure 2-67.

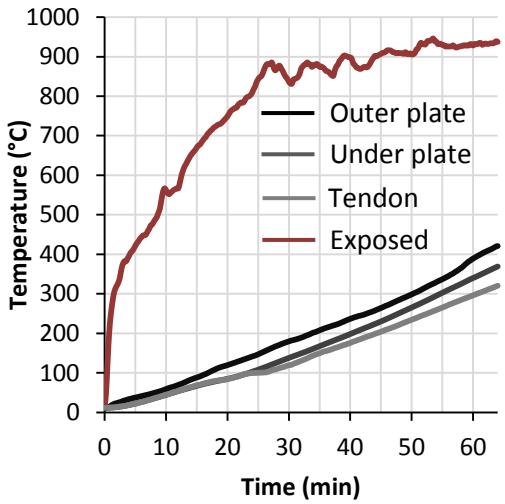

Figure 2-66: Kaowool protected anchorage temperatures

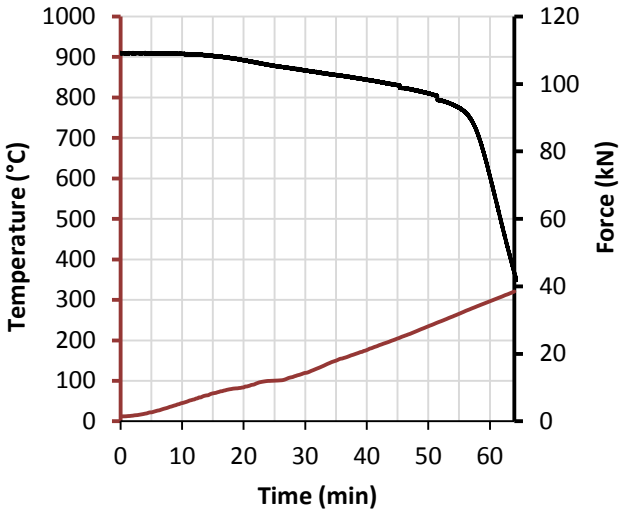

Figure 2-67: Kaowool protected anchorage, tendon temperature near anchorage and remaining tendon force

Timber Protection

The timber-protected anchorages performed well compared to the unprotected anchorages. The temperatures did not rise above 100°C during the 64 minutes of the test. Due to this very slow heating rate the temperatures measured were very similar and differed by less than 5°C. The temperatures stayed close to ambient temperature for approximately 35 minutes where they then started to rise steadily.

In one of the two tests the post-tensioning tendon lost much of its force 2 minutes before the end of the test, as shown in Figure 2-68. This was unexpected as the tendon temperature was still relatively cool. The tendon temperature was only measured near the anchorage; the temperature down the tendon would have been slightly cooler than this measurement. As the tendon length for the anchorage members was only 1.5m long the stiffness was higher than that of the tendons in the longer main beams. This meant the force developed was more sensitive to any movement at the anchorages and thermal strain. The shrinkage of the member, or increased compressive stresses due to the reduction in cross sectional area, may also have been a cause for this loss. The tendon temperature near the anchorage and the remaining post-tensioning force are presented in Figure 2-69.

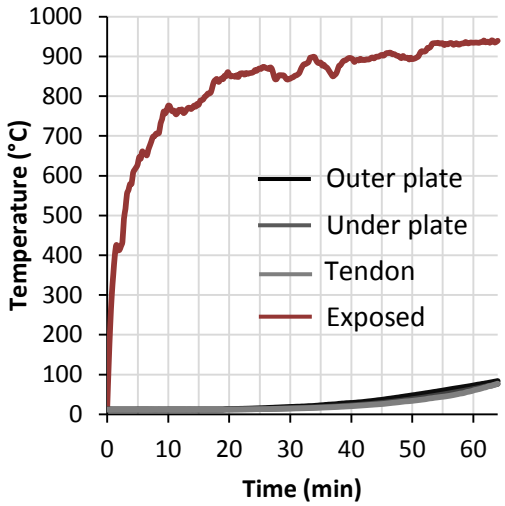

Figure 2-68: LVL Timber protected anchorage temperatures

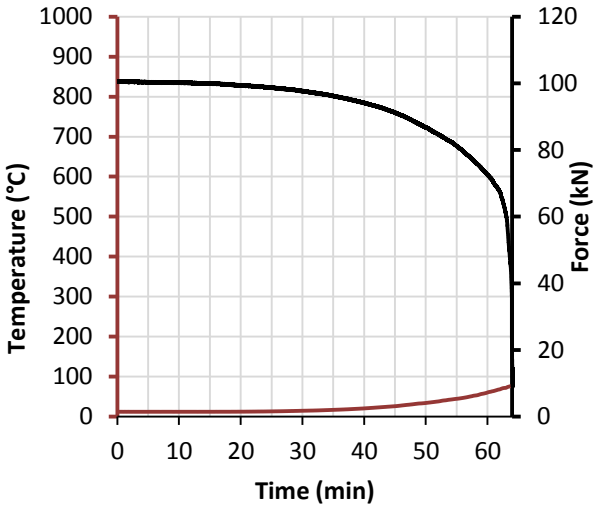

Figure 2-69: LVL Timber protected anchorage, tendon temperature near anchorage and remaining tendon force

GIB Board Protection

The GIB Fyreline protected anchorages performed well during testing keeping temperatures below 200°C and not allowing substantial relaxation of the post-tensioning force. The temperatures of the anchorage quickly warmed to 100°C and remained there for most of the test. At approximately 55 minutes the temperatures started to increase again. During the entire test temperatures did not exceed 200°C. In neither of the GIB board protected tests did the post-tensioning force drop below 85% of the original load during the test. The anchorage temperature profile and the remaining post-tensioning force are presented in Figure 2-70 and Figure 2-71 respectively.

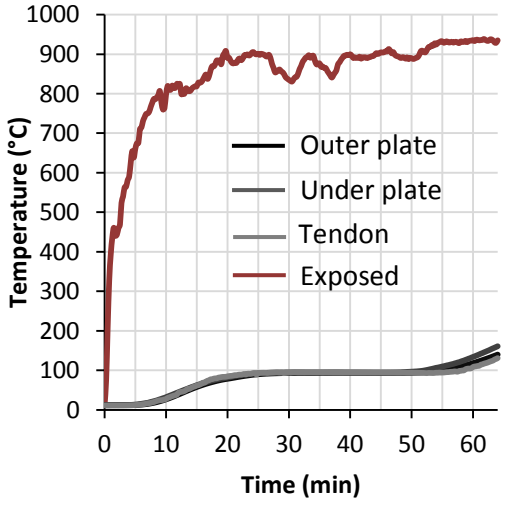

Figure 2-70: GIB Fyreline protected anchorage temperatures

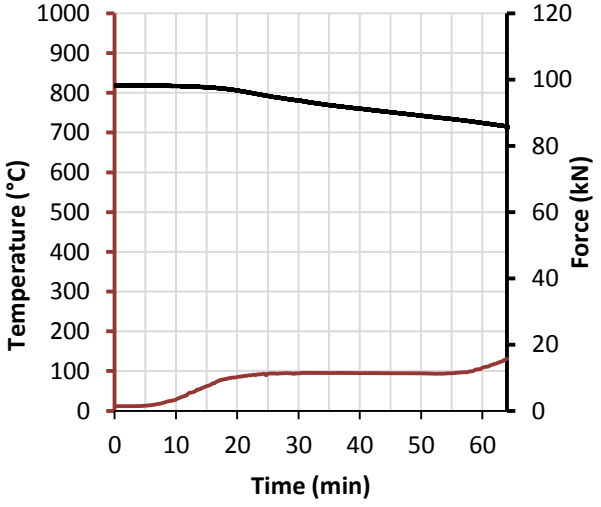

Figure 2-71: GIB Fyreline protected anchorage, tendon temperature near anchorage and remaining tendon force

2.7. Discussion

2.7.1. Failure mechanisms

Unfortunately some of the failure mechanisms exhibited in the test specimens were complex and differed from what was expected. The shear failure in the bottom corner of Beam A was very close to what was expected. However, both bending failures in Beams B and C occurred in an unexpected way.

Shear failure in bottom corner

The shear failure in the bottom corner was expected to split in shear along the beam in the bottom corner. It was also expected that a second shear crack may form higher in the webs closer to the centroidal axis. This was very close to what occurred. Clearly visible on the beam were; a split along the bottom corners, and a split along the web of the beam a short distance below the top flange. Unfortunately due to the extra time the beam was on the furnace to allow for the removal of the loading frame and test specimen a large portion of the beam was burnt away before the beam could be inspected.

The split at the bottom corner was expected to be due to shear forces within the beam reaching a level where the residual cross section was unable to resist them. The bottom corner was important as the geometry of the beam would most likely result in the thinnest portion of the beam occurring there. This is due to the corner rounding which was assumed to continue regardless of the cavity in the beam. Figure 2-72 demonstrates how after charring, the corner thickness could be much smaller than the web or flange thickness.

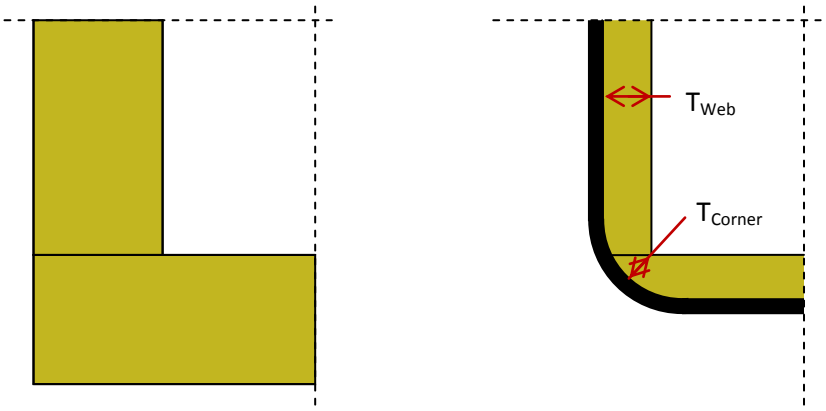

Figure 2-72: Corner rounding and timber thickness, before charring (left), and after charring (right)

The second split near to the neutral axis was expected because during analysis the shear capacity in the web was nearing the demand shortly after corner failure was predicted. When the corner splits, internal stresses have to redistribute in an attempt to continue carrying the load. This was likely to be higher than the web could resist which caused it to fail in shear also.

There was a possibility that the remaining section of the beam, depicted in Figure 2-73, would fail in some other manner. Perhaps the channel which would be formed by the top of the beam would crush and form a plastic hinge. This was not considered particularly likely due to the relatively intact top flange. The residual channel may also have failed in tension near the bottom of the webs. This was considered more likely due to the thin residual webs. This may have occurred in the area of the beam which was burnt away before inspection.

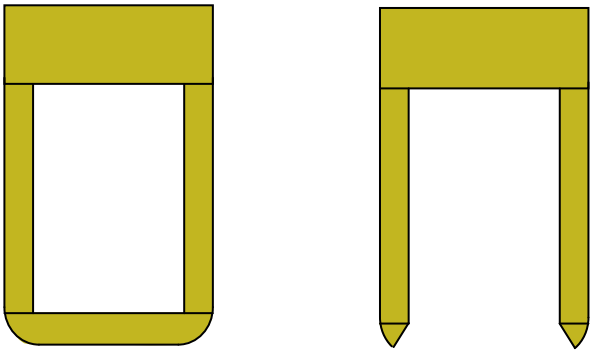

Figure 2-73: Speculative Beam A near failure, before failure (left), after failure (right), Drawing not to scale.

Combined bending and compression due to loading

The combined bending and compression failure mechanism was expected to exhibit crushing in the top of the beam, somewhere between the two load points. This was expected to form a plastic hinge over the entire cross-section. However during both the Beam B and C tests, this did not occur. During the Beam B test where the failure occurred much earlier than expected, the top flange became disconnected from the top of both webs along 80% of the beam length. The bottom channel consisting of the bottom flange and the two webs exhibited crushing in the webs, which formed a plastic hinge. In the Beam C test, in which failure occurred much nearer the predicted time, the webs crushed in a similar manner to the Beam B test, however the wide spread disconnection of the top flange from the webs did not occur. The crushing in the webs was more evident on one side. A crack or split was seen in the web near the top flange, however this only extended from the plastic hinge under the loading point to the plastic hinge at the vertical support.

Combined bending and compression due to post-tensioning.

It is possible that after a certain duration in a fire the post-tensioning end moments can become large enough to cause failure. The moments in the centre of the beam are due to the loading and the post-tensioning; both of which cancel each other out to some extent. Usually the resultant moment is positive resulting in downwards bending.

The centroidal axis moves upwards within the cross section during three sided fire exposure. Material is lost on the lower three sides which means the webs and bottom flange become smaller. Thus the centroid becomes closer to the top flange. This means that over time the post-tensioning eccentricity becomes larger, increasing the effective moment applied at the end of the beam. Therefore near the ends of the beam where the post-tensioning forces are applied the negative post-tensioning moment can become larger than the moment in the centre of the beam. Because the timber member is now no longer symmetrical, both the compression and tension stresses and top and bottom extreme fibres of the beam need to be checked for capacity. In the centre of the beam with positive bending the likely failure is in compression in the top flange. Near the end of the beam the likely failure is in compression on the bottom of the remaining bottom flange. The post-tensioning compressive force in the timber makes a tensile failure unlikely in many cases but not impossible. This indicates that it is possible to get a bending and compression failure at both mid-span and the ends of the beam and also that both compressive and tensile stresses need to be considered during design.

Shear failure in web

Whilst it was not specifically tested for during this series of tests, another potential failure mechanism is the shear failure in the web near the neutral axis. The elastic neutral axis will be the height at which the web experiences the highest shear forces assuming the beam remains elastic.

Whilst the Beam B test was abnormal, the failure exhibited was very similar to what would have been expected in a shear failure high in the web. The shear failure would cause a split or crack which would separate the top of the beam from the bottom. If the crack forms high in the web it would leave the top flange disconnected from the bottom flange and webs. The channel formed by the bottom flange and the webs would then be unable to resist the bending moments applied to it and it would fail in bending. The now unrestrained webs would crush or buckle to allow a plastic hinge to form in the channel. The top flange would be comparatively flexible and not be involved in the crushing and bending failure

Loss of post-tensioning

Another potential failure mechanism is the loss of the post-tensioning. This could be due to the heating of an anchorage which causes the post-tensioning to relax or worse, to break; or for the barrel and wedge mechanism to fail. Also as the timber cross section becomes smaller the compressive stresses and strains increase which will also cause relaxation. When this occurs the timber beam would act as a simply supported beam. It is important that some form of vertical support at the ends of the beam is provided which does not rely on the post-tensioning force; such as a corbel. The effect of this loss can then be calculated using standard calculation methods.

2.7.2. Material Performance

Char rates

The char rates estimated from the remaining timber were similar to the numbers published by the manufacturer (Carter Holt Harvey Woodproducts New Zealand, 2009). However it should be noted that the 0.72mm/min char rate published includes the heat affected layer of wood below the char surface. The manufacturer also presents 0.65mm/min which does not include the effects due to the heated wood. Calculations using 0.65mm/min should include a 7mm to 9mm zero strength layer to take the temperature affected wood into account.

Similarly the char rate estimated is very sensitive to the char depth measurement and the time of charring measurement. The char depth is difficult to measure for two reasons. Firstly, the char depth varies over the surface so a measurement taken at one place on a beam may not reflect the entire surface. Secondly, the distinction between charred wood and un-charred wood is not very clear and is also open to personal interpretation.

Localized increase of char rate

Some of the veneers in the LVL timber exhibited a faster char rate than those around them. This was evident only where charring was perpendicular to the veneer layers. This variability is the nature of timber. Many of the variations in the timber are spread throughout a member when using LVL which leads to a comparatively strong material, as no defect in the wood affects the entire thickness of the member. An example of the veneers affected are presented in Figure 2-74

Whilst for a structural calculation the entire member is used and the effect is minimal as the average char rate remains unchanged, this effect could cause an issue when a calculation is looking at failure in a localised area such as predicting the shear failure in the corner of a post-tensioned timber beam.

Figure 2-74: Veneers charring faster than the average char rate

This faster charring is most probably due to some veneers being less dense than average. It is common practice for LVL manufacturers to use stronger and stiffer veneers near the outside of the material. This allows for efficient use of the timber creating a stiffer, stronger overall material when used in any orientation. The probability of a veneer near a critical area might be sufficiently low to be negligible in the design of these members.

Small corner rounding

Most code calculations assume that the radius of charring is equal to the char depth. However the char radius measured during these tests was in some cases much smaller than the char depth. This suggests that the assumption is conservative. In most structural members the effect of this would be negligible although it may have a greater effect in box beam or similar configurations. Even in these cases it is unlikely to lead to a result which is excessively conservative.

Beam A, which was charred for approximately 66 minutes, had a char radius of approximately 20-25mm, where the char depth was approximately 48mm deep. Figure 2-75 shows the bottom corners of Beam A after charring. Beam B was charred for approximately 25 minutes which gave an approximate char radius of 20mm compared to a char depth of 18mm. Beam C charred for

approximately 58 minutes which resulted in a char radius of 30mm compared to a char depth of 42mm. Figure 2-76 shows the bottom corners of Beam C after charring.

Figure 2-75: The bottom section of Beam A showing the corner rounding.

Figure 2-76: Residual cross section of Beam C test showing corner rounding.

2.7.3. Premature Failure of Beam B

Beam B was originally expected to fail at mid-span in combined compression and bending at approximately 43 minutes of fire exposure. During the test the beam exhibited deflections that began to increase significantly early in the test. At between 21 and 23, minutes two sudden sounds were heard within 5 seconds of each other, these sounds indicated some abrupt movement in the beam. It was thought that these sounds were the webs of the beam becoming detached from the top flange. The beam failed at 23 minutes and the test was stopped.

The bending actions on the beam may also have been higher than was originally planned for due to the bowing induced by the axial loads from the post-tensioning. This was not fully accounted for in the original calculation, but due to this failure and the potential influence, the calculation model was updated to include this. The expected time of failure was then revised to 37 minutes and the beam was still expected to fail in bending and compression. There are two potential causes of this premature failure which are presented in the following sections.

Faulty glue line

The first theory for the premature failure is that the glue line at the interface between the webs and the flanges was for some reason under strength. It was unclear in the beam whether the failure occurred in the timber near the glue line or in the glue line itself, due to the charring that occurred. The glue may have only been strong enough to keep the beam together during construction and then when loaded was unable to resist the shear forces between the web and the flange.

As there is a portion of the beam which did not become disconnected, it would be possible to test the glue line in shear. However there is no guarantee that the strength of the glue in that section of beam represents strength of the glue that may have failed.

Weakness introduced by thermocouple placement

The second theory for the premature failure is that the thermocouple "plugs" may have introduced a discontinuity in the web of the beams severe enough to allow the failure to occur. The thermocouple plugs were placed in a hole which had been drilled from the inside of the cavity (before construction). These plugs were then glued in place by pouring resorcinol glue into the hole and slowing pushing the plug into the hole. This would force the glue around the sides of the plug and glue it in place. However on one of the first plugs placed, it was noted that not enough glue was poured in the hole and after the plug was pushed in the glue was not seen to rise all the way to surface. Unfortunately due to the suction on the plug and the tight fit, it was not possible to remove the plug and add more glue. A small amount of the glue was added to the top of the plug and pushed down into the gap using thin waxed paper. This theory is supported by the fact that a crack is visible running through one of the plug positions which is presented in Figure 2-77. However, the crack may have started elsewhere and merely propagated through the hole in the web.

Figure 2-77: Beam B web thermocouple plug showing crack passing around the plug.

2.7.4. Design considerations

This series of tests have raised some issues which may need to be considered during the fire design of post-tensioned timber members. Some of the aspects unique to post-tensioned timber may require analysis which differs slightly from traditional rectangular section design. The design of these members is very similar to the design of a box section column with lateral loading.

Corner rounding

Due to post-tensioned timber sometimes being constructed from hollow timber sections the shear in the bottom corner can govern the design. This issue is unique to hollow rectangular cross sections. Figure 2-72 on Page 59 shows how the corner rounding due to charring can lead to the thinnest portion part of the beam being in the corner, this is also discussed more fully in Chapter 3. The shear loads at this position are usually very small due to the position in the section. However, because of them causing the thinnest rejoin in the section, they should still be checked during the design along with shear in the web at the centroidal axis.

Changing geometry

During three sided burning, material is lost from the sides and the bottom of a beam which means that over time during fire exposure the geometry of the beam changes significantly. As the top flange is largely unaffected and material is being lost from the webs and bottom flange, the centroid moves upwards towards the top flange over time. The effective eccentricity of the post-tensioning therefore also increases with time. Therefore is it important to monitor this changing centroidal axis, as the increased moment applied to the section through post-tensioning can become critical and cause failure. This was seen in the Beam C test where a plastic hinge was formed near the vertical support.

This effect also means that at mid-span the ability of the post-tensioning to resist bending moments can be increased further than expected, which could lead to an unexpected failure mode. During these tests it was difficult to induce a bending failure due to the post-tensioning making the bending resistance higher than expected.

2.7.5. Test specimen comparison to realistic beams.

Whilst the test specimens were designed to be a good representation of beams which might be used in construction, there were some differences due to the limitations involved with furnace testing. The main constraints were the furnace span and the load able to be applied to the beam. The furnace internal span was 4m which, with the perimeter loading frame, provided a useable beam span of approximately 4.3m. Due to the loading system available the allowable loading force was 40kN. This load was then spread with a large steel spreader bar to give two point loads of approximately 20kN each. The goal was to have a beam fail at approximately 60 minutes to demonstrate that these beams were capable of achieving a reasonable fire resistance rating.

It became difficult to find beam sizes that would exhibit the desired failure mechanisms given these constraints. Due to the short span of the furnace the beams became more likely to fail in shear. More slender beams could have been used to force a bending failure however the size of these beams became impractically small for most cases. Also in order to achieve a 60-minute fire rating a timber thickness of at least 63mm was required. Beam B was designed to fail in bending but encountered problems which were exacerbated by the small eccentricity available in the shallow beam.

Fire test estimate of the ultimate limit state loading

Post-tensioned timber members are usually designed so that the post-tensioning balances the deflections due to some proportion of the ultimate limit state loading. Currently this proportion is the long-term serviceability limit state consisting of the dead load plus the long-term live load. As these loads are dependent on the application, a beam being used in a fire test does have a specific dead or live design action.

The Ultimate Limit State (ULS) is some factor larger than the Fire Limit State (FLS). For these tests this factor has been taken from the preliminary design calculations for a post-tensioned timber building being constructed in Nelson New Zealand from the research of Wouter Van Beerschoten (van Beerschoten, 2011). The ULS/FLS factor for this building was 1.92. The loading during the fire tests were two 20kN point loads. If this is assumed to be the fire limit state loading, based on the factor above the assumed ultimate limit state loading is two point loads of 38.6kN each.

Post-tensioning load balancing ratio

The load-balancing ratio from the preliminary design mentioned above is 0.5185 (1/1.92). This means that the post-tensioning is designed to balance the deflections of 52% of the ultimate limit state loading. Unfortunately this ratio was not able to be achieved easily for a beam designed to fail in bending with a span of 4.36m. The higher this ratio the higher the post-tensioning force and the more bending moment the post-tensioning can resist, therefore larger ratios suggest a beam that performs better in bending. This, however, made a shear failure more likely.

For Beam A a ratio of 0.52 was able to be achieved during testing. Beam B had a ratio of approximately 0.15, and beam C had a ratio of approximately 0.30 during testing. There was a trade-off between being able to cause a bending failure and still being a realistically sized post-tensioned beam.

Test specimen ambient capacity

The ambient condition capacity for a post-tensioned timber member considers both the axial loading and the bending. This can be checked by either checking the compressive and tensile stresses or using an axial and bending combined stress index (CSI). An example of a combined stress index formulae is presented in Eq. 2-2 (Standards New Zealand, 1993). The closer this result is to one the more efficient and close to capacity the beam is.

$$\left(\frac{M^*}{\phi M_n}\right) + \left(\frac{N^*}{\phi N_{nc}}\right) \leq 1.0$$

Eq. 2-2

Where:

M^* is the design bending moment action (kNm)

N^* is the design axial action (kN)

ϕM_n is the factored bending capacity in the direction of bending (kNm)

ϕN_{nc} is the factored axial capacity (kN)

Beam A had an ambient CSI of 0.29, Beam B had a CSI of 1.5, and Beam C had a CSI of 0.82. The CSI for Beam B of above one means that the beam was unrealistic and would not have been acceptable

for ambient designs. However as the fire limit state was less than the ultimate limit state it was calculated that the beam would still provide 37 minutes of fire resistance. For this testing only the fire limit state and the ultimate limit state were compared. No serviceability criteria were considered.

2.8. Conclusions & Recommendations

A series of full-scale furnace tests were conducted on three post-tensioned timber beams. During these tests five types of anchorage fire protection detail were also tested.

2.8.1. Post-tensioned beam results summary

The full-scale tests successfully demonstrated the fire resistance of post-tensioned timber members and also demonstrated many potential failure mechanisms which will need to be considered during design. Beam A successfully demonstrated a longitudinal shear failure in the lower corner of the cross section. The shear failure occurred at the bottom corner due to the geometry of a box section under fire conditions. The external corner of the cross-section charred and rounded whilst the internal corner remained unchanged, which means the thinnest portion of the cross-section occurred here and could potentially fail in shear before the web.

Due to the increased bending capacity of the beams due to post-tensioning the tests were not able to demonstrate a mid-span combined bending and compression failure. The post-tensioning moment and the short beam span available made a shear failure more likely to occur. However Beam C was able to demonstrate a combined axial and bending failure at the end of the beam where, due to the changing cross-section and post-tensioning eccentricity, the post-tensioning moment and axial load caused a plastic hinge to form.

Beam B failed earlier than expected, which lead to improvements in the proposed design method presented in Chapter 3. The design methodology before the Beam B test did not sufficiently consider the added bending moment due to axial loads from post-tensioning on a deflected beam.

2.8.2. Anchorage member results summary

Five different types of post-tensioning anchorage protection details were tested according to ISO834 (The International Organization for Standardization ISO, 1999). Useful information on each method of fire protection was able to be obtained despite being a secondary objective of this research. An unprotected anchorage was able to retain its post-tensioning load for a short duration in the order of 10 minutes. It was found that enclosing the anchorage in timber or GIB Fyreline™ provided the best protection. For timber protection standard charring rate calculation methods can be used to determine the fire resistance rating. For GIB Fyreline™ the anchorage protection should mimic the manufacturer's one-way firewall system.

Intumescent paint protection and Kaowool protection were also demonstrated during the tests. These methods may be able to be made to work appropriately but more research is needed. The Intumescent paint used provided some protection but only in the order of 10 minutes more than an unprotected anchorage. Kaowool was an effective protection detail providing more than 60 minutes protection, but there are currently no simple design methodologies or thickness recommendations available for using it commercially for steel protection.

3. Post-tensioned timber fire design methodology

The proposed design methodology was developed to predict the fire resistance rating of post-tensioned timber beams. The method has been compared against the full scale tests described in Chapter 2. The accuracy and limitations of calculations within this design method are discussed in Chapter 4. The design method focuses on four main failure mechanisms; a shear failure in either the web or in the bottom corner, and a combined bending and compression failure at mid span or and the end of the beam. The analyses described here examine the changing cross section of the beam over the duration of the fire, the secondary effects due to beam deflections, and the loss of post-tensioning force due to temperature on the capacity of the beam in fire. Two aspects of this calculation are non-linear and require iterative solutions. These are the bowing deflections caused by the axial load of the post-tensioning and the effect of end rotations on the tendon force. Methods of solving the iterative calculations are not presented here as modern spreadsheet software is capable of automating these.

The objective of this chapter is to outline the simplified design method recommended for the design of post-tensioned timber members under fire conditions. This is achieved through the following sub objectives;

- present applicable design assumptions and simplifications for fire design,
- present the failure mechanisms which must be checked during fire design,
- discuss practical methods of analysis which allow specific failure mechanisms to be checked.

3.1. Fire design data requirements

The following information is required to check the fire resistance of a post-tensioned timber beam:

- Beam dimensions including web and flange thickness as determined by ambient design.
- Post-tensioning design including the number of tendons, the tendon cross sectional area the post-tensioning force and the position of the tendons within the cavity as determined for ambient design.
- Loading information for the beam
- Material properties for both the timber member and the steel post-tensioning including
    - Timber characteristic strengths
    - Timber modulus of elasticity and rigidity
    - Timber char rate, as quoted by material manufacturer
    - Timber design modification factors including duration and size
    - Material reduction factors for ambient and fire conditions
    - Tendon capacity
    - Tendon Modulus of Elasticity
- Fire duration for design, and therefore the calculated char depth.

3.2. Ambient Capacity Check

It is advised to complete the ambient design, including serviceability, for the beam before calculating its fire resistance. The design methodology for post-tensioned timber is currently undergoing heavy research which may cause the process to change. As such the ambient check presented here is brief and simplified.

3.2.1. Ambient Section properties

The second moment of area of the ambient temperature beam is simple to calculate as it is doubly symmetrical. Eq. 3-1 can be used to calculate the second moment of area for a box beam. The section modulus can then be simply calculated, as shown in Eq. 3-2. Because the beam is symmetric the distance from the centroid to either extreme fibre, y, is the same to the topmost extreme fibre and the lowermost. The cross sectional area can be calculated using Eq. 3-3 and is shown in Figure 3-1.

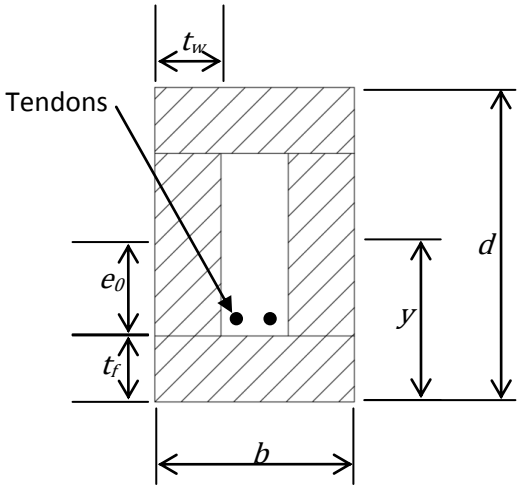

Figure 3-1: Ambient timber cross section dimensions.

$$I_{cold} = \frac{bd^3 - (b - 2t_w)(d - 2t_f)^3}{12}$$

Eq. 3-1

$$Z_{cold} = \frac{I_{cold}}{y} = \frac{I_{cold}}{d/2}$$

Eq. 3-2

$$A_{cold} = bd - (b - 2t_w)(d - 2t_f)$$

Eq. 3-3

3.2.2. Design actions

The design actions should include all actions on the timber member including those induced by the post-tensioning: the external transverse loading actions; and the bending, shear and axial actions due to the post-tensioning. The external actions should be calculated using analyses appropriate to the external loading. The post-tensioning bending actions are due to end eccentricity and uplift at deviators. The shear actions are due to the vertical uplift forces at tendon deviations and the axial load is due to the axial compressive force applied by the tendons.

3.2.3. Bending and compression combined stress

Mid Span

The bending capacity of the timber section is calculated as in NZS3603.

$$\phi M_n = \phi\, k_1\, k_{24}\, f_b\, Z_{Cold}$$

Eq. 3-4

Where:

ϕ is the material strength reduction factor for the ultimate limit state

k_1 is the duration factor

k_{24} is the size factor

f_b is the LVL bending strength

Z_{Cold} is the section modulus for the timber member

To estimate the overall the axial capacity, both the buckling and crushing capacities need to be considered. The overall capacity will be the lesser of these two values. Here it has been assumed that the flooring system for this design is sufficient to resist lateral torsion buckling. Buckling loads need to be investigated further as they rely on the end support conditions, the pinned-pinned condition can be estimated as shown below. The in-plane buckling and crushing capacity is estimated as:

$$\Phi N_{buckling} = \phi \frac{\pi^2 E_T I}{L^2}$$

Eq. 3-5

$$\Phi N_{crushing} = \phi\, k_1\, k_{24}\, A_T\, f_c$$

Eq. 3-6

Where:

E_T is the Young's modulus of LVL

I is the second moment of area of the timber section

L is the length of the beam

A_T is the Area of the LVL cross section

f_c is the LVL compressive stress capacity

The beam has adequate ambient capacity if the combined stress index inequality presented in Eq. 3-7 is true.

$$\frac{M^*}{\Phi M_{nCold}} + \frac{N^*}{\Phi N_{nCold}} \leq 1.0$$

Eq. 3-7

The stresses can also be checked in the top and bottom extreme fibres. Depending on how the actions are calculated this may or may not include the buckling effect. If the moment due to the axial loads acting on an initially deflected member (referred to here as bowing) is included in the calculation of M* then this check does implicitly include the effect of in-plane buckling. This assumes elasticity and that any plastic behaviour denotes "failure". The stress due to bending at the centroid of the cross-section is zero and is therefore only due to the axial load. The stress distribution due to bending can then be calculated and super imposed.

The compressive (positive) stress due to the axial loading is calculated as $\sigma_{NA} = F_{PT}/A_T$. The maximum compressive stress due to bending is calculated as $\sigma_b = M^*/Z_{cold}$. The tensile (negative) stress induced by bending is equal and opposite to the compressive stress calculated. Therefore the top and bottom fibre stress can be calculated as:

$$\sigma_{TopfibreMid} = \frac{F_{PT}}{A_T} + \frac{M^*}{Z_{cold}}$$

Eq. 3-8

$$\sigma_{BottomfibreMid} = \frac{F_{PT}}{A_T} - \frac{M^*}{Z_{cold}}$$

Eq. 3-9

The bending stress capacity can be calculated using the characteristic bending strength for the material and the appropriate modification factors as shown

$$\phi\sigma_{tn} = \phi\sigma_{cn} = \phi\, k_1\, k_{24}\, f_b$$

Eq. 3-10

3.3. Fire Design

3.3.1. Calculation overview

The fire design calculation for post tensioned timber beams including only first order effects is very similar to any other timber beam in fire it includes the following steps:

- Calculate the remaining post-tensioning force including the effects of the tendons decreased strain, due to thermal expansion of the steel and the additional axial compression of the timber, and the reduction of young's modulus of the steel due to its elevated temperature.
- Find the actions on the timber beam including, bending, shear, and compression. It is important to consider actions from both the external loads and the post tensioning system.
- Calculate the reduced section properties using the parallel axis theorem.
- Calculate the stresses induced in the timber beam
- Check the appropriate design equations to ensure the timber can resist the applied stresses.

For this first order calculation it is appropriate to calculate the relaxation of the tendon using the tendons decrease in strain, due to thermal expansion of the steel and the additional axial compression of the timber, and the reduction in young's modulus of the tendon due to its temperature. However, this analysis doesn't capture some of the complexities within the system. In reality the deflections of the beam alter the post tensioning force due to the rotation of the anchorages and due to bowing of the beam under axial loading. These effects make the problem non-linear and more difficult to solve. Methods for dealing with the first order effects and some of these second order effects are presented within this chapter.

3.3.2. Char depth

Eurocode 5 (British Standard Institute, 2004b) and the Australian Timber Structures Standard (Standards Australia, 2006) both incorporate a 7mm zero strength layer beneath the char layer to account for the loss of strength and stiffness of timber affected by increased temperature below the char layer. With the results of the full scale testing and the comparisons presented in chapter 4, it was found that it is important to include a zero strength layer in the design of post-tensioned timber

members. 7mm was found to provide a good correlation between the full-scale tests and the design methodology and has therefore been included here.

The calculation of char depths for post-tensioned timber members is similar to that of normal heavy timber members. It is important to select a charring rate appropriate to the timber product being used. Carter Holt Harvey specifies a char rate of 0.72mm/min or 0.65mm/min with an additional 7mm zero strength layer for their LVL products (Carter Holt Harvey Woodproducts New Zealand, 2009), whereas NZS3603 specifies a char rate of 0.65 mm/min regardless of the type of timber. European and Australian documents recommend the inclusion of a 7-9 mm zero strength layer. A 7mm zero strength layer should be added to the char depth results in this chapter. This is a precaution, as some generic char depth calculations may or may not consider the inclusion of a zero strength layer. The calculations specified here therefore make a clear distinction between the char depth and the zero strength layer. For example the corner-rounding radius is assumed to be equal to the char depth, and not the char depth plus the zero strength layer.

Based on the manufactures recommendation and the results of the full-scale testing it is recommended to assume a char rate of **0.72 mm/min**. It is also recommended to include a **7mm zero strength layer**. This provides the best correlation in failure times between the calculation method and the full-scale tests. The comparisons are presented in Chapter 4.

Table 3-1: Char rate recommendations

Char rate	0.72 mm/min
Zero strength layer	7 mm

3.3.3. Validity check

It is important to ensure that the calculation is being used within their valid range. Much of the design method relies on certain assumptions. Most cases fall within the limits of these assumptions but if the beam is shallower or narrower than usual it is possible for the beam to fall outside the scope of the assumptions. Checks are recommended to detect input errors and to ensure than the values given relate to a valid geometry. It is recommended that the following is adhered to during design:

Tendon stress: Check to ensure that the stress in the tendon is less than its maximum jacking stress. If higher stresses are required more or larger tendons should be used.

Beam width: Ensure that the original width of the beam is greater than four times the char depth at the required fire duration. Timber corners round when they char, it is often assumed that this rounding is circular and its radius is equal to the char depth. If the beam is less than 4 times wider than the char depth then the circular corners start to overlap as shown in Figure 3-2. The calculation will then not represent the physical nature of the charring and introduces errors into the calculation, this should therefore be avoided. If narrower beams are required thermal modelling may allow for a more accurate analysis.

$$4\ Chardepth \leq b$$

Cavity dimensions: Check to make sure the cavity has positive dimensions. If the combined flange or web thickness is greater than the depth or width of the beam respectively, the cavity would have a negative area and would make the geometry impossible.

$$2t_f \leq d$$
$$2t_w \leq b$$

Flange and web thickness: Ensure that there is some remaining thickness in the bottom flange and in the webs.

$$t_w \leq Chardepth$$
$$t_f \leq Chardepth$$

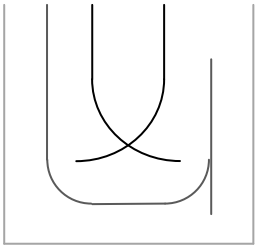

Figure 3-2: Demonstration of corner rounding overlap, to be avoided.

3.3.4. Geometric properties

The geometric properties of the timber section after a specified duration of fire exposure can be estimated based on a set of assumptions on how the cross section changes over the fire duration. The resulting geometry is non-symmetric around the bending axis and will require simplification in order to calculate the section properties. This can be done by breaking the complex shape into smaller simple shapes whose geometric properties are known, and then using parallel axis theorem and superposition to calculate the overall section properties.

The section properties which are to be used further in this calculation are; second moment of area, area, and the centroid. Later in the calculation of shear forces, the first moment of area is calculated in a similar manner.

Incorporating the geometric changes due to charring in this manner is a starting point and is more useful for research than in practice. With future research it may be possible to devise a notional charring rate, and set of design rules which can be used for the design of hollow timber sections without the need to determine section properties in this way. Notional charring rates are more applicable to solid sections, but may be applicable for box section of specific geometries.

Assumptions

The assumptions used to calculate the section properties are:

- A constant char rate of 0.72 mm/min
- A 7mm zero strength and stiffness layer of timber underneath the char layer
- The corner rounding due to charring is equal to the char depth
- The cavity does not affect the corner rounding or char rates
- The beam remains elastic

Parallel axis theorem

For structural engineering the parallel axis theorem is a useful mechanical tool which allows the calculation of the second moment of area of a cross section to be calculated about an axis which is not at its centroid. This allows the calculation of the second moment of area of a complex shape, which is done by breaking the shape into smaller simpler shapes which have known second moment of areas, about their own centroid. The second moment of area for each of these shapes can then be calculated about the entire section's centroid, and can then be superimposed to calculate the overall cross sections second moment of area.

The formulae for the second moment of area around an axis *(z)* parallel to an axis *(cm)* passing through the shape's centre of mass as shown in Figure 3-3 is:

$$I_{zz} = I_{cc} + Ar^2$$

Eq. 3-11

Where:

I_{zz} is the second moment of area around the z axis.

I_{cc} is the local second moment of area around the centroidal (c) axis

A is the area of the shape.

r is the radius/distance between the axes

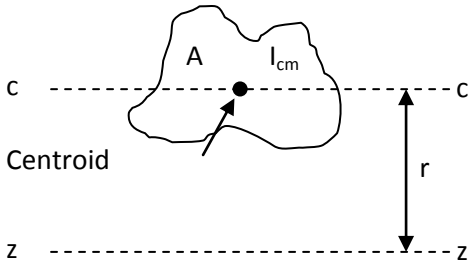

Figure 3-3: Diagram demonstrating the parallel axis theorem

Section shape during fire exposure

The shape of a timber section exposed to fire changes over time. As the timber heats above 300°C it undergoes pyrolysis and turns into char. A layer of char forms quickly in the fire and then progresses through the timber at an approximately constant rate. In reality the char layer progresses faster early in the fire until the char layer forms. Once formed it serves to protect the timber beneath it, causing it to progress slowly. For LVL the char layer moves into the timber at a rate of approximately 0.72mm/min, as presented by the manufacturer.

The corners of a timber section exposed to fire round as it chars. This is due to heat being conducted into the timber from two faces. This can be modelled by assuming the rounding is circular and that the radius is equal to the char depth.

These assumptions can be used to estimate the section geometry over the fire duration. Shown in Figure 3-4 is a visual comparison between the geometry constructed from the above assumptions and a similar timber section which has been exposed to fire.

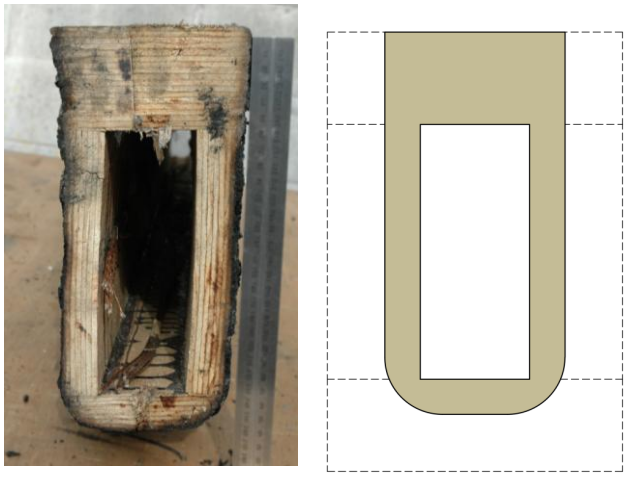

Figure 3-4: Comparison between an actual fire exposed timber section and the model geometry.

Relative dimensions

The model section geometry can be made up from a series of simple geometric shapes, which can then be used to calculate the second moment of area, area, and centroid for the whole cross-section. The dimensions presented in Figure 3-5 and Figure 3-6 allow for the calculation of these section properties. The given dimensions are relative to five principal dimensions, which are; beam depth, beam width, flange thickness, web thickness, and the char depth.

For three sided fire exposure of a post-tensioned timber beam, the following relative dimensions can be used for the calculation of the section properties:

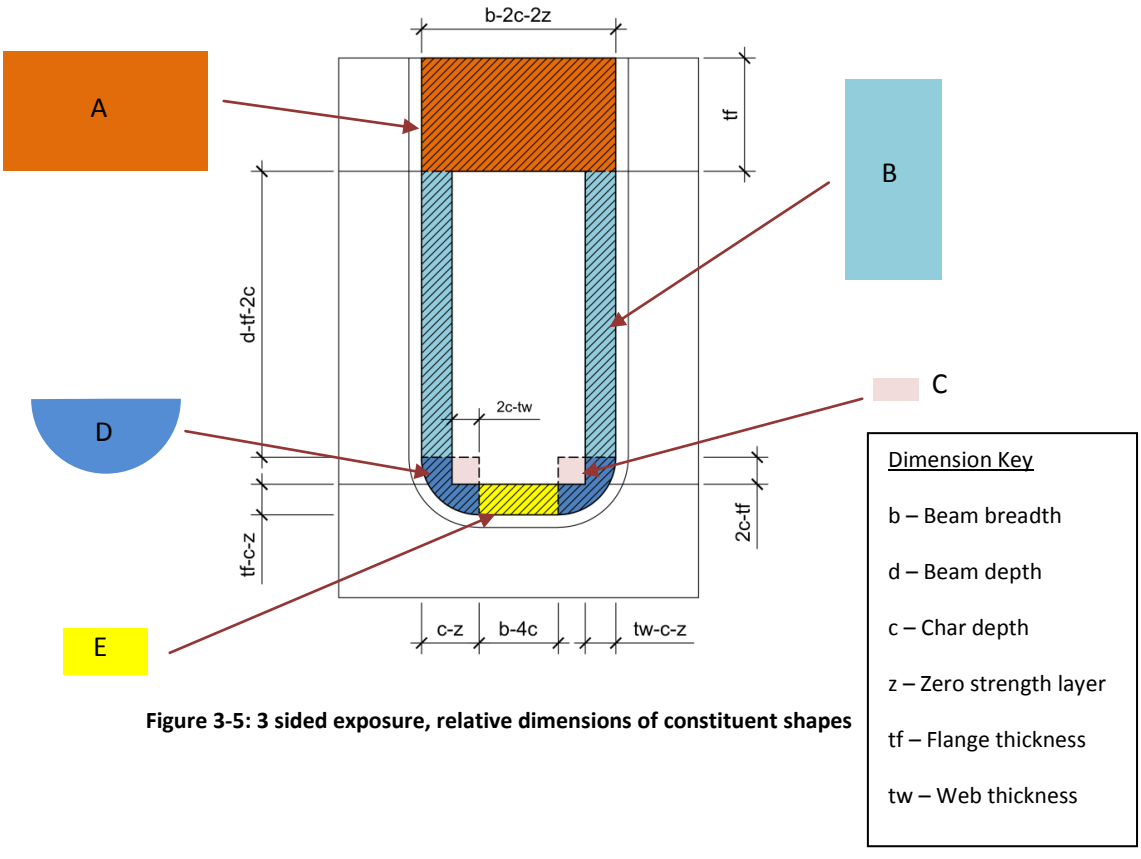

Figure 3-5: 3 sided exposure, relative dimensions of constituent shapes

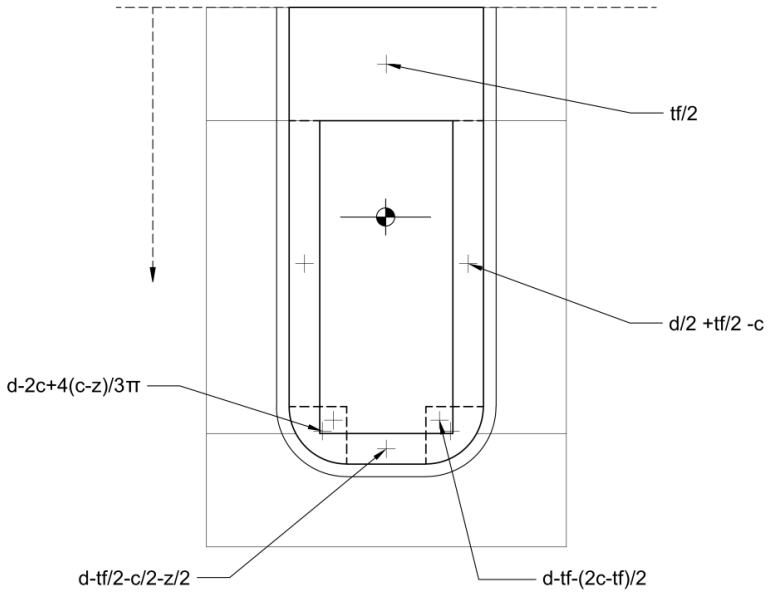

Figure 3-6: 3 sided exposure, relative distances from shape centroid to the top fiber.

Centroid calculation

The location of the section centroid is calculated using the first moment of area around a datum. It is convenient for this calculation to be done about the top fibre of the section. Figure 3-7 shows the shapes and values used in the calculation. An example table is also presented which shows a convenient method for calculating the centroid position.

The first moment of area consists of the area of a shape multiplied by its distance to the datum. The first moments of area for each shape can be super imposed to calculate the first moment of area of the entire section.

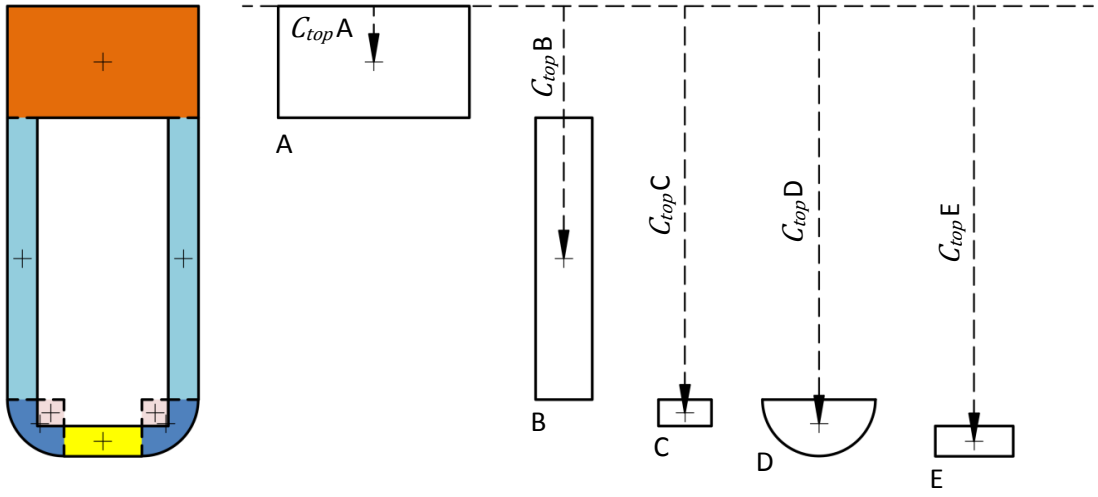

Figure 3-7: Centroid location calculation

Table 3-2: Centroid calculation

Shape	C_{top}	Area	1st Mom. Area
A	$C_{top}A$	$AreaA$	C_{top}-A x $AreaA$
B	$C_{top}B$	$AreaB$	C_{top}-B x $AreaB$
C	$C_{top}C$	$AreaC$	C_{top}-C x $AreaC$
D	$C_{top}D$	$AreaD$	C_{top}-D x $AreaD$
E	$C_{top}E$	$AreaE$	C_{top}-E x $AreaE$
		$\sum Area$	$\sum 1^{st}\ Mom.\ Area$

The distance from the top of the section to the section centroid can then be calculated as:

$$C_{top} = \frac{\sum 1^{st}\ Mom.\ Area}{\sum Area}$$

Eq. 3-12

Where:

$C_{top}X$ is the distance from the top of the section to the centroid of shape X.

$AreaX$ is the area of shape X.

C_{top} is the distance from the section centroid to the top of the section.

$1^{st}\ Mom.$ Area is the first moment of area about the top of the section.

Second moment of area calculation

The second moment of area for the section can be calculated using parallel axis theorem. Using the relative dimensions stated in Figure 3-5 and Figure 3-6 the second moment of area for each component shape about the section's centroid can be calculated. The diagram below shows the dimensions and values used for the calculation of I about the section centroid for shape B. The second moment of area for the entire cross section can then be calculated by the superposition of the global I contribution of each shape.

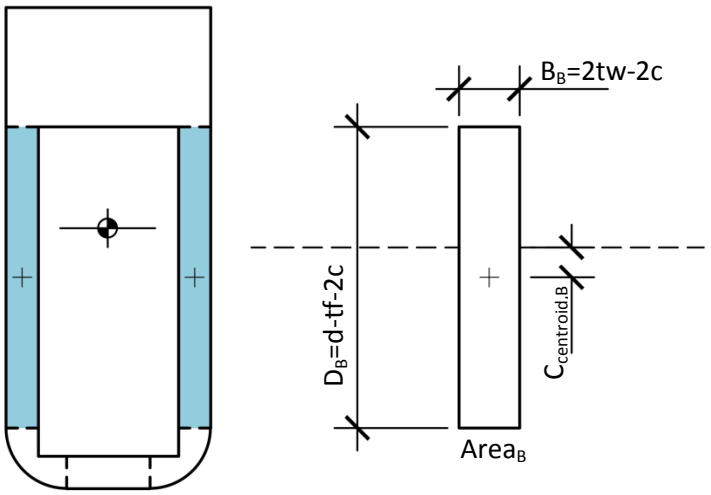

Figure 3-8: Second moment of area calculation. Example showing values used for shape B (shaded).

Table 3-3: Second moment of area calculation

Shape	$C_{centroid}$	Area	I_{local}	I_{global}
A	$Centroid_{top} - C_{top}A$	$AreaA$	I_A	$I_A + AreaA\ C_{centroid}A^2$
B	$Centroid_{top} - C_{top}B$	$AreaB$	I_B	$I_B + AreaB\ C_{centroid}B^2$
C	$Centroid_{top} - C_{top}C$	$AreaC$	I_C	$I_C + AreaC\ C_{centroid}C^2$
D	$Centroid_{top} - C_{top}D$	$AreaD$	I_D	$I_D + AreaD\ C_{centroid}D^2$
E	$Centroid_{top} - C_{top}E$	$AreaE$	I_E	$I_E + AreaE\ C_{centroid}E^2$
			$I_{Fire} =$	$\sum I_{global}$

Where:

$C_{centroid}X$ is the distance of the centroid of shape X from the section centroid. Negative values are below the centroid.

I_{local} or I_X is the local second moment of area of the shape X.

I_{global} is the second moment of area for the section

D_B is the local depth of the shape B

B_B Is the local breadth of the shape B

3.3.5. Tendon relaxation and deflection analysis

The following section describes the analysis required during the design of post-tensioned timber beams for fire conditions. The calculation method seeks to determine the actions acting on the timber beam. These actions include effects such as second order deflections, bowing of the beam due to the axial loads, post-tensioning relaxation due to thermal elongation, the post-tensioning end moments, and the changing geometry of the beam.

Iterative calculation of the remaining post-tensioning force

When heated the post-tensioning loses its tensile force in two ways. The thermal expansion of the steel reduces the mechanical strain on each tendon, and the Young's modulus of the tendon reduces as its temperature increases which reduces the stiffness of the tendons. There are additional changes to the force within the tendons due to the geometry of the beam. As the beam deflects the ends rotate which changes the length of the tendon. Also as the beam chars the compressive stresses increase and the timber compresses more than at ambient temperature conditions. The geometric effects are included as effective strains to analyse the remaining tendon force. Elongation is assumed positive for this calculation. The strain in the tendon can be described as:

$$\varepsilon_{mech\,0} + \varepsilon_{rotation} + \varepsilon_{compression} = \varepsilon_{mechanical} + \varepsilon_{thermal}$$

Eq. 3-13

Where:

$\varepsilon_{mech\,0}$ is the initial mechanical strain on the tendon at ambient conditions after loading;

$\varepsilon_{mechanical}$ is the axial strain due to the applied axial force,

$\varepsilon_{thermal}$ is the thermal strain,

$\varepsilon_{rotation}$ is the effective strain due to the rotation of the anchorages and subsequent elongation of the tendons final length, and

$\varepsilon_{compression}$ is the effective strain due to the increased axial deflections of the timber beam.

There are four main steps to calculate the reduction in post-tensioning force in the tendons:

- Calculate initial tendon length and the mechanical strain
- Estimate tendon temperature
    - Calculate thermal expansion
    - Calculate tendon stiffness
- Calculate total strain
- Calculate relaxed force

This calculation is however complicated by the fact that the beam deflections also affect the strain and forces developed within the tendons. The rotation of the anchorages can elongate or shorten the length of the tendon, as can the increased compression of the timber member due to its reduction in cross section. These become non-linear and need to be solved iteratively as the end rotations and timber compression are dependent on the remaining tendon force. The calculation process is described in Figure 3-9. Each labelled portion of the calculation presented in the flow chart is specifically addressed.

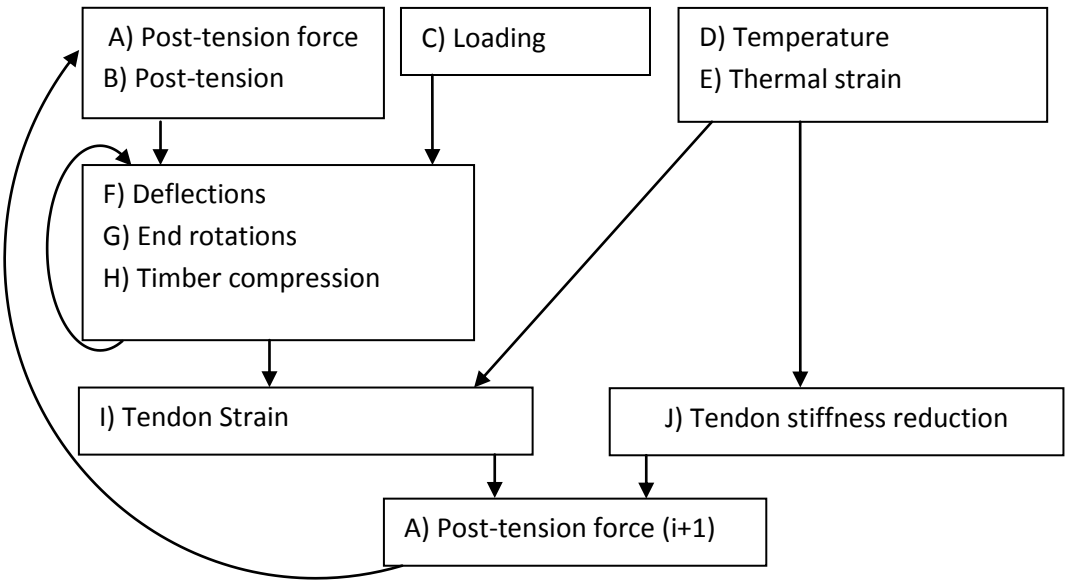

Figure 3-9: Tendon relaxation calculation process flow chart

In-order to calculate the components of strain within the tendon it is important to calculate the initial length of the tendon so that each strain component is calculated with the same reference length. The tendons final length is fixed at the distance between anchorages. However, as the tendon is stretched to this length, the original length, L_o must be determined. The original length is used as the reference length for all strains in this calculation. The original length only needs to be calculated once, based on the ambient design post-tensioning force, and does not need to be recalculated for each iteration. Original length L_o can be calculated as:

$$L_o = \frac{E_{PT} A_{PT} L}{F_{PT} + E_{\mathrm{PT}} A_{PT}}$$

Eq. 3-14

A) Post-tensioning force (i)

The goal is to determine the reduced post-tensioning force in the tendons after certain fire duration. However, due to the non-linear nature of this calculation it is required that an initial value is assumed. It is easiest to assume the ambient temperature post-tensioning force as the initial value, $F_{PT,Fire}^{i=0}$ as it will allow the calculation to converge quickly.

$$F_{PT,Fire}^{i=0} = \varepsilon_{mech,0} E_{cold} A_{PT}$$

Eq. 3-15

$$F_{PT,Fire}^{i} = \varepsilon_{mechanical} E_{fire} A_{PT}$$

Eq. 3-16

B) Post-tensioning moment

The applied post-tensioning moment is determined from the post-tensioning force and the calculated eccentricity. It is important to include the effects of the changing eccentricity due to the changing cross section geometry.

C) Transverse loading

The external loads are determined as dictated by the fire limit state loading and will not change between iterations. AS/NZS 1170 states that the fire limit state load case is the dead load plus 40% of the characteristic live load.

D) Tendon temperature

The temperature of the tendon can be assumed to be the same temperature as the internal surface of the cavity within the timber member. This is a conservative assumption as the tendons will take time to heat. The cavity surface temperature, and therefore the tendon temperature, can be estimated using an assumed temperature distribution for the timber underneath the char layer. Structural design for fire safety (Buchanan, 2001) presents the following parabolic distribution:

$$T(x) = T_i + (T_p - T_i)\left(1 - \frac{x}{a_{heated}}\right)^2$$

Eq. 3-17

Where

$:T(x)$	is the temperature of the timber at a distance x beneath the char layer.
T_i	is the initial or ambient temperature of the timber. Default 20°C.
T_p	is the charring or pyrolysis temperature of the timber. Default 300°C.
a_{heated}	is the thickness of the heat-affected layer. Default 40mm.

It should be noted that this relationship is only valid for values of x between zero and a_{heated}. For a distance greater than a_{heated} the temperature should be taken as T_i. The value x can also be used as the remaining thickness of the timber. This will return an approximate value for the temperature on the internal surface of the timber cavity. If the thickness of the webs and flanges are different it is recommended to use the thickness of the thinnest component which will give a more conservative estimate.

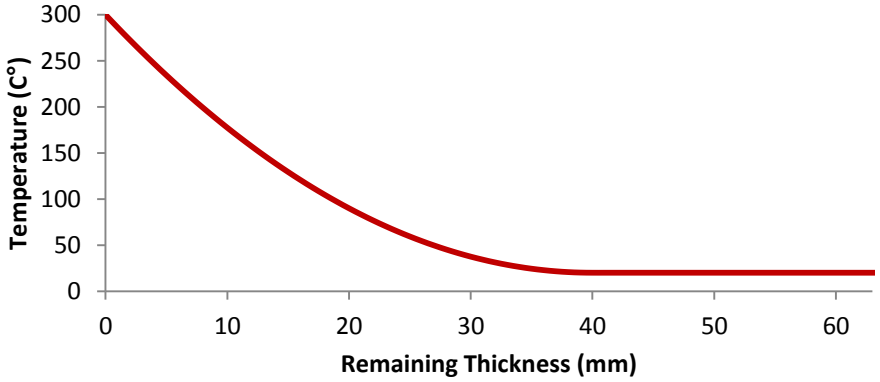

Figure 3-10: Timber temperature profile assumed for a remaining thickness of timber, as calculated with Eq. 3-17.

E) Thermal strain

With the estimated tendon temperature it is possible to calculate the thermal strain in the tendon. Section 3.4 of Eurocode 2 part 1-2 provides a formulae to calculate the thermal strain of pre-stressing steel (British Standard Institute, 2004a). This calculation is intended for use with pre-stressed concrete, as the tendons being used for post-tensioned timber are the same as those used for pre-stressed concrete it is appropriate to use this relationship. In order to fit the sign convention of this calculation the Eurocode formulae has been made to give positive results. The thermal strain of a tendon can be calculated as:

$$\varepsilon_{thermal} = -2.016E^{-4} + \mathrm{E}^{-5}\theta + 0.4E^{-8}\theta^2$$

Eq. 3-18

Where:

$\varepsilon_{thermal}$	is the strain induced in the tendon due to its temperature.
θ	is the temperature of the tendon.

With 63mm LVL after 60 minutes of fire exposure the char depth is approximately 43mm leaving 20mm material remaining. With this remaining thickness the expected cavity temperature is approximately 90°C which induces a thermal strain of 7.5×10^{-4}.

If the entire length of the tendon is heated the above calculation is sufficient to estimate the reduced stiffness. It is however possible that a beam spans across a fire separation and that it is unrealistic to assume the entire length of the beam is exposed to fire at once. The effect of this can be incorporated in the calculation by adjusting the thermal strain. The thermal strain can be reduced proportionally with the proportion of the beam not exposed to fire. If only 30% of the beam is exposed to fire then 30% of the thermal strain calculated above should be used.

F) Beam deflections

Under fire conditions it is important to consider the deflections of a post-tensioned timber beam or laterally loaded column so that the bowing moment induced by the axial loads can be included in the calculation. This is not as important with the ambient design, but becomes more important during fire exposure, as the beam can become comparatively more flexible and slender, especially close to failure. The deflection components which need to be monitored during design are; the flexural deflection due to external loads, the shear deflection due to external loads, the flexural deflections due to the post-tensioning moment caused by the post-tensioning eccentricity, and the bowing deflection caused by the axial post-tensioning force on an initially deflected member.

The moment and deflections due to the axial loads are dependent on the total deflection, which includes a component of its own deflection making this a non-linear problem. The calculation lends itself to being solved in an iterative manner. The initial bowing deflection can be taken as zero. This bowing deflection and moment are denoted with the subscript “bowing”.

The deflections due to the external loads (bending and shear) and the end moment due to the post-tensioning eccentricity are not dependent on the total deflection and are therefore constant whilst solving for the bowing deflection.

It is important to consider the following deflection components:

D_{Load}: Deflections due to bending induced by the external loads

D_{Shear}: Deflections due to shear induced by the external loads

D_{PT}: Deflections due to end moments due to the post-tensioning eccentricity

D_{Bowing}: Deflection due to axial loads acting on an initially deflected member

$$\Delta_{Total} = D_{Load} + D_{PT} + D_{Shear} + D_{Bowing}$$

Eq. 3-19

The mid span deflections due to a non-deviated eccentric tendon can be calculated with:

$$D_{PT} = \frac{M_{PT} L^2}{8EI}$$

Eq. 3-20

$$D_{Bowing} = \frac{F_{PT} \Delta_{Total} L^2}{\pi^2 EI}$$

Eq. 3-21

Deflections for a deviated tendon should be calculated using the same analysis methods as for ambient design. The shear deformations for uplift in a post-tensioned beam with a deviated tendon should be included. For simply supported beams the bowing deflection in Eq. 3-21 still applies, but a more accurate analysis should be done for deviated tendons.

Mid span deflections can be calculated for four point loading using:

$$D_{Load} = \frac{Pa(3L^2 - 4a^2)}{24EI}$$ **Eq. 3-22**

$$D_{Shear} = \frac{0.6Pa}{GA}$$ **Eq. 3-23**

G) Beam end rotations

The rotation at the anchorages affects the forces developed in the tendon. This occurs under both ambient and fire conditions. The beam ends rotate because of; transverse load moments, the post-tensioning moment, and the bowing due to the axial loads. The rotation of the anchorages forces the tendon to elongate. This elongation can be converted to a strain using the initial tendon length, L_o as a reference. An example of how the beam end rotation can cause tendon elongation is presented in Figure 3-11.

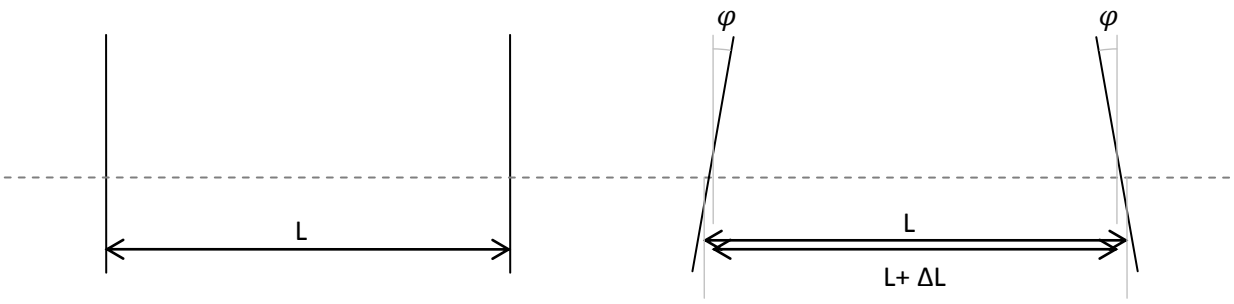

Figure 3-11: End rotation resulting in tendon elongation

The components of the beams end rotation include:

φ_{Load}: End rotations due to the bending induced by the transverse loading

4 point bending: $\varphi_{Load} = \frac{Pa(L-a)}{2EI}$

Eq. 3-24

φ_{PT}: End rotations due to the end moments due to the post-tensioning eccentricity

$$\varphi_{PT} = \frac{M_{PT,Fire}L}{2EI}$$

Eq. 3-25

φ_{Bowing}: End rotations due to the axial loads acting on an initially deflected member

$$\varphi_{Bowing} = \frac{F_{PT,Fire}\Delta_{total}L}{\pi EI}\left(-\cos\left(\frac{\pi L}{4}\right)+1\right)$$

Eq. 3-26

The total rotation for a single anchorage is then calculated as:

$$\varphi_{end} = \varphi_{Load} + \varphi_{PT} + \varphi_{Bowing}$$

Eq. 3-27

The end rotation for both anchorages can then be converted to a strain by multiplying the rotation in radians by the tendons eccentricity and normalising with respect to the initial length of the tendon, which can be done using:

$$\varepsilon_{roation} = \frac{2\varphi_{end}e_{Fire}}{L_o}$$

Eq. 3-28

H) Additional timber compression

As the timber is post-tensioned there are large axial loads which compress the timber. This is implicitly taken into account during stressing. However, during fire exposure the timber area resisting the axial load is reduced, which increases the stress developed in the cross section and therefore compresses the timber more. It is only the change in compressive strain which is of interest during this calculation.

The difference between ambient strain and strain during fire exposure is determined using:

$$\varepsilon_{compression} = \frac{F_{PT,fire}L}{L_oE_TA_{T,fire}} - \frac{F_{PT}L}{L_oE_TA_T}$$

Eq. 3-29

I) Tendon strain

The mechanical strain, which is used to calculate the force within the tendon, can then be calculated using the following:

$$\varepsilon_{mechanical} = \varepsilon_{\text{mech 0}} - \varepsilon_{thermal} + \varepsilon_{rotation} + \varepsilon_{compression}$$

Eq. 3-30

J) Stiffness reduction

As the tendon is heated its young's modulus decreases. Eurocode 2 (British Standard Institute, 2004a) provides a relationship between the reduction of young's modulus and the tendons temperature, which is presented in Figure 3-12.

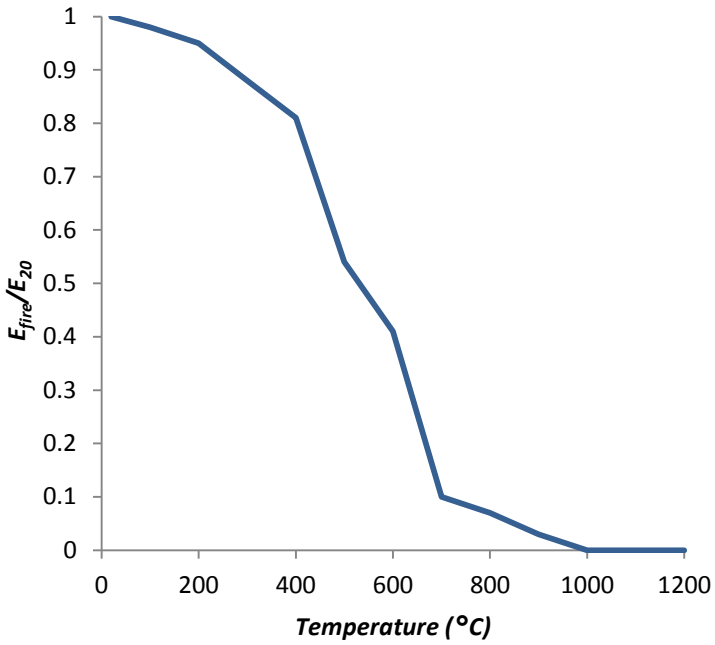

Figure 3-12: Thermal reduction of young's modulus as presented in Eurocode 2 part 1-2 (British Standard Institute, 2004a) table 3.3 column 6 for cold worked pre-stressing tendons.

Where:

Temperature is the temperature of the tendon

E_{fire} is the Young's modulus at the specified temperature

E_{20} is the 20th percentile young's modulus of the tendon

E_{fire}/E_{20} is the Young's modulus reduction factor

A) Post tendon force (i+1)

The reduced tendon force for the current iteration can then be calculated as:

$$F_{PT,Fire}^{i+1} = \varepsilon_{mechanical} E_{fire} A_{PT}$$

Eq. 3-31

3.3.6. Combined bending and compression

Moment actions

The moment acting on the timber member is the summation of the bending moments due to the external loads, the post-tensioning eccentricity, the bowing due to the axial loads, and the uplift due to tendon deviation. This section presents the actions on a straight (un-deviated) tendon; the effect of tendon deviation can be accounted for in a similar manner to the external loads and will follow the ambient design. Each component can be calculated separately and superimposed at any position

along the beam as shown in Figure 3-13. The mid span bending moment is made worse by the loading and the bowing moments and is resisted by the post-tensioning moment. The moment at the end of the beam is due only to the post-tensioning moment. It is important to check the mid span and end moment during the fire design of these beams. When checking stresses the critical stress is commonly the compressive stress as the tensile stress is reduced by the compression due to post-tensioning.

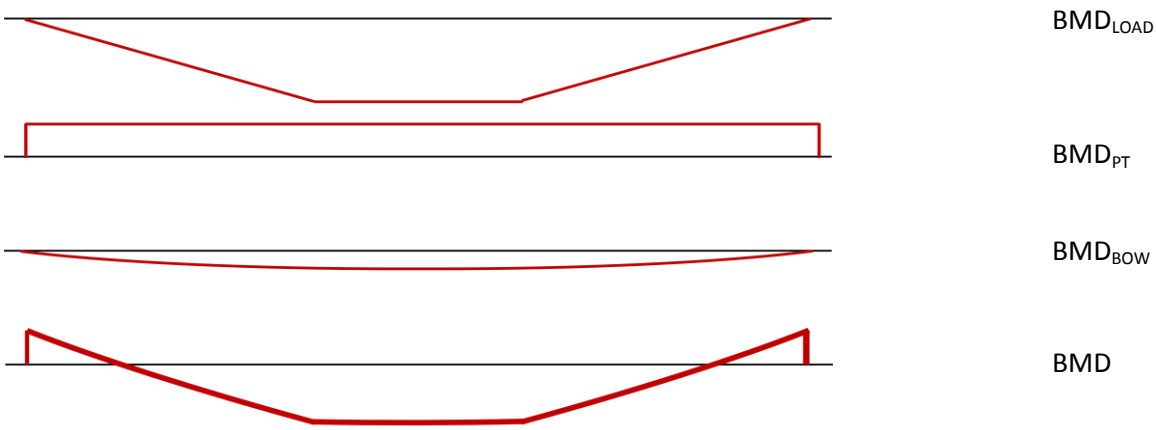

Figure 3-13: Bending moment diagram for a straight eccentric tendon, post-tensioned timber member.

M_{LOAD}

The moment due to external loading is calculated in the standard manner depending on the loading configuration. An example formula to calculate the mid span bending moment for four point simply supported loading configuration is presented in Eq. 3-32. These formulae and others are available in many mechanical texts.

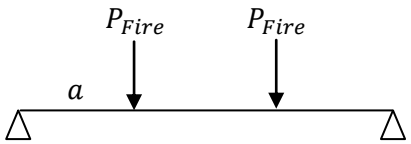

$$M^*_{Load,Fire} = P_{Fire} \times a$$

Eq. 3-32

Where:

$M^*_{Load,Fire}$ is the mid-span moment due to the external loads on the member (kNm).

$Pointload_{Fire}$ is the value of one of the two point loads on a member (kN).

a is the distance from the vertical support to the nearest point load (m).

L is the length between vertical supports on a simply supported beam (m).

M_{PT}

The bending moment due to the eccentric post-tensioning is constant along the length of the beam regardless of deflections. The deflections of the beam will increase the bowing moment but not the post-tensioning moment. This is due to the post-tensioning acting on the beam only at the anchorages and not interacting with the beam at any other position.

During fire exposure the moment due to the eccentricity increases. This is because as material is removed from the bottom of the section the centroid moves upwards towards the relatively unaffected top flange. This increase in moment means that it is important to monitor end moments during fire design. The resultant cross-section and increased eccentricity is shown in Figure 3-14.

The moment due to the post-tensioning eccentricity can be calculated with:

$$M_{PT}^{*} = F_{PT,Fire} e$$

Eq. 3-33

$$e = e_0 + \frac{d}{2} - C_{top}$$

Eq. 3-34

Where:

$F_{PT,Fire}$ is the temperature reduced horizontal post-tensioning force as calculated in the tendon relaxation section above.

e is the increased eccentricity calculated for an initially vertically symmetric member.

e_0 is the initial eccentricity at ambient conditions.

d is the initial depth of the member.

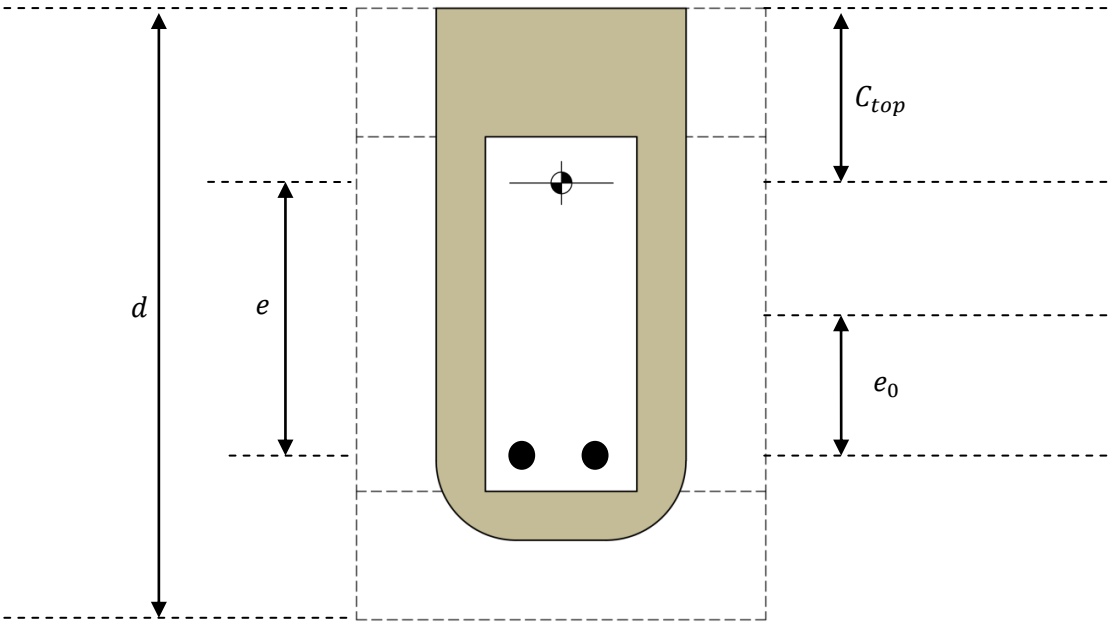

Figure 3-14: Increased tendon eccentricity due to 3 sided charring

M_{BOW}

The mid span moment due to the axial loads can be calculated if the total deflection is known. A method to calculate the deflection is discussed in Section 3.3.5. As the deflection is maximum at mid span and zero at either end the moment is also maximum in the centre and zero at either end. The moment in the centre is simple to calculate as shown in Figure 3-15. If a moment distribution for the entire length is desired, it is simple to fit a sinusoidal or parabolic distribution.

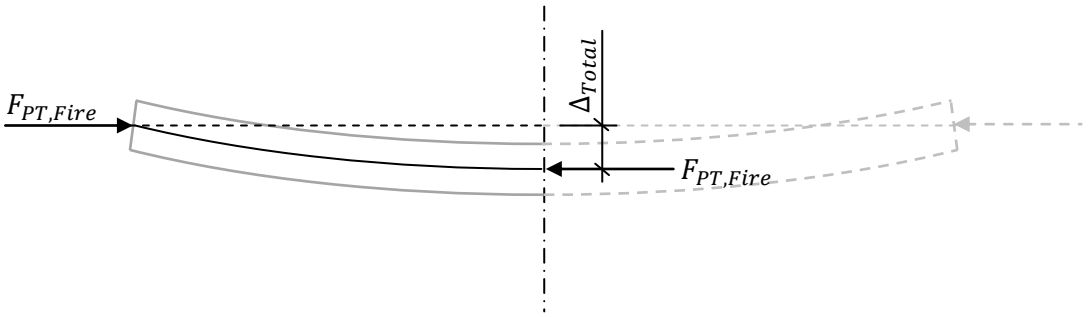

Figure 3-15: Bowing moment calculation

The bending moment at mid span due to bowing can be calculated as:

$$M^*_{Bow} = F_{PT,Fire}\Delta_{Total}$$

Eq. 3-35

Where:

$F_{PT,Fire}$ is the temperature reduced horizontal post-tensioning force as calculated in the tendon relaxation section above.

Δ_{Total} is the increased total deflection of the beam as calculated above in the deflection section.

M_{Fire}

The total mid-span moment is the sum of the previously described moments.

$$M^*_{Fire} = M^*_{Bow} + M^*_{PT} + M^*_{Load,Fire}$$

Eq. 3-36

Axial action

The axial action on the beam should include the reduced post-tensioning force calculated previously and any external axial loads on the beam. For a simply supported beam with an un-deviated tendon the axial action is:

$$N^*_{Fire} = F_{PT,Fire}$$

Eq. 3-37

Where:

N^*_{Fire} is the axial action on the member during fire exposure.

$F_{PT,Fire}$ is the reduced post-tensioning force.

Mid-span moment capacity

The bending capacity can be calculated similar to NZS3603 as shown in Eq. 3-38.

$$\phi M_{n,Fire} = \phi\, k_1\, k_{24}\, f_b\, Z$$

Eq. 3-38

Where Z is the section modulus for the timber member at mid-span. For compression at mid-span the section modulus can be calculated as:

$$Z = \frac{I_{fire}}{C_{top}}$$

Eq. 3-39

The mid-span bending producing compressive stresses in the top flange. For the moment capacity at the end of the beam it may be appropriate to use the distance from the centroid to the lower extreme fibre. Eq. 3-40 can be used as the section modulus for the timber member at the end of the beam. The difference between these section moduli is demonstrated in Eq. 3-40.

$$Z = \frac{I_{fire}}{d - C_{top} - chardepth}$$

Eq. 3-40

Nominal Axial capacity

The axial capacity of the member is the lesser of the buckling capacity and the crushing capacity. Lateral stability has not been investigated in this research as it was assumed that a flooring system will always be in place to provide lateral restraint along the top flange of the beam. The inclusion of a buckling check is redundant as the bowing moment is included in the moment calculation. However, it has been included for this style of check to ensure buckling is incorporated in all possible cases.

The in plane buckling capacity is calculated as:

$$\phi N_{buckling} = \phi\, \frac{\pi^2 E I_{fire}}{L^2}$$

Eq. 3-41

Where:

ϕ is the material strength reduction factor for the fire limit state

E is the youngs modulus of LVL

I_{fire} is the second moment of area of the timber section after the specified burning duration

L is the length of the beam

The crushing axial capacity is calculated as:

$$\phi N_{crushing} = \phi\, k_1\, k_{24}\, A_{T,Fire}\, f_c$$

Eq. 3-42

Where:

ϕ is the material strength reduction factor for the fire limit state

k_1 is the duration factor. For NZS3603 for most fire cases this is taken as 1 for brief loading.

k_{24} is the size factor

$A_{t,Fire}$ is the Area of the LVL cross section

f_c is the LVL crushing strength

Therefore the axial capacity is the lesser of the buckling and crushing capacity:

$$\phi N_{n,Fire} = \mathrm{Min}(\phi N_{Buckling}, \phi N_{crushing})$$

Eq. 3-43

Combined bending and compression stress index check

The overall combined stress index of the beam can then be calculated as in NZS3603. If the following inequality is true then the beam can withstand its loading for the specified fire duration.

$$\frac{M^*_{Fire}}{\phi M_{n,Fire}} + \frac{N^*_{Fire}}{\phi N_{n,Fire}} \leq 1.0$$

Eq. 3-44

Stress check

A more elegant method to check the adequacy of the beam is to compare the stresses due to the axial and bending loads to the allowable tension and compression stresses. This method again includes the effect of in plane buckling, as the moment induced by the axial loads is calculated and included in the stress calculation. The stress due to bending at the centroidal axis is zero and is therefore due only to the post-tensioning axial loading component. The stress distribution due to bending can then be calculated and super imposed as shown in Figure 3-16.

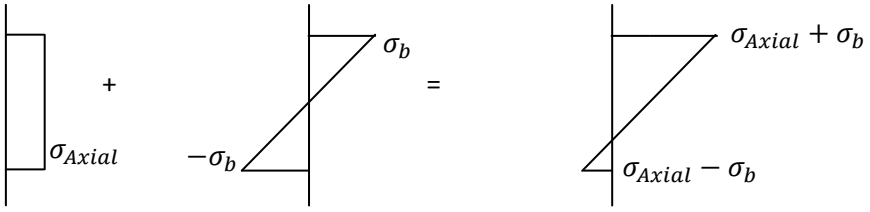

Compressive stress due to axial load | Bending stress due to Bending moments | Resultant stress distribution

Figure 3-16: Simplified stress distribution for post-tensioned timber beam

The positive, compressive, stress is calculated as

$$\sigma_{Axial} = F_{PT,Fire}/A_{T,Fire}$$

Eq. 3-45

The maximum compressive bending stress is calculated as

$$\sigma_b = M^*_{fire}\, y / I_{Fire}$$

Eq. 3-46

Where, y is the distance from the centroid to the extreme fibre being considered. As the section becomes non symmetrical during burning the y value for the top of the section and for the bottom of the section become different as shown in Figure 3-17. It is important to maintain the sign convention that values above the centroid are positive and values below the centroid are negative. The y value for compression at mid-span and tension at the end of the member, in the top of the section should be taken as:

$$y = C_{Top}$$

Eq. 3-47

The y value for compression at the end of the member and tension mid-span, in the bottom of the section should be taken as:

$$y = -d + C_{Top} + Chardepth$$

Eq. 3-48

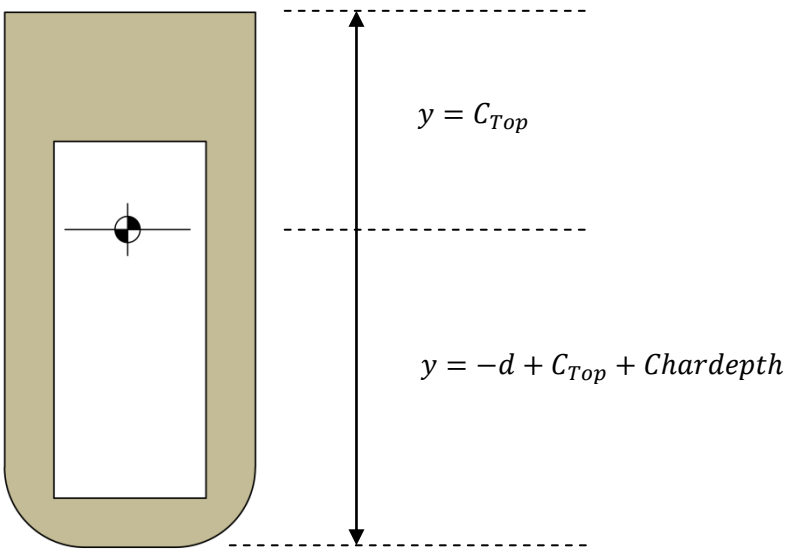

Figure 3-17: Distances from the centroid to the extreme fibers

The tensile or negative stress induced by bending is equal and opposite to the compressive bending stress as demonstrated in Figure 3-16. Therefore the mid-span top and bottom fibre stress can be calculated as:

$$\sigma_{TopChordMid} = \frac{F_{PT,fire}}{A_{T,fire}} + \frac{M^*_{fire}\, C_{Top}}{I_{fire}}$$

Eq. 3-49

$$\sigma_{BottomFibreMid} = \frac{F_{PT,fire}}{A_{T,fire}} + \frac{M^*_{fire}\,(-d + C_{Top} + Chardepth)}{I_{fire}}$$

Eq. 3-50

As M_{PT} is a negative by convention the maximum compressive stress at the end of the beam will be in the bottom flange. The end of beam top and bottom fibre stresses can be calculated as:

$$\sigma_{TopFibreEnd} = \frac{F_{PT,fire}}{A_{T,fire}} + \frac{M^*_{PT}\, C_{Top}}{I_{fire}}$$

Eq. 3-51

$$\sigma_{BottomChordEnd} = \frac{F_{PT,fire}}{A_{T,fire}} + \frac{M^*_{PT}\,(-d + C_{Top} + Chardepth)}{I_{fire}}$$

Eq. 3-52

The allowable stress capacity can be calculated as

$$\sigma_{Cn} = \sigma_{Tn} = \phi\, k_1\, k_{24}\, fb$$

Eq. 3-53

3.3.7. Shear

It is important to consider shear in two places in the cross section with post-tensioned timber members in fire. Firstly it is important to check the shear in the webs at the centroidal axis, as this is where the shear flow is maximum. Secondly it is also important during the fire case to consider shear at the bottom corners of the section. This is because the presence of corner rounding and the internal cavity can cause the timber to become thinner in the corners than in the web. The shear stress may be maximum at either position and therefore both must be checked.

Shear action

The shear flow, or shearing force per metre length, can be calculated between a discrete portion of the cross section and the rest of the cross section. The interface between these two sections can be considered as a "cut" through the section. The shear flow across this interface is dependent on the total shearing force applied to the member and the position of the cut. It doesn't matter which portion of the section is used to calculate the first moment of area, but sometimes one portion is easier to calculate than another.

The shear flow formula is:

$$q = \frac{VQ}{I}$$

Eq. 3-54

Where:

q is the shear flow at the cut (kN/m)

V is the shear force (kN)

I is the second moment of area (m^4)

Q is the first moment of area of one portion of the section around the section centroid (m^3)

Web Shear Action

As the shear flow is not constant through the web the action should be calculated at the centroid where the shear flow is at its maximum. The first moment of area for the portion below the cut is demonstrated in Figure 3-18. It is simpler to calculate the first moment of area for the upper portion

as it does not involve the rounded corners at the bottom of the section; however, for demonstration purposes the more complicated portion is presented.

To calculate Q the first moment of area of the portion below the centroid the shape must be broken into simple geometric shapes whose geometric properties are known. The shaded area in Figure 3-18 shows the portion for which the first moment of area (Q) will be calculated. In order to capture the geometry with simple shapes, three rectangular and one semi circular shape are used.

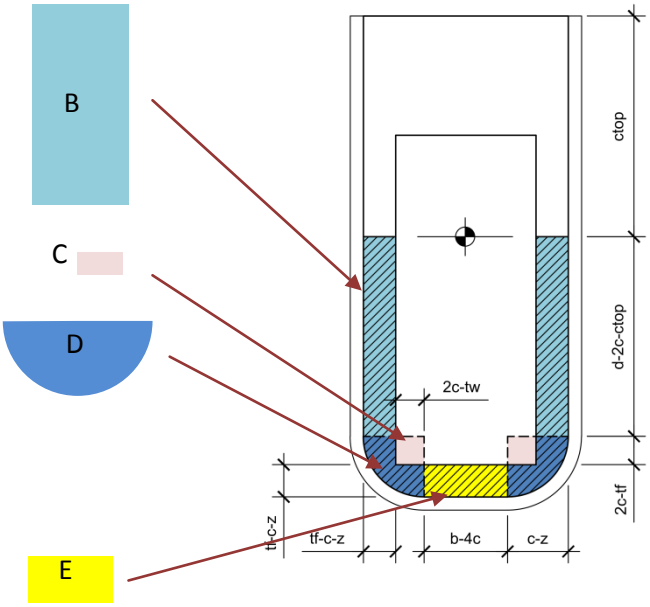

Figure 3-18: Geometric shapes used to calculate the shearing action in the web.

As the second moment of area and the centroid have already been calculated in Section 3.3.3, the Q calculation simply involves summing the product of the shape areas and their distances from the centroid of the section. The same geometric shapes are used as in the calculation of the second moment of area. Again as the geometry is complex and a negative area shape (C) is required.

$$Q_i = Area_i \times C_{Centroid}i$$

Eq. 3-55

$$Q_{w,fire} = \sum_{i=1}^{n} (Area_i \times C_{Centroid}i)$$

Eq. 3-56

Table 3-4: First moment of area for web shear calculation.

Shape	$C_{centroid}$	Area	1st Mom. Area
B	$C_{centroid}B$	$AreaB$	$C_{centroid}B \times AreaB$
C	$C_{centroid}C$	$AreaC$	$C_{centroid}C \times AreaC$
D	$C_{centroid}D$	$AreaD$	$C_{centroid}D \times AreaD$
E	$C_{centroid}E$	$AreaE$	$C_{centroid}E \times AreaE$
		$\sum Area$	$\sum 1^{st}\ Mom.\ Area$

Centroid shear action

For some beams with large flanges it may be that the centroid is within the top flange. If this is the case it is important to check the shear at both the web flange interface and at the centroid depth. For shear at the web flange interface the capacity will be calculated from the remaining thickness of

the webs. For the shear in the centroid in the top flange the capacity should be calculated from the remaining width of the top flange.

Corner shear action

The shapes used to create the required portion for which the first moment of area will be calculated are; a sector of a circle with angle 2α, a triangle and a rectangle. Again a negative shape is required to create the geometry of the corner. The shapes and their positions are shown in Figure 3-19.

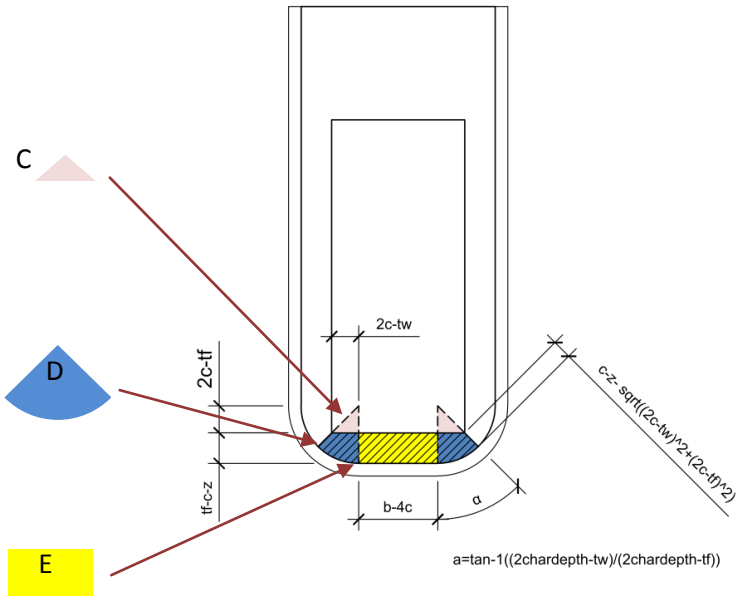

Figure 3-19: Geometric shapes used to calculate the shearing action in the lower corners.

The shear in the lower corner is slightly more complicated to calculate as the line of least thickness through the corner will depend on the position of the centre of the corner rounding radius and also the relative dimensions of the webs and flanges. The calculation is only valid when the centre of corner rounding radius is within the cavity. If this centre is not within the cavity the corner will not be the thinnest portion of the section.

The thinnest part of the section will lie on a line drawn from the centre of the corner-rounding radius through the corner of the cavity and extended outward. Examples of this are shown in Figure 3-20 for equal thickness webs and flanges. If the web and flange have the same thickness this line will always be 45° from vertical. Drawings C and D in Figure 3-20 show that if the centre of the charring radius is not within the cavity then the calculation method will give erroneous results and the thinnest part of the section will not lie in the corner. In example D the remaining web thickness will be thinner than the corner, and as the web will be designed according to its maximum shear at the neutral axis there is no need to check the shear in the corner. If the centre of the charring radius is in the webs as shown in example C the bottom flange will become the thinnest point and should still be checked.

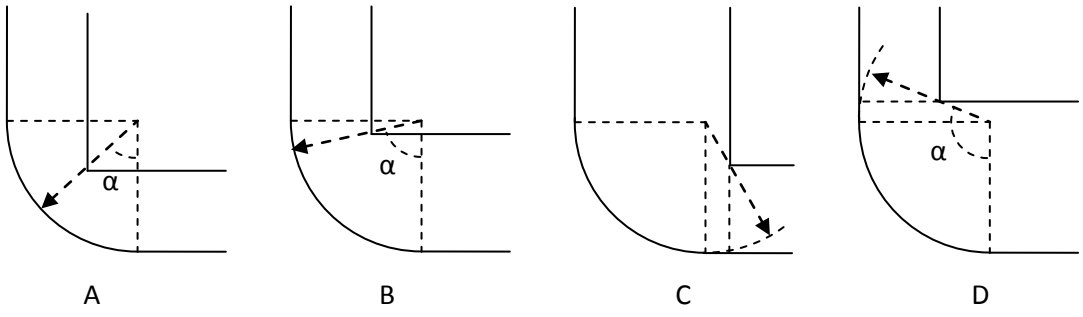

Figure 3-20: Calculation of the thinnest portion of the section in the bottom corner.

This line can be characterised by the angle α which can be calculated as:

$$\alpha = \tan^{-1}\left(\frac{2Chardepth - t_w}{2Chardepth - t_f}\right)$$

Eq. 3-57

$$Q_i = Area_i \times C_{Centroid}i$$

Eq. 3-58

$$Q_{w,fire} = \sum_{i=1}^{n}(Area_i \times C_{Centroid}i)$$

Eq. 3-59

Table 3-5: First moment of area for bottom corner shear calculation.

Shape	$C_{centroid}$	Area	1st Mom. Area
C	$C_{centroid}C$	$AreaC$	$C_{centroid}C \times AreaC$
D	$C_{centroid}D$	$AreaD$	$C_{centroid}D \times AreaD$
E	$C_{centroid}E$	$AreaE$	$C_{centroid}E \times AreaE$
		$\sum Area$	$\sum 1^{st}\ Mom.\ Area$

Nominal shear capacity

The shear capacity of the timber can be calculated if the effective width of remaining material is known. For ease the capacity can be obtained in terms of shear flow, kN/m. The nominal shear capacity can be calculated with the following formula:

$$\phi q_n = \phi t f_s$$

Eq. 3-60

Where:

ϕq_n, is the nominal shear capacity of the timber at the specified cut in the cross section.

ϕ, is the material reduction factor for timber, under fire conditions this is commonly taken as 1.0

t, is the thickness of the timber at the specified cut in the cross section.

f_s, is the characteristic shear stress in the appropriate orientation.

After this check, it is also important to ensure that the lower corner has some remaining thickness and has not burnt through. It is possible that the lower corner may burn through and the remaining beam still has enough capacity to resist the load, however the post-tensioning will be exposed to the fire and if this is relied upon the beam will fail shortly.

$$t_{c,fire} \geq 0$$

Eq. 3-61

Web shear capacity

The thickness of the LVL in the webs can be calculated as:

$$t_{w,fire} = 2(t_w - chardepth - zerostrength)$$

Eq. 3-62

The coefficient of two is because there are two webs in a box beam and the total thickness at the cut is used to calculate the shearing action and therefore capacity as shown in Figure 3-21. The thickness should include the 7mm zero strength layer in the timber due to thermal degradation.

Therefore the nominal shear capacity in the web can be calculated as:

$$\phi q_{w,n} = \phi f_s 2(t_w - chardepth - zerostrength)$$

Eq. 3-63

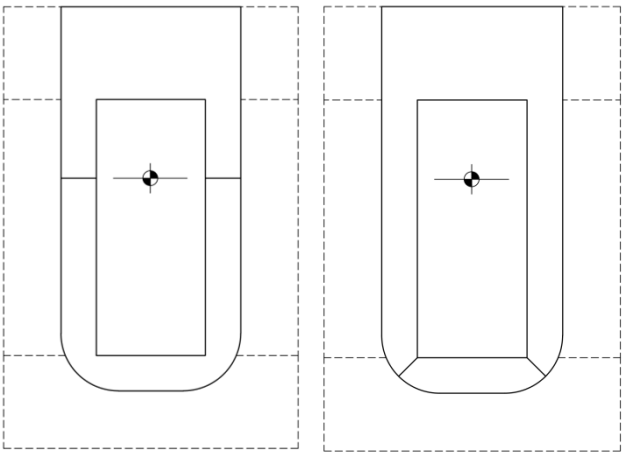

Figure 3-21: Web thickness (right) and corner thickness (left) for the calculation of shear capacity.

Corner shear capacity

The thickness of the LVL in the webs can be calculated as:

$$t_{corner,fire} = \min \left| \begin{array}{c} 2chardepth - 2\sqrt{(2chardepth - t_w)^2 + \left(2chardepth - t_f\right)^2} \\ 2(t_{flange} - chardepth) \end{array} \right.$$

Eq. 3-64

This thickness is calculated along a line from the centre of the charring radius passing through the corner of the section. Therefore the calculation breaks down if the centre of the charring radius is not within the cross section. If the centre of the radius is not inside the cavity then the corner thickness won't govern and the thickness should be taken as the remaining bottom flange thickness.

Therefore the nominal shear capacity in the web can be calculated as:

$$\phi q_{c,n} = \phi f_s t_{c,fire}$$

Eq. 3-65

Shear stress check

The member is adequate in shear if the nominal shear capacity exceeds the shear action in both the web and the lower corner after the allotted fire duration.

$$q_w^* \leq \phi q_{w,n}$$

Eq. 3-66

$$q_c^* \leq \phi q_{c,n}$$

Eq. 3-67

3.3.8. Dissipater fire resistance

In order to perform well under seismic conditions sacrificial mild steel members are used to dissipate energy. These dissipaters are often exposed in order to provide easy access to allow their replacement after a seismic event. In some designs these dissipaters might also be used to provide some moment resistance under the ultimate limit state gravity loading. As these dissipaters are small exposed steel members they do not have significant fire resistance.

However, fire resistance is not required if the frame is designed to resist the fire limit state loading without the dissipaters. The New Zealand Standard for structural design actions requires structures exposed to fire to resist the dead load and the long-term live load (often 40% of the live load). Therefore it is recommended to ensure the frame can withstand this loading for the desired fire duration without any assistance from the dissipaters.

If it is desirable to give the dissipaters some fire resistance, they can be protected in a similar manner to the post-tensioning anchorages. It is important to monitor temperatures developed within the dissipater for each protection method and ensure that the dissipater is capable of providing adequate resistance at the expected temperatures.

3.4. Chapter Conclusions

Chapter 3 introduced and outlined the recommended design methodology for post-tensioned timber under fire conditions. Limitations and comparisons of this design methodology are presented in Chapter 4.

Whilst the reality of a post-tensioned timber beam is complex and non-linear it is possible to obtain reasonable accuracy with a first order calculation. In order to design a post-tensioned timber beam for fire conditions the following steps are recommended:

- Calculate the remaining post-tensioning force including the effects of the tendons decreased strain, due to thermal expansion of the steel and the additional axial compression of the timber, and the reduction of young's modulus of the steel due to its elevated temperature.

- Find the actions on the timber beam including, bending, shear, and compression. It is important to consider actions from both the external loads and the post tensioning system.
- Calculate the reduced section properties using the parallel axis theorem.
- Calculate the stresses induced in the timber beam
- Check the appropriate design equations to ensure the timber can resist the stresses applied to it.

Parallel axis theorem is a simple calculation tool which can be used to analyse the effect of charring and the changing geometry on a beam during fire exposure. The charred cross section properties such as the second moment of area can be constructed mathematically from simple geometric shapes with known properties.

Tendon relaxation is estimated by assuming a temperature profile for the timber and assuming that the tendon is at the same temperature as the internal surface of the cavity within the timber. This is then used to calculate the thermal strain and the reduction in the modulus of elasticity of the tendon. These, when incorporated with any losses due to anchorage rotation and beam compression, are able to estimate the relaxation of the post-tensioning tendons.

It is important to check shear for post-tensioned timber members as the post-tensioning can substantially increase the bending capacity of a beam but does not affect the shear capacity. This can lead to higher loading resulting in higher shear actions. It was also found that it is important to check the shear stress in both the web at the centroid and in charred corners of the member. Whilst the shear flow is maximum in the web at the centroid the timber thickness at the bottom corner can be much thinner than the webs leading to a potentially greater shear stress.

It is important to include secondary effects in the analysis. The axial loads of the post-tensioning can induce bending moments in the beam due to not only their eccentricity but also a bowing effect very similar to P-delta effects. The axial loads induce a bending moment due to the beam's initial deflections. The additional deflections for this effect can be calculated iteratively.

3.5. Design Recommendations

Chapter 4 makes the following recommendations for the design of post-tensioned timber under fire conditions:

- Consider all potential failure mechanisms, including:
    - Combined bending and compression failure at mid span, specifically by checking top and bottom extreme fibre stresses.
    - Combined bending and compression failure at the beam anchorage, also by check top and bottom extreme fibre stresses.
    - Longitudinal shear in the webs at the centroidal axis.
    - Longitudinal shear in any charred corner which undergoes corner rounding.
- Monitor the remaining post-tensioning force on the beam
- Use a char rate of 0.72mm/minute and include an additional 7mm zero strength layer.
- Include secondary effects such as, axial bowing (P-Delta), anchorage rotation, and increased beam compression.

4. Comparisons and Discussions

This chapter presents comparisons of results from the full scale tests presented in Chapter 2, the proposed design method presented in chapter 3, and thermal numerical modelling which is presented in this chapter. The goal of these comparisons is to validate the proposed design method against the two successful tests, beam A and beam C, and to provide discussion on the testing, calculation, and modelling results. The thermal modelling is provided as a basis for potential future mechanical numerical modelling for post-tensioned timber members.

The numerical thermal modelling completed with Abaqus (Dassault Systèmes Simulia Corporation, 2010) is presented here, including results and discussion on the modelling process. A discussion on the results of the full-scale testing is also presented. Analysis of the simplified calculation method results are also presented and discussed. Then comparisons and contrasts are made between the full-scale tests, the simplified calculation method, and the thermal modelling.

4.1. Timber thermal modelling

Timber Is a complex material, and even more complex under fire conditions. The timber undergoes a dramatic change when it chars. Some of the material undergoes pyrolysis and is burnt but the remaining portion of the material remains as char. This char layer is much less dense than the timber which slows the heat transfer into the timber below it. Also, due to shrinkage, cracks form in the char layer which slightly diminishes its insulative properties. Timber charring is very complex and as of yet it has not been able to be numerically modelled reliably and simply enough to be useful for structural engineering purposes. However the process can be simplified to a thermal conduction problem. This involves incorporating the effects of the char layer, and its associated insulation and cracking, the thermal effects of pyrolysis, and the effects of moisture in the timber, into a set of effective thermal properties.

In order to thermally model timber in Abaqus for fire conditions there are a series of properties and inputs that are required. The geometry must be implemented in either one, two or three dimensions depending on the member and what is being looked at. The effective thermal properties for the timber must be defined. The geometry must be discretised or meshed into individual elements, and the element types must be defined.

Three main thermal properties are required to model temperature conduction; thermal conductivity (k), density (ρ), and specific heat (c_p). If there is a phase change, then latent heat (L) is also involved but is often incorporated into the specific heat value. Due to the complex nature of timber in fire and the changes which occur to timber these values are not constant, but vary with temperature. Many sets of properties have been published by various authors, a selection of which are discussed by König (König, 2006). For this modelling the values published in Eurocode 5 part 2 annex B were used (British Standard Institute, 2004b). Figure 4-1 shows the Eurocode timber thermal properties.

The density value given in the Eurocode thermal properties is a ratio of the timbers initial density. LVL density is increased due to the gluing and compression of laminates. As the charring largely isn't effected by the glue, using a higher density with the Eurocode properties may result in an un-realistically low charring rate. To compare this, the real density of the LVL (620 kg/m^3), the average published density of the radiata pine used to create LVL (510 kg/m^3) and an arbitrary lower density value of 450 kg/m^3 were used in modelling. The lower density value was used to try and capture the

comparatively faster charring rate of New Zealand LVL and pine in comparison to European pine, and is the characteristic density quoted for charring rates in Eurocode 5 Table 3.1.

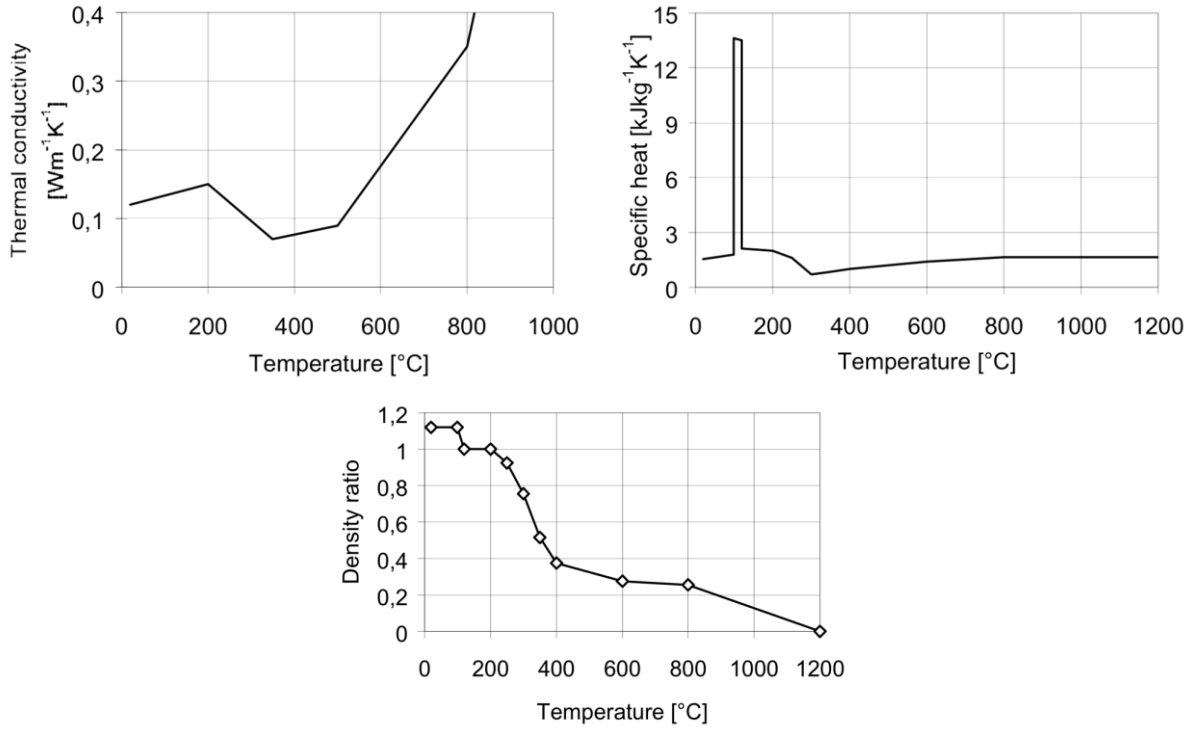

Figure 4-1: Eurocode 5 timber thermal properties

The latent heat of water evaporation has been included in the specific heat. The peak at 100°C corresponds with a moisture content of 12%. Because of the mechanics within Abaqus and other thermal models it can be sometimes useful to remove this peak from the specific heat and define it in as a latent heat value. When the software is solving for the temperature of an element and the temperature is changing rapidly it is possible that the specific heat peak may be skipped or may induce numerical instabilities due to the rapidly changing property. If the latent heat in defined as a latent heat in Abaqus the software is able to use an entropy calculation to calculate the timber temperatures. As the enthalpy function is a cumulative function of specific heat and latent heat the large peak is not used and the software is considerably more numerically stable. This allows for the use of larger mesh sizes and time steps leading to faster computation.

Other material properties are required to define the boundary interactions. The boundary is heated via convection and radiation. Convection requires a heat transfer coefficient and radiation requires an emissivity. Eurocode 1 part 2 section 3 provides a convective heat transfer coefficient of 25 W/m^2K and Eurocode 5 part 2 section 2 provides a timber emissivity of 0.8. Whilst these values also change over the duration of the fire they provide reasonable results. The flame emissivity and shape factor are taken as one because the member is assumed to be completely surrounded and immersed in the flame.

4.1.1. Model setup

For comparison to the full-scale test results beam C was modelled. The member was modelled with a 3 mm mesh size. A 3mm mesh is a good trade-off between geometric accuracy and computational complexity (Werther et al., 2012). Decreasing the mesh size beyond this yields limited increases in

accuracy and increases the calculation time substantially. The mesh was generated automatically with Abaqus. It was generated using the structured technique resulting in square and regular elements. The element type was two-dimensional 4-node heat transfer, DS4 in Abaqus notation.

A two dimensional slice of Beam C was chosen to be modelled (Figure 4-2), as the exposed temperature should not vary greatly along the length of the beam and modelling the beam in three dimensions would be computationally wasteful. Beam C was modelled with a width of 189mm instead of the full 190 mm so that it would line up with a 3mm mesh size. The beam depth was modelled as 300mm. The cavity dimensions are 63mm wide by 174mm deep which corresponds to a web and flange thickness of 63mm.The outside surface boundary was given an emissivity of 0.8 and a convective heat transfer coefficient of 25 W/m^2K on the lower three edges, the upper surface was left as adiabatic. This is to model three sided burning where the top edge is protected by the flooring system. The internal surfaces of the cavity were also left as adiabatic. A more complex cavity model could have been implemented such as incorporating radiative or convective interaction between an element representing a tendon and the cavity surface; however this was not completed during this research.

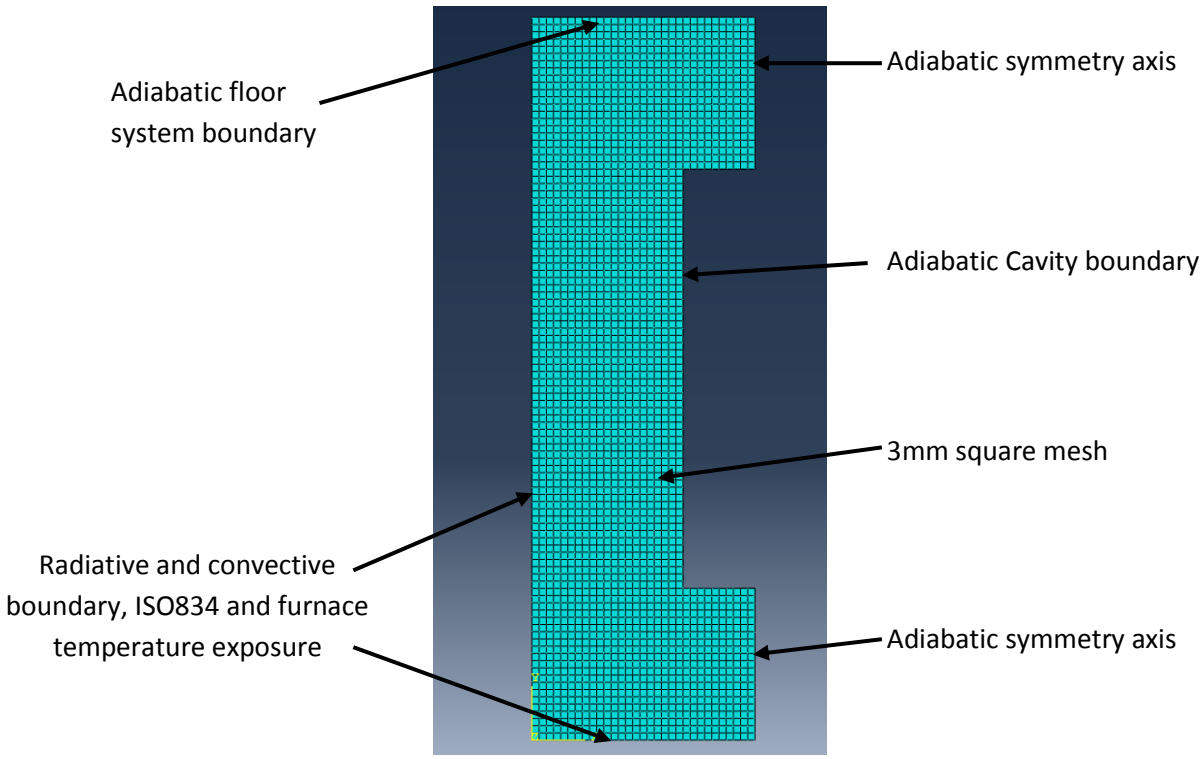

Figure 4-2: Abaqus screen shot showing model geometry and annotated boundary and mesh details

When using the latent heat/enthalpy model in Abaqus it is possible to use almost any time step. However, when using the standard model Abaqus requires very small time steps to avoid numerical instabilities. Abaqus allows a maximum, minimum and initial time step to be defined. When the solver is unable to find a solution or the solution is too large then the software automatically selects a smaller time step down to the minimum defined. For this modelling an initial time step of 1 second was defined with a minimum of 0.001 seconds allowed.

The exposed fire temperature modelled was that of the ISO834 standard fire. However in order to compare the modelling results and accuracy to the full-scale experiment, the furnace temperatures measured during the full-scale test were also used.

4.1.2. Results

The geometry of Beam C was modelled with the ISO834 standard fire exposure, the flange temperature profile is presented in Figure 4-3. This shows the progression of a thermal wave through the timber. Temperature is measured at points 0,6,18,27,39,51 and 63mm from the surface. This was designed to line up with the temperature measurement points in the full-scale testing, however due to mesh constraints some measurement points are 1mm away from the corresponding depth in the full-scale test. This is still within the accuracy at which the holes and thermocouples were placed in the timber and should therefore still provide comparable results.

The hottest data series presented below is the surface temperature; this was not measured during the full-scale tests however the darker cooler series all line up with a measurement point from the full-scale tests. There are small plateaus in each data series between 99 and 120 degrees. These are due to the effect of moisture evaporation captured by the inclusion of the latent heat of water in the modelling. The temperatures and the smoothness of the line are affected by mesh size, the results are usually more accurate and the series are usually smoother for smaller mesh sizes. Through trial and error it was found that a mesh size of 3mm yields a good trade off between accuracy and smoothness, and the computational complexity and therefore time required to run each simulation (Werther et al., 2012).

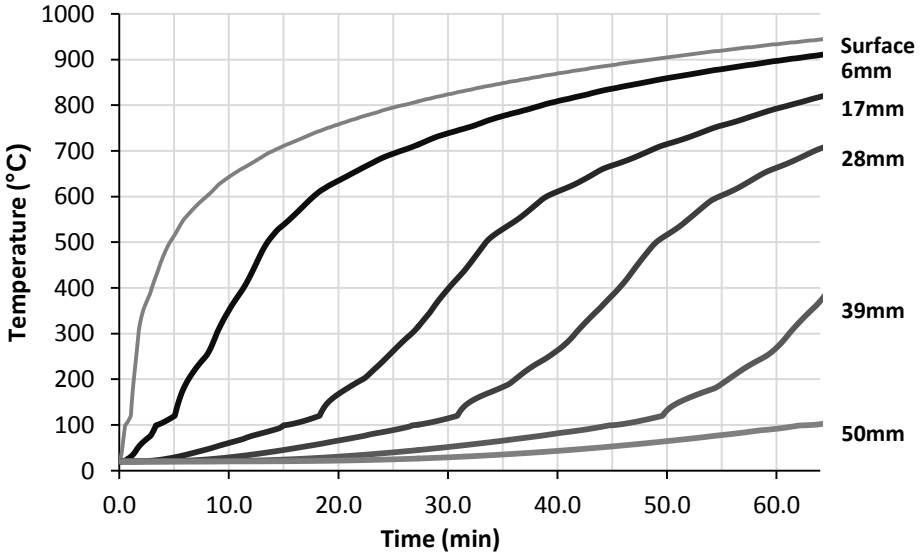

Figure 4-3: Typical timber temperature distribution for a 63mm bottom flange of a post-tensioned timber member. Numerical thermal model, flange temperatures, density: 510 kg/m^3, ISO834 exposure.

Figure 4-4 demonstrates the minor difference in temperatures between the web and flange of a box beam that were captured by the numerical model. This simulation did not take into account any difference in radiation view factors between the vertical webs and the horizontal flanges, or the radiation lost to the potentially cooler roof or other surroundings. These simplifications are valid assuming the member is completely submerged in flame which is optically thick, because the distance to the radiator or flame is very small which forces the radiative view factor asymptotically towards unity.

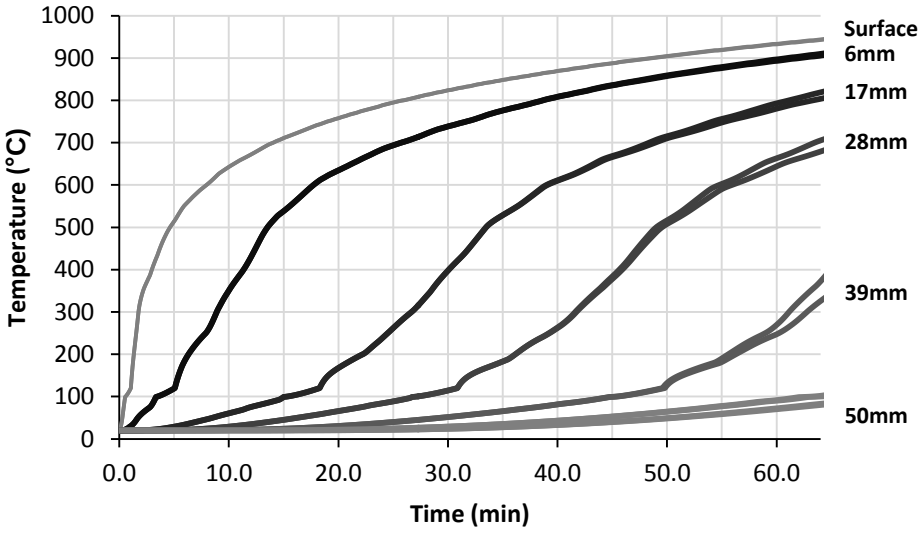

Figure 4-4: Numerical model results: Temperature distribution comparison between flange and web of beam. For each depth two curves are presented representing the flange (hotter) and the web (cooler).

The thermal penetration is strongly effect by the material density. The temperature distributions for densities of 480, 510 and 620 kg/m^3 are presented in Figure 4-5. Char rates were calculated from these distributions based on the 300°C isotherm. The 27mm depth temperature series was used to calculate these char rates for each density and have been presented in the first row of Table 4-1.

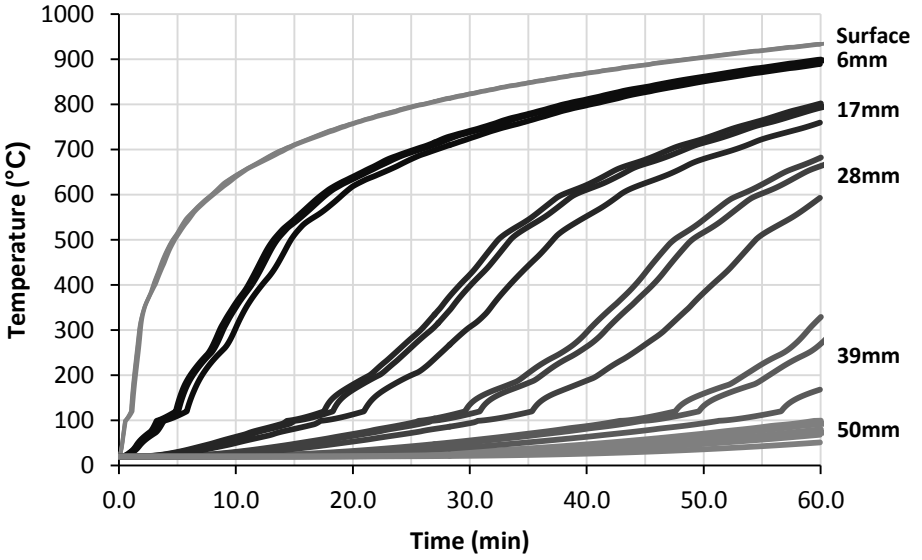

Figure 4-5: Numerical model results: Temperature distribution comparison for different wet density values including 12% moisture. For each depth 3 curves are presented from the left to right they represent densities of 480, 510, 620 kg/m^3.

The ISO834 standard provides a set of tolerances because it is difficult to achieve an exact temperature profile. As such, the actual furnace temperatures vary slightly from the ideal ISO834 fire. In order to compare the numerical thermal modelling results as closely as possible to the full-scale tests the actual furnace temperature in the centre of the furnaces was also used as the fire exposure input in the numerical modelling. The effect of the differing exposed temperature profiles on the internal temperature distributions has been presented in Figure 4-6. The 300°C isotherm char

rates for 27mm of depth were again calculated and are presented in the second row of Table 4-1. These both show that the effect of the differing fire exposure temperatures is small, and becomes lesser at greater depths.

Table 4-1: Numerical model results: Calculated char rates for the 300°C isotherm for a depth of 27mm.

	Density including 12% moisture, ρ		
	480	**510**	**620**
ISO834 exposure	0.672	0.649	0.578
Furnace exposure	0.677	0.653	0.584

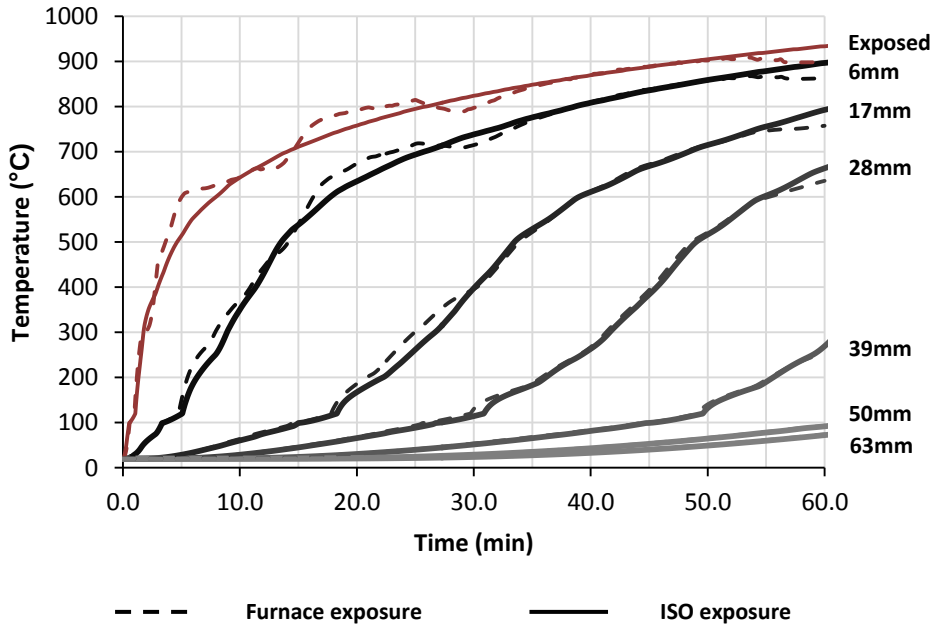

Figure 4-6: Numerical model results: Temperature profile comparisons for ideal ISO834 fire and the actual exposed furnace profile of the full-scale test.

The corner rounding can be estimated by tracking the 300°C isotherm and then fitting a circular curve to it. In Abaqus the char layer can be visualised by setting the limits of the temperature colour map to a minimum of 300°C and a maximum of 500°C. This will then show the 300°C and 500°C isotherm as the boundaries between the rainbow temperature contour map and the solid grey colours. Dark grey represents uncharred timber and light grey represents material which has been burnt away, the rainbow contour represents the char layer. AutoCAD was then used to fit a circle tangent to the three lines shown in Figure 4-7. The result of this was a circle of radius 40.8mm.

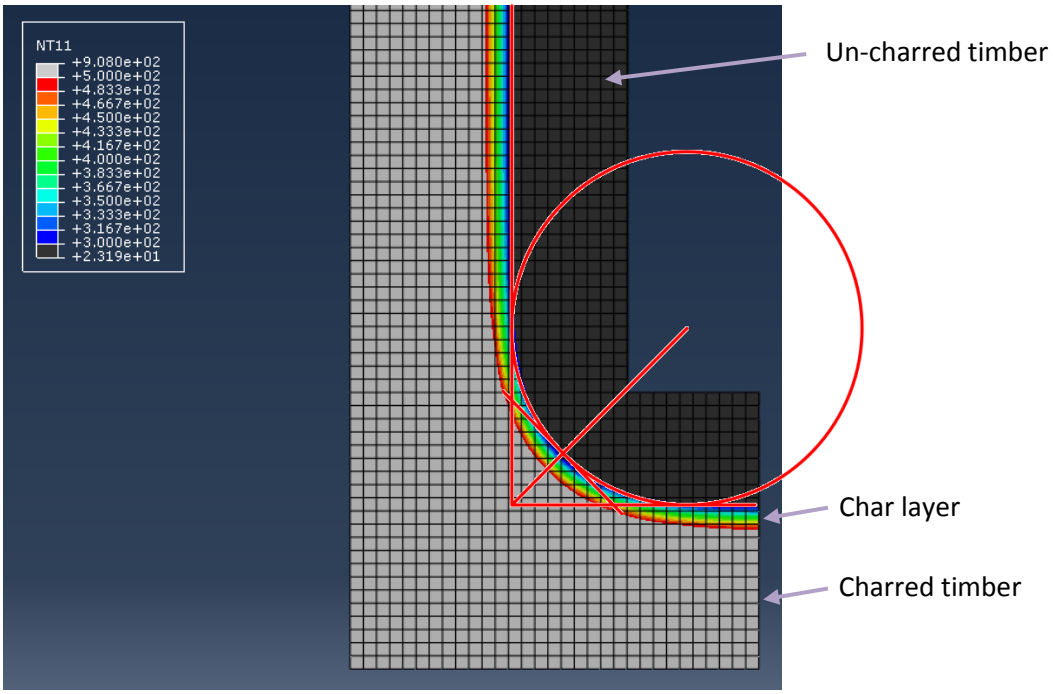

Figure 4-7: Abaqus 300°C isotherm and AutoCAD overlay. Dark grey: Un-burnt timber, Rainbow distribution: Char layer.

The temperature of the inner cavity surface was tracked at the centre of the web and bottom flange, and the lower corner of the cross section. It was expected that the temperature in the corner would be greater than at the web and flange. The middle of the, webs and bottom flange are exposed to approximately 1D heating and charring where as the corner is being heated from two directions which causes the corner to round and the expected temperature increase. Figure 4-8 shows that the corner temperatures were above those of the webs and bottom flange but only by less than 10°C for most of the fire duration.

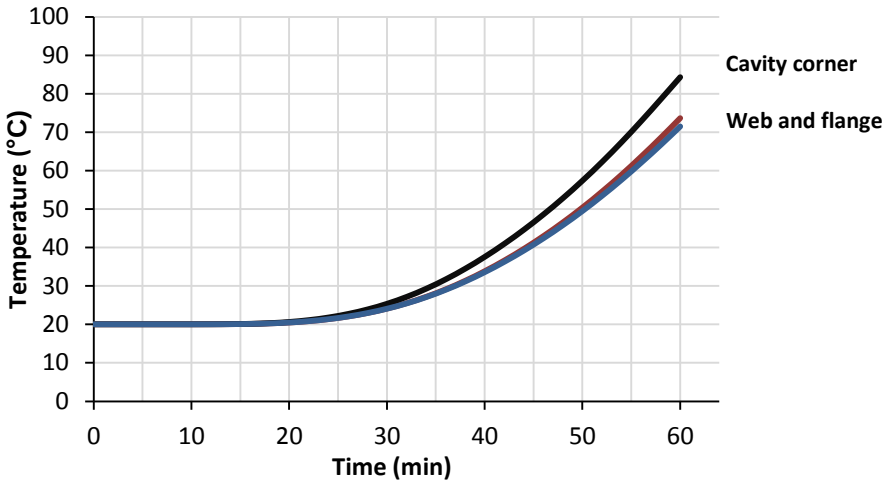

Figure 4-8: Numerical model results: Cavity surface temperatures as determined by 2D thermal modelling

4.2. Full-scale experiment discussion

The full-scale tests described in Chapter 2, provided thermal data for post-tensioned timber cross sections. Presented here is a brief overview of the relevant test details and results processed in a way to make them comparable to the thermal modelling and the simplified calculations. For more information on the full-scale tests, particularly the mechanical response, refer to Chapter 2.

The dimensions of Beam C were 300mm high by 190mm wide with web and flange thicknesses of 63mm. Timber material is LVL13 from Carter Holt Harvey New Zealand. The beams were exposed to an ISO834 standard fire.

4.2.1. Thermal properties

The thermal properties of timber are difficult to determine at ambient temperature and even more difficult and impractical to measure during fire exposure. This is due to the complex process of timber charring and combustion, which involves phase changes, moisture migration, pyrolysis, density changes, and many other complicating factors. Therefore it is not possible to present a set of thermal properties that are comparable to the properties used in the numerical thermal modelling above.

The simplest thermally relevant properties able to be measured or determined are the ambient density, the char rate when exposed to a standard fire and the moisture content. Also due to the nature of timber, only approximate average values for any of these properties are able to be measured. The density of the LVL used is quoted by the manufacturer as 620 kg/m^3. This density is larger than that of the timber used to create it. The radiata pine quoted density is between 460 and 560 kg/m^3 the central value of this range is 510 kg/m^3. The manufacturers quoted charring rate for LVL is 0.72mm/min which includes the loss of strength and stiffness of timber due to thermal degradation, or 0.65 mm/min which requires an additional 7mm zero strength layer to be incorporated. Neither of these quoted charring rates include the effect of corner rounding on solid members. The commonly assumed moisture content for timber is 12%. This can be used to calculate the latent heat of vaporization of water per kilogram of timber. The latent heat of water is 2,260 MJ/kg$_{water}$ to convert this to per kilogram of timber it is multiplied by the water content of 12% giving a value of 271.2 kJ/kg$_{timber}$.

4.2.2. Temperature distributions

The temperature distributions measured during the full scale tests were measured at depths of 6, 17,28,39,50, and 63mm from the exposed surface. Presented in Figure 4-9 are the temperature distributions of the flange and web of Beam C during the ISO834 fire exposure. The web temperature lagged approximately 4.5 minutes behind the flange temperature 6mm from the surface but caught up further into the timber. At 17mm depth the web lagged approximately 3.5min behind and at 28mm depth lagged only 1.5min behind. These values are calculated at 300 °C. The maximum difference in temperatures occurs between 100 and 600 °C; above and below these temperatures there was only a small difference in temperature. 6mm from the surface at 15 minutes the flange is approximately 125°C hotter than the web. At 30 minutes, 17mm below the surface the flange is approximately 66°C hotter and at 45 minutes, 28mm from the surface the flange is only 26°C hotter than the web.

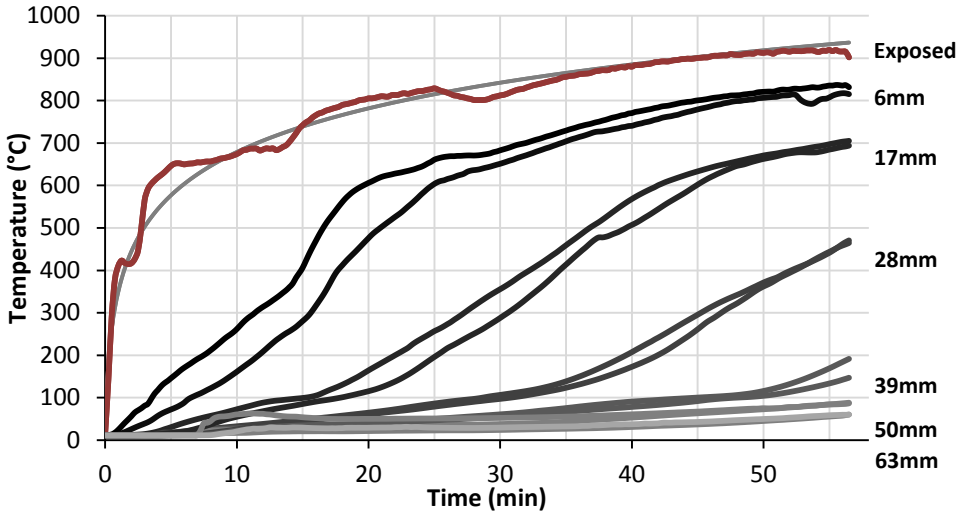

Figure 4-9: Full-scale furnace tests, Beam C, web (cooler) and bottom flange (warmer) temperature distributions.

The temperatures measured on the internal surface of the beam's cavity vary slightly with their position. All the temperatures stayed below 100 °C. The temperatures which were recorded on the web and the flange showed some anomalous peaks and fluctuations in heating in Beam C (Figure 4-10) which may have been due to their proximity to the plugs of timber which were wired with thermocouples and glued into the beam for temperature recording. These peaks also differed randomly with the plugs position along the beam. The temperature recordings in the corners of the beam were consistent and closely spaced with no peaks or jumps in the temperature. Figure 4-11 shows a similar scatter for Beam A; however there are no sharp jumps in temperature but still a number of variations. This may be partly due to noise in the measurement being recorded or some process happening which causing these fluctuations in temperature such as moisture being driven off the timber and a steam jet extruding from the plugs and impinging on the thermocouples.

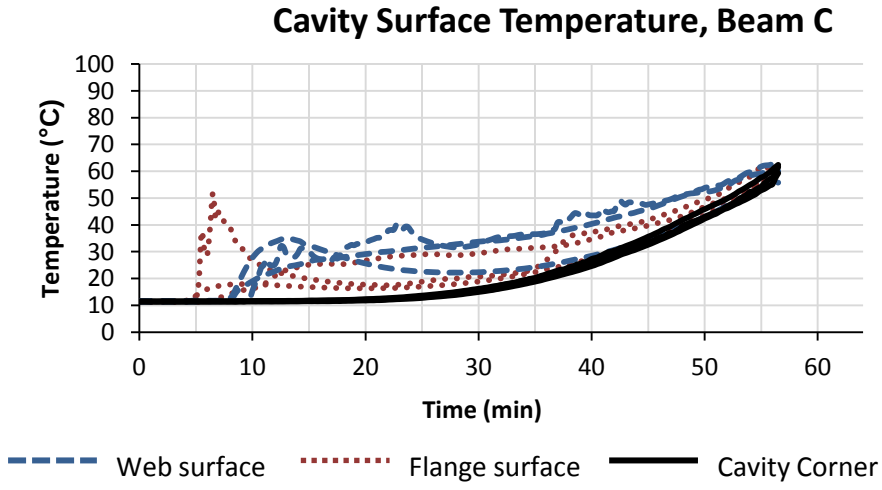

Figure 4-10: Beam C, cavity internal surface temperature on the web flange and bottom corner.

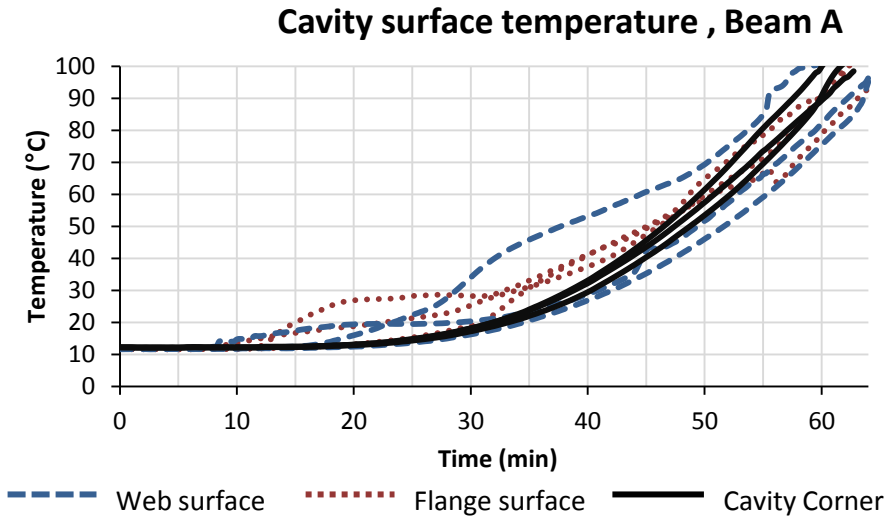

Figure 4-11: Beam A, cavity internal surface temperature on the web flange and bottom corner.

4.2.3. Char rate

The char rate of the full-scale tests can be determined in two main ways; calculation from the 300°C isotherm, and by physically measuring the char depth after the test. Calculating the char depth from the 300°C isotherm can yield results that are more precise, but the assumption that 300°C depicts the surface of the char layer is somewhat arbitrary, the result may not be as accurate as implied by the calculations precision. It is also difficult to know that the act of measuring temperatures within the wood doesn't affect the results. The holes drilled for the thermocouples may allow hot gasses to enter the area around each thermocouple early. Likewise measuring the char depth after a full-scale test is difficult. It is difficult to expose the char surface and to determine exactly where it is. The black char layer can be scraped away to expose un-charred but heat effected material of varying shades of dark brown. This layer of darkened but un-charred timber is multiple millimetres thick. There is then the difficulty of measuring depth from the original surface which no longer exists. The method used to get around this issue was to subtract the remaining thickness of the timber material from the original thickness. These difficulties lead to an estimated uncertainty of ±2-3mm.

There are also difficulties in estimating the actual charring time of the timber. The test may have been ended and measured at a specific time however the timber in the furnace is still hot and continues to decompose. There are approximately 5 minutes required to remove the loading frame and then lifting the specimen somewhere where it can be hosed down. The temperature exposed to the timber during this time was however much lower than the ISO834 temperatures. An effective additional charring time was estimated at 2 minutes per test.

The 300°C char rates are presented in Table 4-2. The depth used for calculation was determined as the deepest thermocouple which reached 300°C during the test. The char rate was then calculated for every measurement plug and the average value is presented. The 80% confidence interval error and a ±1mm positional error were combined and also presented.

Because beam B was not exposed to the fire for very long only the 6mm deep thermocouple reached above 300°C. This meant that the ±1mm error had a large influence on the total error. For the other beams the statistical error was dominant with the positional error accounting for only 2-4% error.

Table 4-2: 300°C isotherm char rates calculated from experimental data, repeated from Section 2.3.

	Char Depth (mm)	Char Rate (mm/min)	Error (mm/min)
Beam A	39	0.74	0.11
Beam B	6	0.61	0.20
Beam C	28	0.61	0.08

The measured char rates are presented in Table 4-3. The char depths were measured from cut cross sections exposing the un-burnt timber and the temperature-affected timber. Also measured and presented is an estimated corner rounding radius.

Table 4-3: Char rates measured from full-scale test, repeated from Section 2.3

	Char time (min)	Char Depth (mm)	Charring rate (mm/min)	Corner rounding (mm)
Beam A	66	47.5	0.72	20-25
Beam B	25	18	0.72	20
Beam C	58	40	0.69	30
Anchorage members	58	42	0.72	30

4.2.4. Inside corner temperature

The cavity corner temperature was recorded to provide data which would allow some comparison of the 2D heat transfer in the corner of the section. The corner temperatures are presented in Figure 4-10 and Figure 4-11 where they are presented in comparison to the cavity temperatures on the webs and bottom flange of the beam. The temperatures stay below 70°C during the test and are on average slightly cooler than the average web and flange temperatures for Beam C. It was expected that they would be warmer than the web and flange surfaces as the corner thickness is thinner due to corner rounding and the increased heat flux due to the beam corner. The slightly cooler values are probably due to the unexpected fluctuations in temperature in the web and flanges and may not be significant.

4.2.5. Tendon temperature

The temperatures of the tendons in Beam C are presented in comparison to the timber cavity corner temperatures, in Figure 4-12. The tendons temperatures were measured at three positions along the tendon and there were two tendons, each of these temperature profiles are plotted below. There is only small scatter between the measurement points indicating an almost homogenous temperature distribution along the tendons. The tendons showed no real deviation from the timber surface temperature for 30 minutes then the timber started to increase in temperature at a faster rate than the tendon.

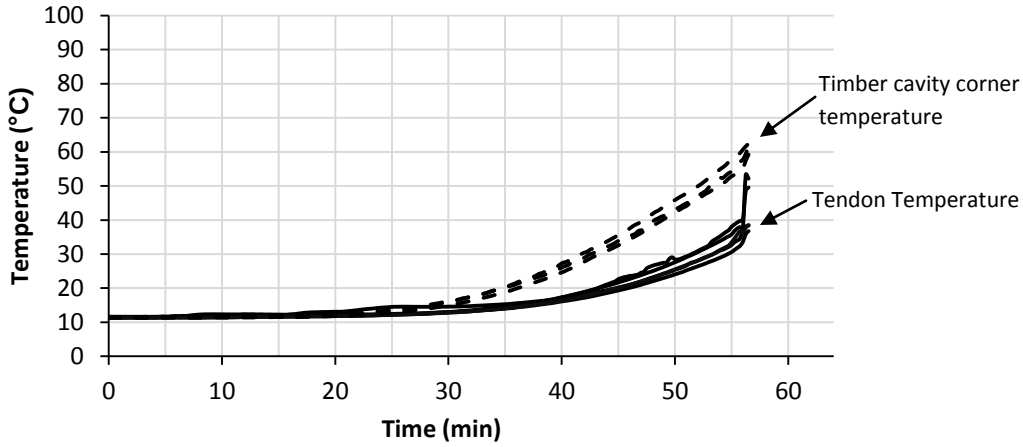

Figure 4-12: Tendon temperature compared to timber surface temperature, Beam C

4.2.6. Simplified calculation method discussion

Char rate

Eurocode 5 and NZS3603 state that the charring rate of LVL should be taken as 0.65mm/min. The Eurocode provides more detailed advice on charring rates depending on the type of timber and its density. The 0.65mm/min char rate is for LVL with a characteristic density of greater than 480 kg/m^3. NZS3603 provides a blanket char rate of 0.65mm/min regardless of the type of timber or its density. Both codes are intended for use with rectangular cross sections and have methods for taking corner rounding into consideration. The Eurocode provides two charring rates one for one dimensional charring which ignores corner rounding, and another slightly faster notional charring rate which is meant to implicitly take the corner rounding of a rectangular section into account. NZS3603 takes the corner rounding into account by assuming the corner radius is equal to the char depth and calculating section properties with this geometry.

The LVL manufacturer, Carter Holt Harvey Wood Products, provides some recommendations on char rates in their LVL design information. Their recommendations apply to LVL at least 90mm thick. The recommendation is to use a char rate of 0.65mm/min but to include a 7mm zero strength layer in the calculations, or to use a char rate of 0.72mm/min which does not require an additional zero strength layer to be included. These recommendations are based on research by Warren Lane (Lane, 2005).

The char rate which is recommended in this research for the design of post-tensioned timber members is 0.72mm with an additional 7mm zero strength layer. This char rate gave the best correlation between expected failure times and the actual failure times during the full scale testing. These values are higher or more severe than the existing published char rate recommendations and are discussed and justified later in Section 4.6.

Temperature distribution

The simplified temperature distribution beneath the char layer presented in Structural Design for Fire safety (Buchanan, 2001) can be used to calculate simplified temperature distributions for given depths in the same form as those measured during the full scale testing. The temperature distribution can be calculated for a given charring rate. The charring rate dictates the speed at which

the pyrolysis temperature, T_p, isotherm moves through the cross section. The thickness of thermally effected timber, a_{heated} dictates the width of the parabolic temperature distribution. This method can only be used to estimate temperature values below T_p which has been assumed as 300°C.

$$T(x) = T_i + (T_p - T_i)\left(1 - \frac{x}{a_{heated}}\right)^2$$

Eq. 4-1

The values of β and a_{heated} can be tuned to change the shape of the distribution. With the values $a_{heated} = 35mm$ which is recommended by Janssens and White (Janssens and White, 1994) and $\beta = 0.65mm/min$ which is recommended by the LVL manufacturer and NZS3603, the temperature distributions do not match the recorded distributions very well. Figure 4-13 depicts the simplified distributions with these values compared with the temperature distributions measured for beam C. At depths 39 and 50 mm the distribution matches better and is reasonably conservative.

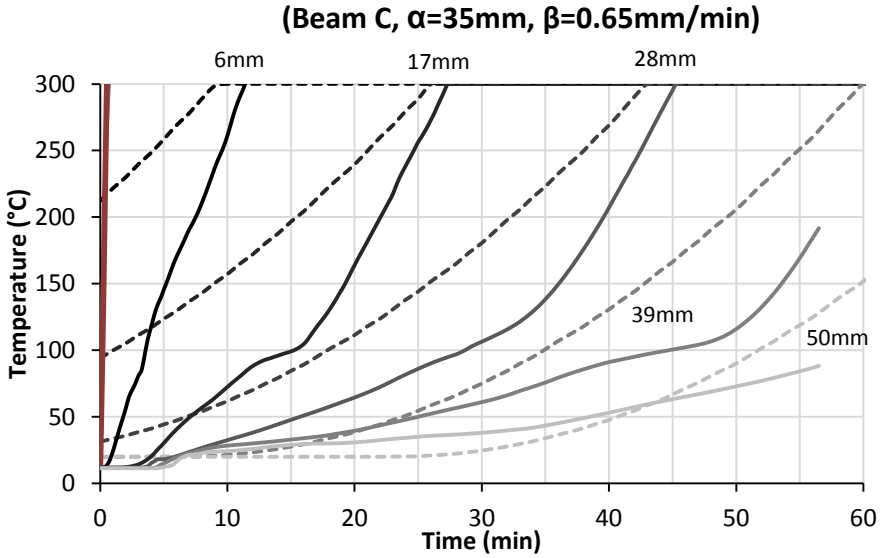

Figure 4-13: Simplified temperature distribution. a=35mm, B=0.65mm/min

A better fit can be achieved for the Beam C temperature distributions with the values $a_{heated} = 17mm$ and $\beta = 0.62mm/min$ which were found through trial and error and simple optimisation. These temperature distributions are presented in Figure 4-14. The char rate value was tuned by matching the time for the simplified profiles to reach 300°C with the time the measured profiles crossed 300°C. This shows that the progression of the char layer or the 300°C isotherm is reasonably constant, except for early and close to the surface. The a_{heated} values were then tuned by matching the slope of the two distributions. These values predict the timber temperature with some accuracy above 100°C and below 300°C.

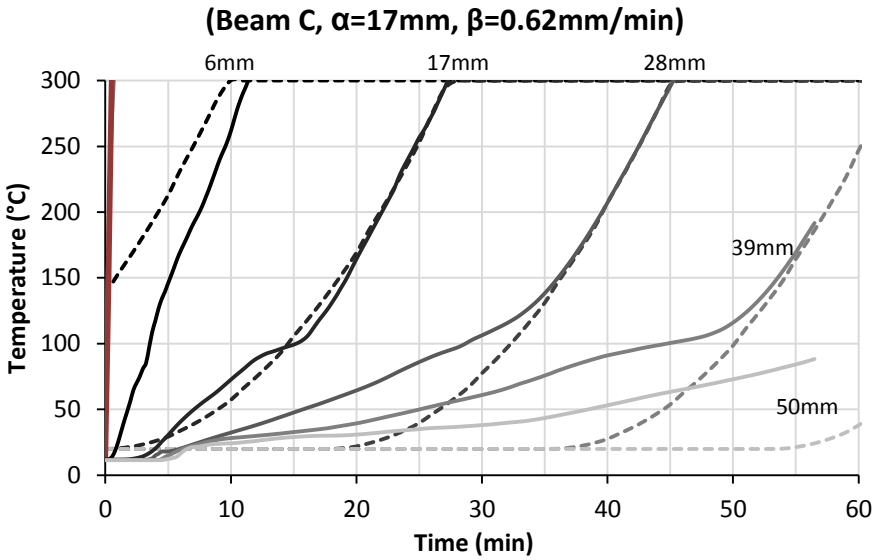

Figure 4-14: Simplified temperature distribution (Beam C). a=17mm, B=0.62mm/min

As with the Beam C temperature distributions, the simplified temperature distribution can be fitted to the Beam A temperature profiles. However the values required to match the profiles differ. Beam A is more closely matched with the values $a_{heated} = 22mm$ and $\beta = 0.74mm/min$. This shows how sensitive the distributions are on the char rates and the depth of temperature effected timber assumed. This is presented in Figure 4-15.

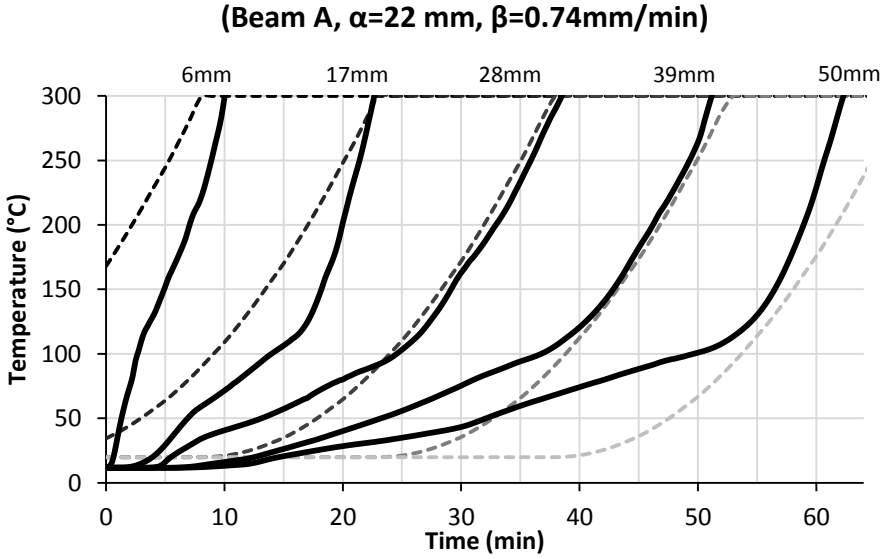

Figure 4-15: Simplified temperature distribution (beam A). A=22mm, B=0.62mm/min

Inside Surface temperature and tendon temperature

Using the same technique as mentioned above the temperature of the internal surface can be calculated over time. This method ignores any increased heating due to the insulation of the cavity. In reality the timber would heat slightly faster because the air in the cavity does not remove heat as efficiently as conducting it away into other timber. Also this method is only as good as the $T(x)$ calculation model. This model fails to capture some of the complexity of charring timber but for certain depths and applications it can be tuned to give reasonable results. Figure 4-16 shows the

calculated timber surface temperature in comparison to the temperature measured in beam C as presented previously. It shows that with the values $a_{heated} = 40mm$ and $\beta = 0.65mm/min$ the calculated temperature mimics the actual temperatures, which gives results slightly cooler than measured.

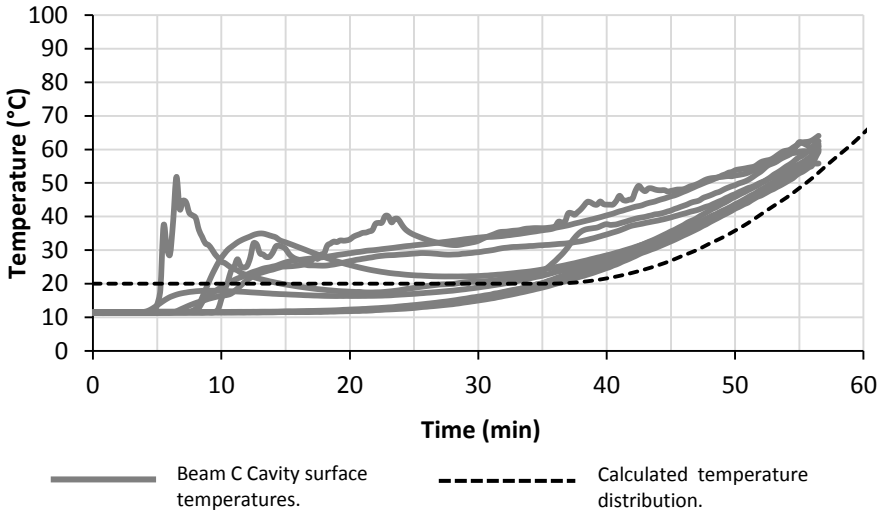

Figure 4-16: Cavity surface temperature profile, a=40mm, B=0.65mm/min

It should be noted that it changing other values, such as the ambient temperature value, drastically changes the temperature profile. It may seem that a better match may be obtained by inputting the actual $T_i$value of 12°C, however changing this value changes the rest of the profile making it an even worse match for the measured results.

4.3. Timber thermal comparisons

There was a strong agreement between the full-scale temperature distributions and the thermal modelling. The thermal modelling and full-scale test temperature distributions are presented for comparison in Figure 4-17. The best agreement was found when a density of 510 kg/m^3 was used. This is the published average density of the Radiata Pine used to manufacture the LVL. There is a very close agreement between the results below 100°C. The disagreement is greatest between 100°C and 600°C. The depth of 28mm shows the most disagreement. The difference becomes less pronounced deeper into the timber section and for the 60-minute exposure, depths greater than 50mm show very little deviation.

The exposed temperature used for the thermal modelling was taken from the full-scale tests. The fire profile was taken from the four furnace temperature probes closest to the thermocouple plug used for comparison. The results shown in Figure 4-17 are from the full-scale test of Beam C and the thermal modelling completed here.

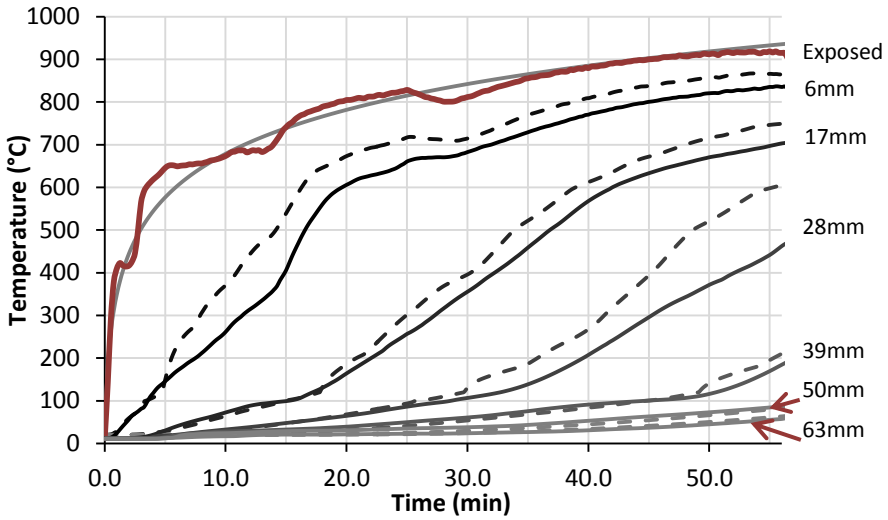

Figure 4-17: Comparison between full-scale thermal profiles (solid lines) and the results of 2D thermal modelling (dashed lines)

The thermal modelling gave a 300°C isotherm char rate of 0.65 mm/min. This numerical char rate was determined with a density of 510 kg/m^3, which relates to the density of the timber material used to create the LVL not the density o f the final LVL product. These results are discussed above in Section 4.1.2. The full scale testing gave a modal (most common number) measured char rate of 0.72 mm/min and a mean (average) measured char rate of 0.68 mm/min. The manufacturers recommended char rates are 0.72 mm/min and 0.65mm/min with an additional 7mm zero strength layer, which were determined by Lane (2005) based on his furnace testing of solid beams and his small scale cone calorimeter tests. The average measured char rate compares reasonably with the numerical model char rate of 0.65 mm/min and the manufacturers recommended char rate of 0.65 mm/min with an additional 7 mm zero strength layer. The modal measured char rate compares very well with the manufacturers recommended char rate of 0.72 mm/min with no additional zero strength layer.

The agreement between the temperature development in the full scale tests is practically reasonable and conservative but could be stronger. Furnace testing is not as accurate as smaller scale testing. There are a large number of variables and parameters which affect the tests. These include physical inaccuracies in thermocouple placement, material dimensions, and the inherent variability in thermocouples. Also the furnace temperature is not perfectly even everywhere. Some areas are exposed to higher temperatures than others; this was also difficult to measure as the thermocouples measuring the furnace temperatures are not located near the specimens. There is also some variability and inaccuracy with numerical thermal modelling. Parameters such as mesh resolution, timestep sizes and numerical techniques also slightly alter the results. This has been explored in more detail in Werther et al (2012).

The internal cavity temperatures have also been compared, and are presented in Figure 4-18. The modelling results have been shifted by -8°C to match the ambient temperature during the test. The thermal modelling again shows a close match to the data recorded during the full-scale test. The largest discrepancies are seen in the flange and web measurements. The flange and web temperature measurements exhibit the unexpected jumps and variation that were discussed previously. The corner temperature results match the measured temperature very closely with a

difference of less than 5°C. The web and flange measurements match very closely before 5 minutes in the flange and 10 minutes in the web. They also match with reasonable accuracy after approximately 40 minutes but still show a 10-20°C difference with the modelling results being cooler.

The thermal modelling results for the web and flange are cooler than the measured results. This is due to the anomalous temperature readings during the test possibly due to moisture migration or warm gases escaping though small gaps not filled with glue. However because the surface temperature is not in itself an important value and is only used to estimate the tendon temperature which will always be slightly cooler than the timber temperature, the temperatures are still useful and valid.

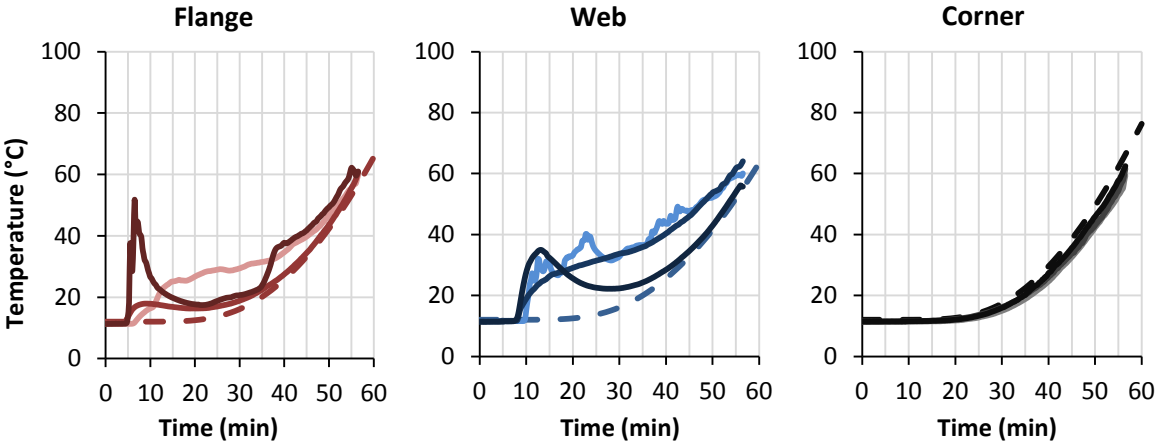

Figure 4-18: Cavity surface temperature comparison between full-scale test results and thermal modelling results

The hand calculation method of estimating the temperature of the inner surface of the timber has been shown to provide reasonable results, and is able to be used to estimate the tendon temperature conservatively. The hand calculation method gives results slightly cooler than those observed on the timber surface but approximately 10°C higher than the tendon temperatures recorded anywhere in the cavity. The temperatures of the timber cavity surface, the tendons as recorded during the full-scale test, and as predicted with the hand calculation method are compared in Figure 4-19. The timber cavity temperatures presented are those recorded in the corner of the cavity. This is because they were most stable in comparison to the web or flange measurements.

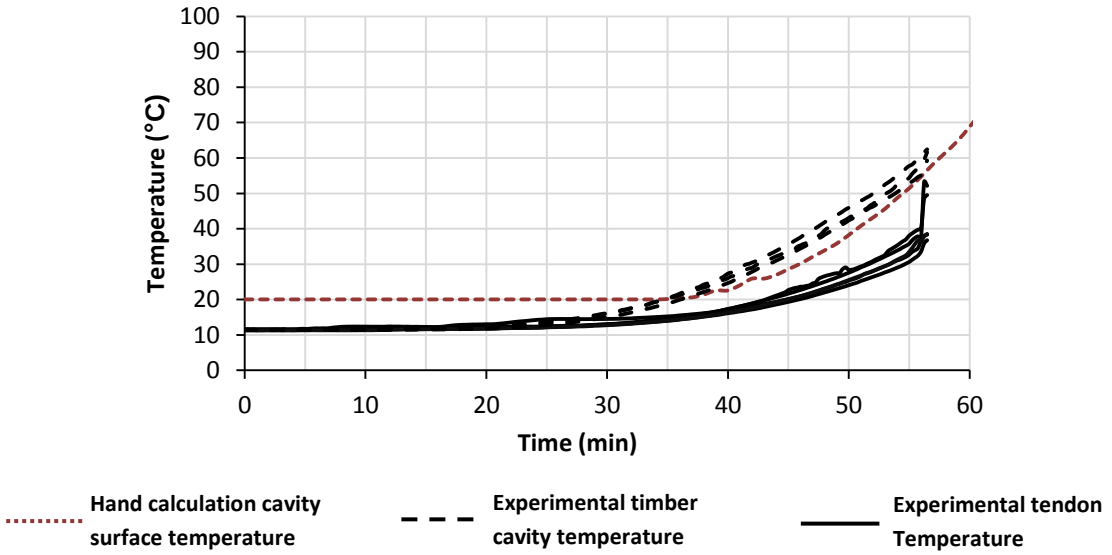

Figure 4-19: Tendon temperatures as estimated by hand calculations and as recorded during full scale testing of beam C.

The corner-rounding radius, calculated and modelled, closely agree with each other. However, the measured corner-rounding radius was smaller than predicted. The hand calculation prediction based on the corner radius being equal to the char depth and the char rate being 0.72mm/min gives a corner radius of 41.8mm after 58 minutes of fire duration. The thermal modelling after 58 minutes of fire duration fits a circle of 40.8mm radius. The full-scale test gives a corner-rounding radius of approximately 30mm. Measuring the corner radius after a fire test is not easy and is therefore not very accurate.

The corner rounding during the test may have been affected by phenomenon not modelled or expected for the hand calculation methods. The hand calculation method is only an approximate method and in most situations is only used to calculate section properties for rectangular cross sections. This may mean that its inherent accuracy is not intended for modelling the corner radius in a lot of detail. However both the hand calculations and the thermal modelling methods are still conservative giving larger radiuses than measured, which in turn gives a thinner corner thickness and more material loss.

Table 4-4: Corner rounding as calculated, modelled and measured for Beam C

	Hand Calculation (0.72mm/min)	Thermal Modelling	Full Scale Test
Corner radius (beam C)	41.8mm	40.8mm	30mm

4.4. Tendon relaxation

The tendons relaxed their post-tensioning force as they increased in temperature. The relaxation remained less than approximately 5% while the temperature of the tendon remained below 20°C which is an 8°C rise from ambient temperatures. The tendon temperature and loading profiles of the full-scale tests are presented in Figure 4-20.

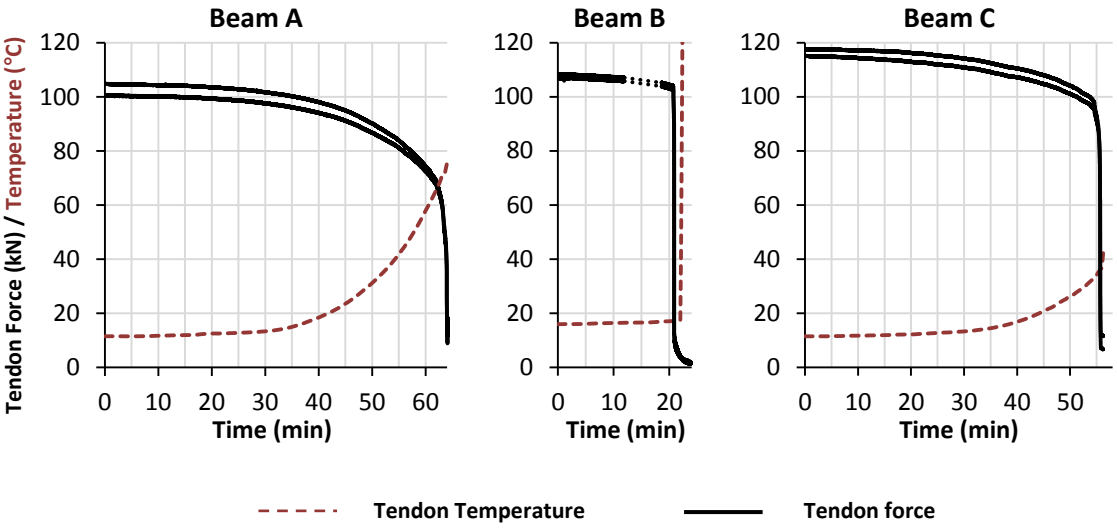

Figure 4-20: Tendon temperature and force during full scale testing

The simplified calculation method provides a reasonable estimate of the relaxation of the post-tensioning tendons. Figure 4-21 shows the calculated tendon strength for beam A and C compared to the full-scale experimental results. The tendon force for Beam A, which of the beams tested was the stiffest and least flexible, was predicted accurately within 2% of the measured values for the majority of the test. The tendon strength for Beam C, which was comparatively more flexible than Beam A, was again accurately predicted.

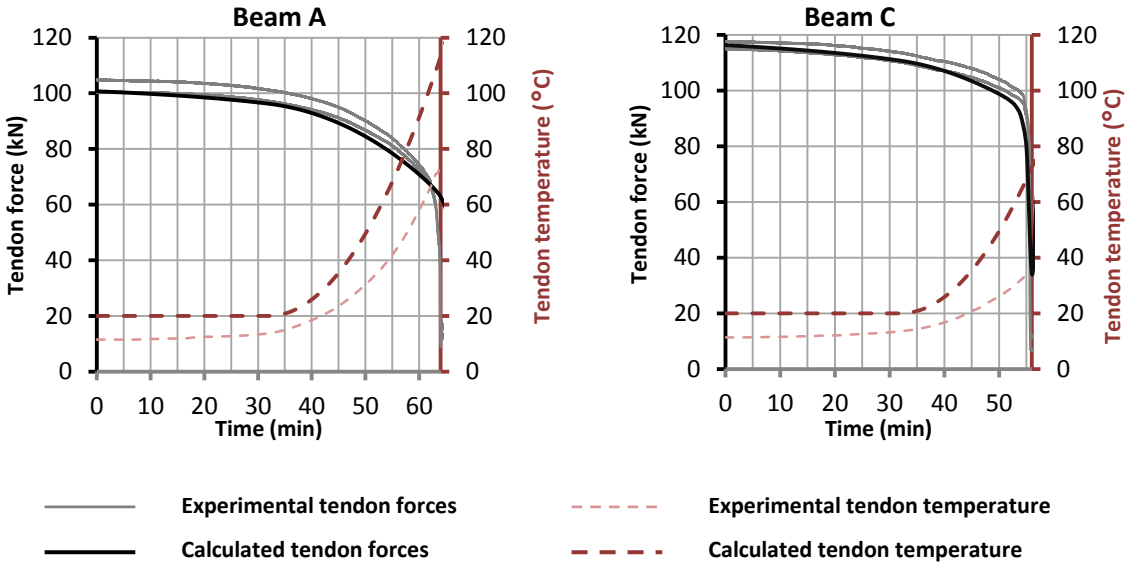

Figure 4-21: Simplified calculation method tendon relaxation for beam A (left) and beam C (right) compared to experimental results

It was found that the tendon force is significantly better modelled by including the effects of tendon elongation or shortening due to end rotations and increased timber compression as well as the loss of stiffness and the increased thermal strain. The rotation of the anchorages causes the tendon to be pulled more tightly which increases the strain in the tendon. The compression stresses and strains in the timber due to the axial post-tensioning increase during the fire due to the reduction in timber cross section. Before including these effects the relaxation calculation depended only on the thermal

strain and reduction of Young's modulus and greatly over predicted the remaining force in the post-tensioning.

4.5. Deflections

Unfortunately the deflections calculated by the hand calculation method differ substantially from the measured deflections. Figure 4-22 shows the calculated deflections for both beams compared to the experimental deflections recorded. As the experimental deflections were measured at the loading points, the mid span deflections were slightly more than shown. The calculated deflections of Beam A are positive due to the post-tensioning moment overcoming the loading and causing the beam to deflect upwards. The calculated deflections for Beam C follows the shape of the recorded deflections better than Beam A but still under predicts the actual deflection. Due to the non-linear nature of the deflection calculation it can become numerically unstable and not reach a solution. This however should not occur before the calculation method predicts failure. Possible reasons for this disagreement include; errors in the deflection calculation and insufficient complexity in the design calculation.

Further analysis at ambient temperature in the research of van Beerschoten (2011) should be able to refine the deflection calculations of post tensioned timber and ambient conditions. This should help to refine the deflection calculation for the fire case.

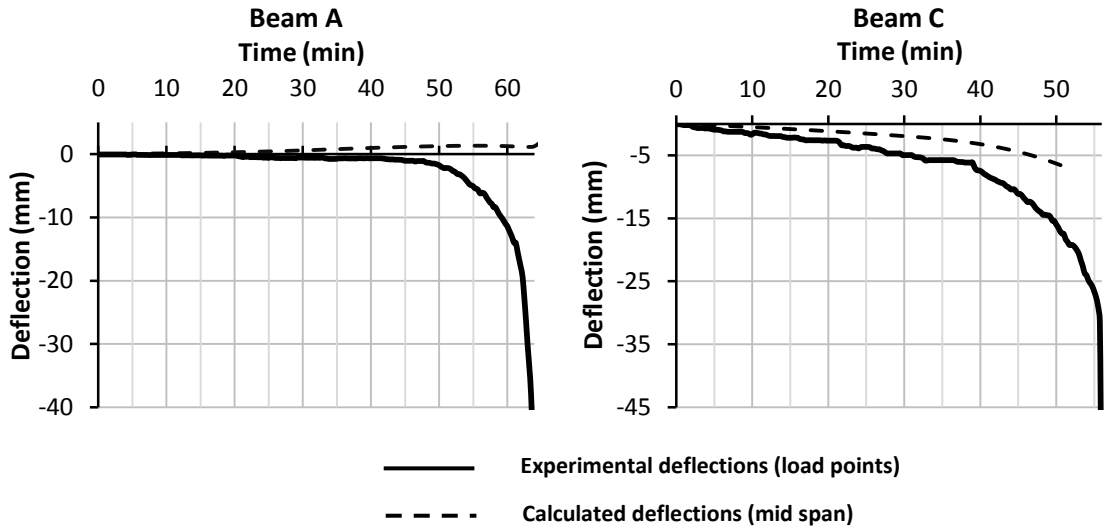

Figure 4-22: Calculated and experimental beam deflections

4.6. Failure times

The simplified calculation method was used to predict the failure times for the full-scale test specimens. This was done by completing the calculation check at minute intervals. The failure times predicted depend on the input assumptions. The most important input is the char rate of the timber.

The failure times recorded during the full-scale tests are summarised in Table 4-5. These values can be used to compare the physical state of the beams with the predicted state. The remaining thickness of the web and flange is useful to compare, as well as the failure times, as it shows how well the calculation method is approximating the physical reality.

Table 4-5: Char depths and failure times measured from the full-scale test series.

	Char depth	Failure time
Beam A	48mm	64 min
Beam B	18mm	22 min
Beam C	40mm	56 min

With a char rate of 0.65mm/min as published in NZS3603 the calculation method over predicted the time to failure and therefore the beam's fire resistance rating. Beam A was then predicted to fail at 73 minutes of fire exposure with a shear failure at the bottom corner of the section. The corner thickness was predicted to be 4.7mm thick and a flange and web thickness of 15.5mm was predicted due to a 47.5mm char depth. Whilst the char depth reflects the measured char depth at failure, the time to reach failure is 9 minutes later than during the full-scale test. With the 0.65mm/min char rate Beam B was predicted to fail at 50min with a combined bending and compression failure at mid span. The remaining flange and web thickness would have been 30.5mm with a char depth of 32.5mm. Beam B was unlikely to correlate to predictions as its failure mechanism was unexpected. Beam C, with a 0.65mm char rate was predicted to fail at 70min with the end of the beam failing in combined bending and compression. Char depth at failure of beam C with this char rate would have been 45.5mm. A summary of these values is presented in Table 4-6.

Table 4-6: Predicted failure times for 0.65mm/min char rate

	Char depth	Failure time
Beam A	47.5 mm	73 min
Beam B	32.5 mm	50 min
Beam C	45.5 mm	70 min

The LVL manufacture quotes two char rates for LVL the first is 0.65mm/min with an additional 7mm zero strength layer to account for thermally degraded material. Using this char rate and zero strength layer Beam A was predicted to fail at 68 minutes. The predicted failure mechanism was still a shear failure in the bottom corner of the section. The predicted corner thickness for this char rate is 2.6mm, and the char depth plus zero strength layer would have been 51mm leaving only 12mm of material in the flange and webs of the beam. Beam B was predicted to fail at 40 minutes for this char rate and zero strength layer, with a mid span bending and compression failure. This failure time would have resulted in a char depth of 33mm. Beam C was predicted to fail at 59 minutes with a combined bending and compression failure at the end of the beam. This would have resulted in a char depth of 45.5mm which is slightly more than the char depth measured after the test; the time to failure is also within 3 minutes of the measured time. A summary of these values is presented in Table 4-7.

Table 4-7: Predicted failure times for 0.65mm/min char rate and a 7mm zero strength layer.

	Char depth	Failure time
Beam A	51 mm	68 min
Beam B	33 mm	40 min
Beam C	45.5 mm	59 min

The LVL manufacture also gives a char rate of 0.72mm/min but without an additional zero strength layer. With this char rate Beam A was predicted to fail at 66 minutes, with a shear failure in the

bottom corner. This predicts a remaining corner thickness of 4.4mm and a char depth of 47.5mm leaving 15.5mm of material in the webs and flanges. Beam B was predicted to fail at 45min with this char rate. The expected failure mechanism was again mid span bending and compression. The predicted char depth was 32mm. Beam C was predicted to fail at 63 with a combined bending and compression failure at the end of the beam. Again the predicted char depth at failure was 45mm leaving 18mm of the flange and web.

Table 4-8: Predicted failure times for 0.72mm/min char rate and a 7mm zero strength layer.

	Char depth	Failure time
Beam A	47.5 mm	66 min
Beam B	32 mm	45 min
Beam C	45 mm	63 min

The char rate recommendation of this research is 0.72mm/min with an additional 7mm layer. Using this recommended char rate Beam A was predicted to fail at 61 minutes, again with a shear failure in the bottom corner. The remaining corner thickness was predicted at 3.6mm with a char depth of 51mm. Beam B was predicted to fail at 37 minutes with a mid-span bending and compression failure. The predicted char depth at failure was 33.5mm. Beam C was predicted to fail at 53 minutes with a combined bending and compression failure at the end of the beam. The predicted char depth was again 45mm.

Table 4-9: Predicted failure times for 0.72mm/min char rate and a 7mm zero strength layer.

	Char depth	Failure time
Beam A	47.5 mm	61 min
Beam B	33.5 mm	37 min
Beam C	45 mm	53 min

The recommended char rate of 0.72mm/min with an additional 7mm zero strength layers gave failure times which were conservative enough for design, even though the measured and calculated char rates seem to be less than this. A possible reason for the required increase in char depth to predict failure conservatively is that the thickness of the timber remaining can become relatively thin. The full-scale tests were designed with 63mm thick webs and flanges which after 60 minutes of charring at any char rate discussed left less than approximately 20mm of material remaining. When dealing with such thin timber the effect of defects and variations in timber strength start to become more pronounced. LVL goes a long way to reducing the variations in timber by using thin veneers to spread defects among the timber, and placing stronger veneers near the surface. But with 20mm remaining there are only approximately six veneers left there may be knots in some veneers or finger joints between layers, which can weaken the remaining timber. These reductions in strength could be incorporated into material reduction factors, but it seems simpler for design to use an increased char rate.

The full-scale tests were completed only on beams made from 63mm thick material. Further research may be appropriate to determine if a slower char rate may be applicable for beams made of thicker LVL, glue laminated post-tensioned timber beams, post-tensioned timber beams with additional webs or beams with smaller cavities.

It was also noted that some veneers charred faster than those round them causing areas which charred further into the timber. Figure 4-23 shows an example of the fast charring layers encountered during the full scale testing. These veneers are most likely due to lower density timber being used in some layers. It is common practice to include these layers in the LVL to use the timber most efficiently. This may be an issue for LVL beams in a box configuration where shear in the lower corner may govern and the increased char rate and reduced timber properties may lead to premature failures.

Figure 4-23: Fast charring veneers. A larger version is presented in Figure 2-74.

4.7. Chapter Conclusions

Many aspects of this research were compared in Chapter 4. Some numerical thermal modelling was completed and compared to the full-scale test results and the simplified design methodology. The tendon relaxation, as calculated using the simplified design method and recorded during the full-scale tests, was also compared and contrasted. The predicted times to failure were also investigated with regards to how the char rate assumed affected the predictions.

It was found that the density assumed for thermal modelling affects the resultant char rate; as expected, increased density slows the propagation of the 300°C isotherm which is analogous to the char rate of timber. The most accurate density to assume for the LVL used was 510 kg/m^3 which was the density of the timber used to create the LVL and not the density of the LVL itself. The thermal modelling did not produce any significant variation in thermal propagation between the webs and the bottom flange. A more complex model may be able to capture this effect. Thermal modelling predicted a corner-rounding radius very similar to hand calculations' assuming the radius was equal to the char depth. However, the measured corner radius of the full-scale tests was less than either of these methods predicted. But, as this is a conservative estimate, both methods are applicable for post-tensioned timber.

It was found that the assumed temperature distribution below the char layer, presented in Chapter 3, matched the measured temperature profiles adequately but was sensitive to the values assumed for the heat affected thickness and timber char rate. Temperatures near the char layer were predicted well with the exception of temperatures below 150°C. A heat-affected thickness equal to 35mm and a char rate of 0.65mm/min provided an adequate prediction of the lower temperatures deeper in the timber.

It was found that a char rate for the design of post-tensioned timber members of 0.72 mm/min with an additional 7mm zero strength layer was able to conservatively predict the failure times for the beams tested.

5. Conclusions

5.1. Full-scale furnace tests

A series of full-scale furnace tests were conducted on three post-tensioned timber beams. These box beams were fabricated with using LVL in configurations intended for use in multi-storey timber structures. During these tests five types of anchorage fire protection detail were also tested.

5.1.1. Post-tensioned beam results summary

The full-scale tests successfully demonstrated the fire resistance of post-tensioned timber members and also demonstrated many potential failure mechanisms which will need to be considered during design. Beam A successfully demonstrated a longitudinal shear failure in the lower corner of the cross section. The shear failure occurred at the bottom corner due to the geometry of a box section under fire conditions. The external corner of the cross-section charred and rounded whilst the internal corner remained unchanged, which means the thinnest portion of the cross-section occurred here and could potentially fail in shear before the web.

Due to the increased bending capacity of the beams due to post-tensioning the tests were not able to demonstrate a mid-span combined bending and compression failure. The post-tensioning moment and the short beam span available made a shear failure more likely to occur. However Beam C was able to demonstrate a combined axial and bending failure at the end of the beam where, due to the changing cross-section and post-tensioning eccentricity, the post-tensioning moment and axial load caused a plastic hinge to form.

Beam B failed earlier than expected, which lead to improvements in the proposed design method presented in Chapter 3. The design methodology before the Beam B test did not sufficiently consider the added bending moment due to axial loads from post-tensioning on a deflected beam.

5.1.2. Anchorage member results summary

Five different types of post-tensioning anchorage protection details were tested according to ISO834 (The International Organization for Standardization ISO, 1999). Useful information on each method of fire protection was able to be obtained despite being a secondary objective of this research. An unprotected anchorage was able to retain its post-tensioning load for a short duration in the order of 10 minutes. It was found that enclosing the anchorage in timber or GIB Fyreline™ provided the best protection. For timber protection standard charring rate calculation methods can be used to determine the fire resistance rating. For GIB Fyreline™ the anchorage protection should mimic the manufacturer's one-way firewall system.

Intumescent paint protection and Kaowool protection were also demonstrated during the tests. These methods may be able to be made to work appropriately but more research is needed. The Intumescent paint used provided some protection but only in the order of 10 minutes more than an unprotected anchorage. Kaowool was an effective protection detail providing more than 60 minutes protection, but there are currently no simple design methodologies or thickness recommendations available for using it commercially for steel protection.

5.2. Design methodology

Chapter 3 introduced and outlined the recommended design methodology for post-tensioned timber under fire conditions. Limitations and comparisons of this design methodology are presented in Chapter 4.

Whilst the reality of a post-tensioned timber beam is complex and non-linear it is possible to obtain reasonable accuracy with a first order calculation. In order to design a post-tensioned timber beam for fire conditions the following steps are recommended:

- Calculate the remaining post-tensioning force including the effects of the tendons decreased strain, due to thermal expansion of the steel and the additional axial compression of the timber, and the reduction of young's modulus of the steel due to its elevated temperature.
- Find the actions on the timber beam including, bending, shear, and compression. It is important to consider actions from both the external loads and the post tensioning system.
- Calculate the reduced section properties using the parallel axis theorem.
- Calculate the stresses induced in the timber beam
- Check the appropriate design equations to ensure the timber can resist the stresses applied to it.

Parallel axis theorem is a simple calculation tool which can be used to analyse the effect of charring and the changing geometry on a beam during fire exposure. The charred cross section properties such as the second moment of area can be constructed mathematically from simple geometric shapes with known properties.

Tendon relaxation is estimated by assuming a temperature profile for the timber and assuming that the tendon is at the same temperature as the internal surface of the cavity within the timber. This is then used to calculate the thermal strain and the reduction in the modulus of elasticity of the tendon. These, when incorporated with any losses due to anchorage rotation and beam compression, are able to estimate the relaxation of the post-tensioning tendons.

It is important to check shear for post-tensioned timber members as the post-tensioning can substantially increase the bending capacity of a beam but does not affect the shear capacity. This can lead to higher loading resulting in higher shear actions. It was also found that it is important to check the shear stress in both the web at the centroid and in charred corners of the member. Whilst the shear flow is maximum in the web at the centroid the timber thickness at the bottom corner can be much thinner than the webs leading to a potentially greater shear stress.

It is important to include secondary effects in the analysis. The axial loads of the post-tensioning can induce bending moments in the beam due to not only their eccentricity but also a bowing effect very similar to P-delta effects. The axial loads induce a bending moment due to the beam's initial deflections. The additional deflections for this effect can be calculated iteratively.

5.3. Investigation comparisons

Many aspects of this research were compared in Chapter 4. Some numerical thermal modelling was completed and compared to the full-scale test results and the simplified design methodology. The tendon relaxation, as calculated using the simplified design method and recorded during the full-

scale tests, was also compared and contrasted. The predicted times to failure were also investigated with regards to how the char rate assumed affected the predictions.

It was found that the density assumed for thermal modelling affects the resultant char rate; as expected, increased density slows the propagation of the 300°C isotherm which is analogous to the char rate of timber. The most accurate density to assume for the LVL used was 510 kg/m^3 which was the density of the timber used to create the LVL and not the density of the LVL itself. The thermal modelling did not produce any significant variation in thermal propagation between the webs and the bottom flange. A more complex model may be able to capture this effect. Thermal modelling predicted a corner-rounding radius very similar to hand calculations' assuming the radius was equal to the char depth. However, the measured corner radius of the full-scale tests was less than either of these methods predicted. But, as this is a conservative estimate, both methods are applicable for post-tensioned timber.

It was found that the assumed temperature distribution below the char layer, presented in Chapter 3, matched the measured temperature profiles adequately but was sensitive to the values assumed for the heat affected thickness and timber char rate. Temperatures near the char layer were predicted well with the exception of temperatures below 150°C. A heat-affected thickness equal to 35mm and a char rate of 0.65mm/min provided an adequate prediction of the lower temperatures deeper in the timber.

It was found that a char rate for the design of post-tensioned timber members of 0.72 mm/min with an additional 7mm zero strength layer was able to conservatively predict the failure times for the beams tested.

5.4. Recommendations for design

Chapter 4 makes the following recommendations for the design of post-tensioned timber under fire conditions:

- Consider all potential failure mechanisms, including:
    - Combined bending and compression failure at mid span, specifically by checking top and bottom extreme fibre stresses.
    - Combined bending and compression failure at the beam anchorage, also by check top and bottom extreme fibre stresses.
    - Longitudinal shear in the webs at the centroidal axis.
    - Longitudinal shear in any charred corner which undergoes corner rounding.
- Monitor the remaining post-tensioning force on the beam
- Use a char rate of 0.72mm/minute and include an additional 7mm zero strength layer.
- Include secondary effects such as, axial bowing (P-Delta), anchorage rotation, and increased beam compression
-

5.5. Recommendations for further work

5.5.1. Timber box beam fire performance

The fire performance of timber box beams without any post tensioning is presently not well understood. This should be studied in more detail. It would be useful for this research as well as practical design if an accurate and reliable design model based on the Reduced Cross-Section Method (RCSM) was developed.

5.5.2. Numerical modelling

A 3-Dimensional mechanical model with a 2-Dimensional thermal model as input should be constructed to allow for further investigations into the mechanical response of post-tensioned timber beams under fire conditions. Numerical modelling will allow for further exploration of phenomena and failure mechanisms related to post-tensioned timber where full-scale testing is difficult and expensive.

A fully coupled thermal-mechanical numerical model of the tendon behaviour would allow for further investigation into the tendon relaxation. The intention of this is to be able to improve the relaxation calculation used in the design methodology presented here. The modelling should then be extended to include thermal and mechanical modelling of an anchorage and tendon where the anchorage is exposed to fire. This will provide useful insight into the fire design of the post-tensioned anchorages.

5.5.3. Full-scale testing

Where practical the full-scale testing program should be extended to demonstrate two more potential failure mechanisms which were unable to be achieved during the series of tests described. The two failure mechanisms are: a bending and compression failure at mid-span where the top flange crushes and forms a plastic hinge; and a bending and compression failure where the bending stresses overcome the axial compression and cause a tensile failure in the bottom flange.

5.5.4. Small-scale testing

A series of small-scale tests on anchorage protection details will allow for a better understanding of how the anchorages perform during a fire. This coupled with numerical modelling may allow for more efficient and safer anchorages to be designed, and may provide an architect with more options and flexibility in the anchorages.

References

AALAMI, B. (2007) Critical Milestones in Development of Post Tensioned Buildings. *Concrete International, October***,** Volume 29, Issue 10, Pages 52-56.

BRITISH STANDARD INSTITUTE (2002a) Eurocode 1: Actions on structures BS EN 1991-1:2002.

BRITISH STANDARD INSTITUTE (2002b) Eurocode 1: Actions on structures, part 1-2: General actions - actions on structures exposed to fire BS EN 1991-1-2:2002.

BRITISH STANDARD INSTITUTE (2002c) UK National Annes for Eurocode 0: Basis of structural design BS EN 1990:2002.

BRITISH STANDARD INSTITUTE (2004a) Eurocode 2: Design of concrete structures - part 1-2: General rules - Structural fire design. U.K.

BRITISH STANDARD INSTITUTE (2004b) Eurocode 5: Design of timber structures EN 1995-1:2004. U.K.

BUCHANAN, A. (2001) *Structural design for fire safety*, Wiley Chichester, UK.

BUCHANAN, A. (2007) *Timber Design Guide,* Wellington, New Zealand Timber Industry Federation Inc.

BUILDING RESEARCH ASSOCIATION OF NEW ZEALAND (2011) About BRANZ http://www.branz.co.nz/about_branz. Porirua City.

CARTER HOLT HARVEY WOODPRODUCTS NEW ZEALAND (2009) LVL Specific Design Infomation.

CARTER HOLT HARVEY WOODPRODUCTS NEW ZEALAND (2011) Community, Be inspired.

CARTERHOLTHARVEY WOODPRODUCTS NEW ZEALAND (2009) hySPAN Span Tables for Residential Buildings, Edition 3.

CONSTRUCTION TECHNIQUES LTD (2007) Prestressing Technology.

CREWS, K. (2002) An Overview of the Development of Stress Laminated Timber Bridges in Australia. *Behaviour and Critical Limit States of Transversely Laminated Timber Cellular Bridge Decks.* University of Technology, Sydney - Australia.

DASSAULT SYSTÈMES SIMULIA CORPORATION (2010) *ABAQUS version 6.10* Providence, RI, USA.

ELLOBODY, E. & BAILEY, C. G. (2009) Modelling of unbonded post-tensioned concrete slabs under fire conditions. *Fire Safety Journal,* Volume 44, Issue 2, Pages 159-167.

FORMAN BUILDING SYSTEMS (2002) KAOWOOL Product Data Sheet.

FRANGI, A. & FONTANA, M. (1998) Fire Behaviour of Timber-Concrete Composite Slabs. *the 5th World Conference on Timber Engineering.* Montreux, Switzerland.

GALES, J. (2009) Transient High-Temperature Prestress Relaxation of Unbonded Prestressing Tendons for use in Concrete Slabs. Kingston, Ontario, Queen's University.

GIB (2006) GIB Fire Rated Systems. IN WINSTONSE WALLBOARDS LIMITED (Ed.).

IQBAL, A., PAMPANIN, S., PALERMO, A. & BUCHANAN, A. H. (2010) Seismic performance of full-scale post-tensioned timber beam-column joints. *The 11th World Conference of Timber Engineering.* Riva del Garda, Trentino Italy.

JANSSENS, M. L. & WHITE, R. L. (1994) Temperature profiles in wood memebers exposed to fire. *FIRE AND MATERIALS,* Volume 18, Pages 263-265.

JOHN, S. (2008) Environmental Impacts of Multi-Storey Buildings Using Different Construction Materials. MAF

JOHN, S., PEREZ, N. & BUCHANAN, A. H. (2010) The Carbon Footprint of Multi-storey Timber Buildings Compared with Conventional Materials WCTE 2010. *11th World Conference on Timber Engineering.* Riva del Garda, Trentino, Italy.

KÖNIG, J. (2005) structural fire design according to Eurocode 5- design rules and their background. *FIRE AND MATERIALS*, Volume 29, Pages 147-163.

KÖNIG, J. (2006) Effective thermal actions and thermal properties of timber members in natural fires. *FIRE AND MATERIALS*. Volume 30, Issue 1, Pages 56-63.

KYLEK (2010) Designing in the deep end, Diocesan aquatic. IN CARTERHOLTHARVEY WOODPRODUCTS NEW ZEALAND (Ed.).

LANE, W. P. (2005) Ignition, Charring and Structural Performance of Laminated Veneer Lumber. *Department of Civil Engineering.* Christchurch, University of Canterbury.
MCGECHIE, M. (2011) Innovative post-tensioned Expan timber building. *Build* Wellington New Zealand, BRANZ.
MIN, J.-K., ABU, A. K., MOSS, P. J., DHAKAL, R. P. & BUCHANAN, A. H. (2012) Verification of code fire ratings of precast prestressed concrete slabs. IN FONTANA, M., FRANGI, A. & KNOBLOCH, M. (Eds.) *The 7th International Conference on Structures in Fire proceedings* Zurich, Switzerland.
MINISTRY OF AGRICULTURE AND FORESTRY (2011) Forestry and the New Zealand Economy.
NAWY, E. G. (2003) Historical development of prestressing. *Prestressed concrete: a fundamental approach 4th ed.* Upper saddle river, New Jersey, Pearson Education, Inc.
NEWCOMBE, M. (2007) Seismic Design of Multistory Post-Tensioned Timber Buildings. Pavia, University of Pavia.
NEWCOMBE, M. P., MARRIOTT, D., KAM, W. Y., PAMPANIN, S. & BUCHANAN, A. (2011) Design of UFP-coupled post-tensioned timber shear walls, Paper 132 *the Ninth Pacific Conference on Earthquake Engineering* Auckland, New Zealand.
NZWOOD (2011a) EXPAN – a wealth of timber technology put into action.
NZWOOD (2011b) Timber Design Awards 2011
Entrants: NMIT Arts & Media: Landmark Timber Design.
O'NEIL, J., ABU, A., CARRADINE, D., MOSS, P. & BUCHANAN, A. (2012) Modelling prefabricated timber floors in fire. *The 12th World Conference on Timber Engineering proceedings.* 218-226 Auckland, New Zealand.
O'NEIL, J. W. (2009) The Fire Performance of Timber-Concrete Composite Floors. *Department of Civil and Natural Resources Engineering.* Christchurch, University of Canterbury.
PALERMO, A., PAMPANIN, S., BUCHANAN, A. & NEWCOMBE, M. (2005) Seismic Design of Multi-storey Buildings using Laminated Veneer Lumber (LVL). *Annual NZSEE Technical Conference.* Paper 14, Wairakei.
PALERMO, A., PAMPANIN, S., CARRADINE, D., BUCHANAN, A. H., LAGO, B. D., DIBENEDETTO, C., GIORGINI, S. & RONCA, P. (2010) Enhanced Performance of Longitudinally Post-Tensioned Long-Span Lvl Beams. Paper 59. CECCOTTI, A. (Ed.) *World Conference on Timber Engineering.* Riva del Garda, Trentino, Italy.
PAMPANIN, S., PAGANI, C. & ZAMBELLI, S. (2004) Cable-stayed and suspended post-tensioned solutions for precast concrete frames: the Brooklyn system. *New Zealand Concrete Society Conference.* Queenstown.
PRECAST NEW ZEALAND LIMITED - STRESSCRETE (2003) Fundamentals of Prestressing.
PRIESTLEY, M. J. N., SRITHARAN, S., CONLEY, J. R. & PAMPANIN, S. (1999) Preliminary Results and Conclusions from the PRESSS Five-story Precast Concrete Test-Building. *PCI Journal,* 44**,** 42-67.
ROWE, D. M. (2006) Thermoelectric and Thermomagnetic Effects. IN ROWE, D. M. (Ed.) *Thermoelectrics Handbook - Macro to Nano.* Boca Raton, CRC Press, Taylor & Francis Group.
SMITH, T. J. (2008) Feasibility of Multi Storey Post-Tensioned Timber Buildings: Detailing, Cost and Construction. *Department of Civil and Natural Resources Engineering.* Christchurch, New Zealand, University of Canterbury.
STANDARDS AUSTRALIA (2006) AS 1720.4 Timber Structures : Fire-resistance of structural timber members.
STANDARDS NEW ZEALAND (1993) AS/NZS 3603:1993 Timber Structures Standard.
STANDARDS NEW ZEALAND (2002) AS/NZS 1170:2002 Structural design actions.
STIC LTD. (2009) STIC. Sustainable Buildings of the Future: Our programme , http://www.stic.co.nz/programme. Christchurch
THE INTERNATIONAL ORGANIZATION FOR STANDARDIZATION ISO (1999) ISO 834-1:1999 Fire-resistance tests - elements of building construction. Switzerland.

TSAI, W.-H. (2010) Charring Rates for Different Cross Sections of Laminated Veneer Lumber (LVL). *Department of Civil and Natural Resources Engineering* Christchurch, University of Canterbury.

VAN BEERSCHOTEN, W., PALERMO, A., CARRADINE, D., SARTI, F. & BUCHANAN, A. (2011) Experimental Investigation on the Stiffness of Beam- Column Connections in Post Tensioned Timber Frames. *Structural Engineers World Congress 2011.* Italy.

WERTHER, N., O'NEILL, J. W., SPELLMAN, P. M., ABU, A. K., MOSS, P. J., BUCHANAN, A. H. & WINTER, S. (2012) Parametric study of modelling structural timber in fire with different software packages. FONTANA, M., FRANGI, A. & KNOBLOCH, M. (Eds.) *7th International Conference on Structures in Fire proceedings.* Zurich, Switzerland. 427-438

Appendix A: Shape properties

The following geometric shapes are used to make up the section geometry after fire exposure. Presented below are: the areas; the second moment of area around the centroid; and the location of the centroid for each shape.

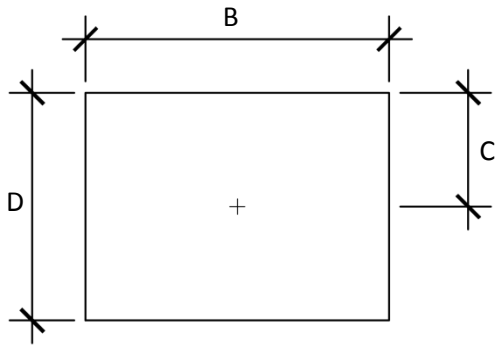

$$C_{rectangle} = D/2$$

$$Area_{rectangle} = BD$$

$$I_{rectangle} = BD^3/12$$

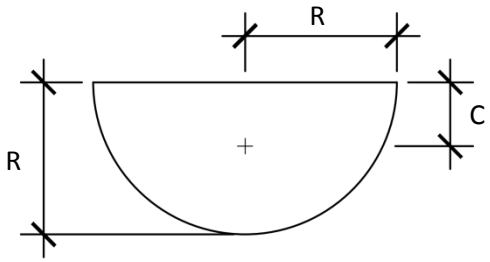

$$C_{semicircle} = 4R/3\pi$$

$$Area_{semicircle} = \frac{\pi R^2}{2}$$

$$I_{semicircle} = \left(\frac{\pi}{8} - \frac{8}{9\pi}\right) R^4$$

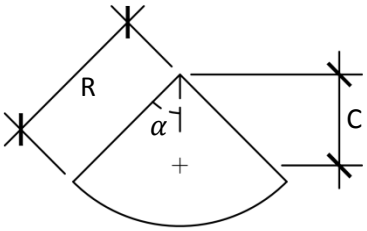

$$C_{sector} = \frac{2R\,sin\alpha}{3\alpha}$$

$$Area_{sector} = R^2\alpha$$

$$I_{sector} = \frac{1}{4}R^4\left[\alpha + \frac{1}{2}\sin(2\alpha)\right] - \frac{4}{9\alpha}R^4 sin^2(\alpha)$$

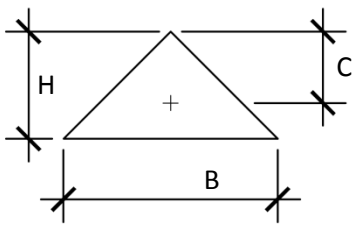

$$C_{triangle} = 2H/3$$

$$Area_{triangle} = BH/2$$

$$I_{triangle} = BH^3/4$$

Where:

B, is the breadth of a shape

D, is the depth of a shape.

H, is the height of a shape.

C, is the distance from the top of the shape to its centroid.

Area, is the area of the shape.

I, is the second moment of area of the shape around its centroid in the orientation shown.

Appendix B: Design Example

A simply supported post-tensioned timber beam of 4.36 m with un-deviated tendons and loaded has with two central point loads of, 20 kN for the fire limit state, and 38.6 kN for the ultimate limit state, 1.5m apart. It was previously found that a post-tensioning force of 232kN would balance the design long-term deflections.

Check the beam beams adequacy for a fire resistance rating of 60 minutes (60/-/-). The beam dimensions and other relative information are given below in Figure B-1 and Table B-1.

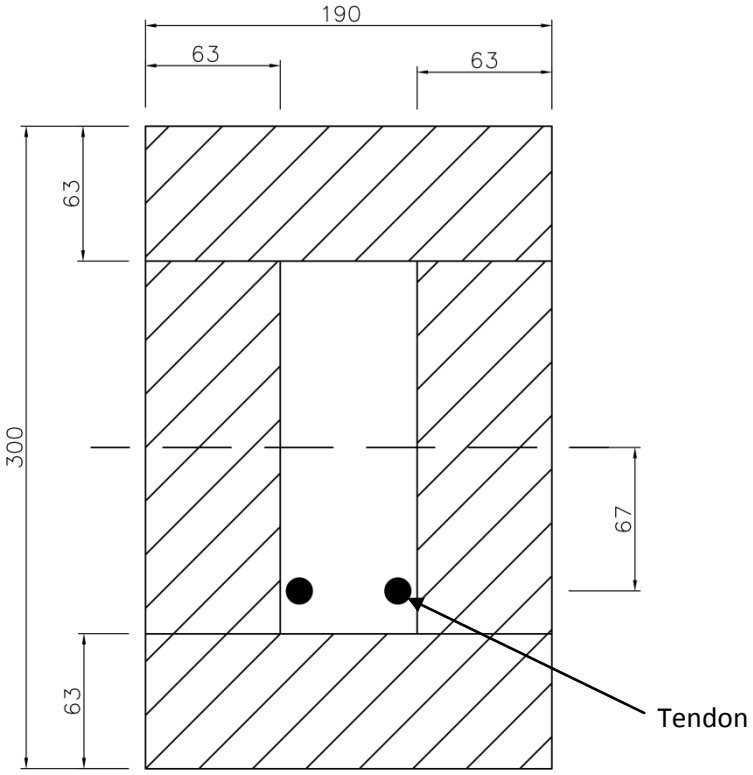

Figure B-1: Design example beam dimensions

Tendon	Area	99 mm^2
	Number	2 tendons
	Eccentricity	67 mm
	Group load	232 kN
	1% Yield stress	1890 MPa
	Material reduction factor	0.7
Timber	Characteristic bending strength	48000 kPa
	Characteristic shear strength	6000 kPa
	Characteristic compressive stress	45000 kPa
	Modulus of elasticity	13 GPa
	Modulus of rigidity	660 MPa
	Characteristic Char rate	0.72 mm/min
	Zero strength layer	7mm

Table B-1: Design example material parameters

Ambient capacity check

Calculate initial actions on the beam:

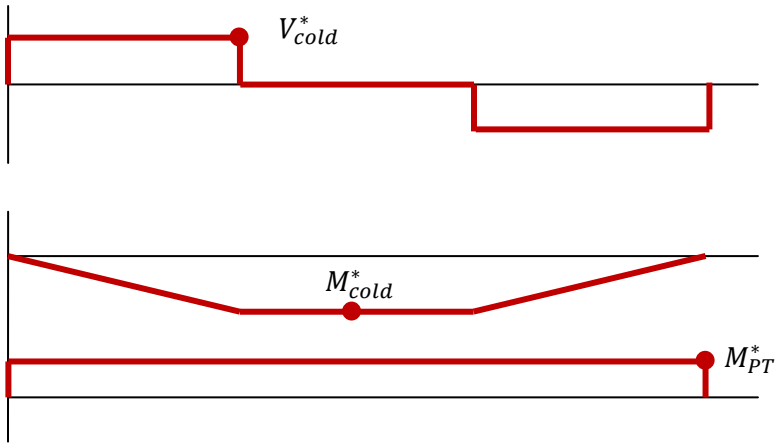

Figure B-2: Design example, initial external actions.

$$V^*_{cold} = 38.6\ kN$$

$$M^*_{cold} = 55.2\ kNm$$

$$M^*_{PT} = -15.5\ kNm$$

Calculate the section properties:

$$I_{cold,timber} = \frac{bd^3 - (b - 2t_w)\left(d - 2t_f\right)^3}{12}$$

$$= \frac{190 \times 300^3 - (190 - 2 \times 63)(300 - 2 \times 63)^3}{12}$$

$$= 399 \times 10^6\ mm^4 \quad or \quad 399 \times 10^{-6}\ m^4$$

$$A_{cold,timber} = bd - (b - 2t_w)\left(d - 2t_f\right)$$

$$= 190 \times 300 - (190 - 2 \times 63)(300 - 2 \times 63)$$

$$= 45{,}800\ mm^2 \quad or \quad 0.0458\ m^2$$

Calculate the deflections due to the loading, bending, and shear, and the post-tensioning:

$$D_{Load,Bending} = \frac{Pointload_{cold}\, a(3L^2 - 4a^2)}{24 E_{Timber} I_{cold}} = \frac{38.6 \times 1.43(3 \times 4.36^2 - 4 \times 1.43^2)}{24 \times 13 \times 10^6 \times 399 \times 10^{-6}} = 0.0216m$$

$$D_{Load,Shear} = \frac{Pointload_{cold}\, a}{G_{Timber} A_{cold}} = \frac{38.6 \times 1.43}{660 \times 10^3 \times 0.0458} = 0.00182m$$

$$D_{PT} = \frac{M_{PT}^{*} L^2}{8 E_{Timber} I_{cold}} = \frac{-15.5 \times 4.36^2}{8 \times 13 \times 10^6 \times 399 \times 10^{-6}} = -0.00711m$$

Calculate additional deflection and moment due to bowing:

$$D_{Bow} = \frac{F_{PT} D_{Total} L^2}{\pi^2 E_{Timber} I_{cold}}$$

$$D_{Total} = D_{Load,Bending} + D_{Load,Shear} + D_{PT} + D_{Bow}$$

Solve D_{Bow} iteratively, assuming an initial value of zero.

D_{Total}(m)	D_{Bow}(m)
0.0163	0.00000
0.0177	0.00141
0.0178	0.00153
0.0178	0.00154

$$D_{Total} = 0.0178\, m$$

$$D_{Bow} = 0.00154\, m$$

Therefore the mid-span bowing moment can be calculated.

$$M_{Bow}^{*} = F_{PT} D_{Total} = 232 \times 0.0178 = 4.15\, kNm$$

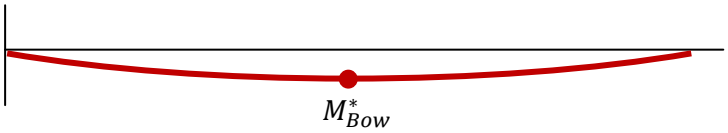

Figure B-3: Moment due to axial loads

Actions Summary.

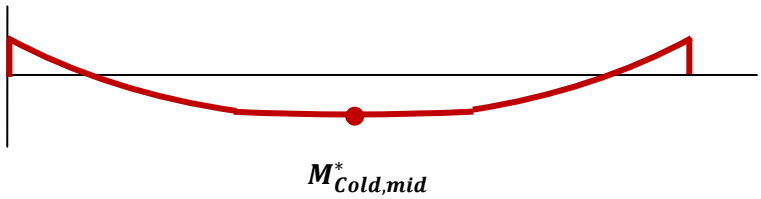

Figure B-4: Ambient moment

Mid-span actions

$$M_{cold}^{*} = 55.2\, kNm$$

$$M_{PT}^{*} = -15.5\, kNm$$

$$M_{Bow}^{*} = 4.15\, kNm$$

$$\boldsymbol{M_{Cold,mid}^{*} = M_{fire}^{*} + M_{PT}^{*} + M_{Bow}^{*} = 43.8\, kNm}$$

$$\boldsymbol{N_{PT}^{*} = 232\, kNm}$$

End actions

$$\boldsymbol{M^*_{PT} = -15.5\ kNm}$$

$$\boldsymbol{N^*_{PT} = 232\ kNm}$$

$$\boldsymbol{V^*_{cold} = 38.6\ kN}$$

Stress check mid-span

Positive = compression

$$\sigma_{TopChordMid} = \frac{N^*_{PT}}{A_{cold,timber}} + \frac{M^*_{Cold,mid} \times {}^{d}/_{2}}{I_{cold,timber}}$$

$$= \frac{232}{0.0458} + \frac{43.8 \times {}^{0.3}/_{2}}{399 \times 10^{-6}} = 21{,}500\ kN/m^2$$

$$\Phi\sigma_{Cn} = \Phi \times k_1 \times f_b = 0.8 \times 0.6 \times 48000 = 23{,}000\ kN/m^2$$

Top fibre mid-span OK

$$\sigma_{BottomChordMid} = \frac{N^*_{PT}}{A_{cold,timber}} + \frac{M^*_{Cold,mid} \times {}^{-d}/_{2}}{I_{cold,timber}}$$

$$= \frac{323}{0.0458} + \frac{43.8 \times {}^{-0.3}/_{2}}{399 \times 10^{-6}} = -11{,}400\ kN/m^2$$

$$\Phi\sigma_{Tn} = \Phi \times k_1 \times f_b = 0.8 \times 0.6 \times -48000 = -23{,}000\ kN/m^2$$

Bottom fibre mid-span OK

Fire Design Capacity Check

$$Chardepth = \beta \times Duration = 0.72mm/min \times 60\ min = 43.2mm$$

$$t_{f,fire} = t_{w,fire} = 63mm - 43.2mm = 19.8mm$$

Initial actions on the beam:

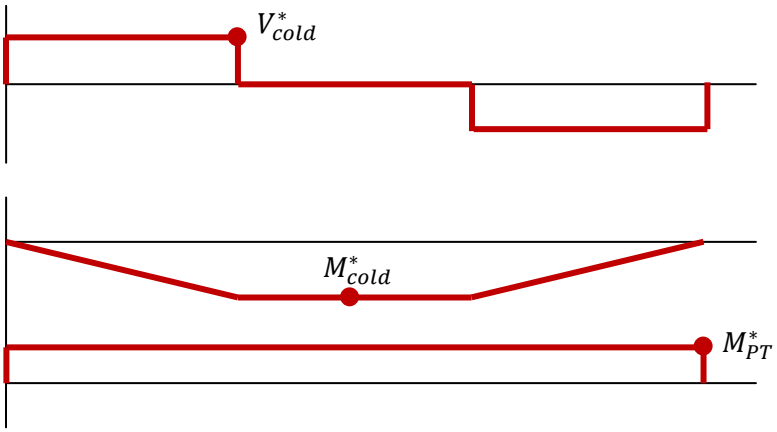

Figure B-5: Actions on post-tensioned timber beam under fire conditions

$$V^*_{Fire} = 20\ kN$$

$$M^*_{Fire} = 28.6\ kNm$$

$$M^*_{PT} = -15.5\ kNm$$

Section properties

Using the geometric shapes and the relative dimensions provided in Section 3.3.4 populate the following table and calculate the area, second moment of area, and centroid position of the charred section. For brevity on the calculation for shape D is shown here.

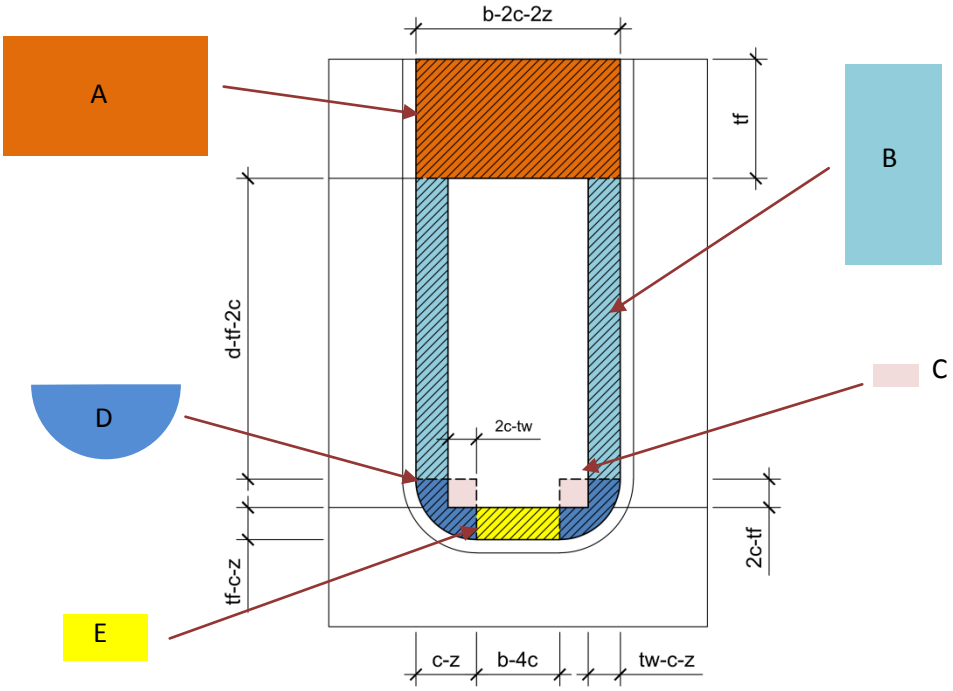

Figure B-6: Second moment of area calculation for charred cross-section

	Area (mm^2)	c_{top} (mm)	First mom. of area (mm^3)	$c_{centroid}$ (mm)	I_{local} (mm^4)	I_{global} (mm^4)
A	5644.8	31.5	177811.2	61.1	1867018	22931604
B	3855.4	138.3	533196.3	-45.7	7286746	15343040
C	-1095.1	225.3	-246730.5	-132.7	-49970	-19337896
D	2058.4	229.0	471306.9	-136.4	188480	38472250
E	220.2	243.4	53586.9	-150.8	3006	5010417
Totals	10,684		989,171			62,419,416

$$\boldsymbol{Area_D} = \frac{\pi R^2}{2} = \frac{\pi(chardepth - z)^2}{2} = \frac{\pi(43.2 - 7)^2}{2} = 2058\ mm^2$$

$$\boldsymbol{c_{top,D}} = d + 2chardepth + \frac{4(chardepth - z)}{3\pi}$$

$$= 300 + 2 \times 43.2 + \frac{4(43.2 - 7)}{3\pi} = 225.3mm$$

$$\boldsymbol{First\ mom.\ area_{top,D}} = Area_D \times c_{top,D}$$

$$= 2058 \times 225.3 = 471306.9\ mm^3$$

$$\boldsymbol{Centroid_{top}} = \frac{\sum 1^{st}\ Mom.\ Area}{\sum Area} = \frac{989,171}{10,684} = 92.6mm$$

$$\boldsymbol{c_{centroid,D}} = Centroid_{top} - c_{top,D} = 92.6 - 225.3 = -136.4mm$$

$$\boldsymbol{I_{D,local}} = \left(\frac{\pi}{8} - \frac{8}{9\pi}\right)R^4 = \left(\frac{\pi}{8} - \frac{8}{9\pi}\right)(43.2 - 7)^4 = 188{,}480mm^4$$

$$\boldsymbol{I_{D,global}} = I_{D,local} + Area_D \times {c_{centroid,D}}^2 = 188{,}480 + 2058 \times -136.4^2 = 38{,}472{,}250mm^4$$

$$\boldsymbol{Area_{fire}} = \sum_{i=A}^{E} Area_i = 10{,}684\ mm^2\ or\ 0.0107\ m^2$$

$$\boldsymbol{I_{fire}} = \sum_{i=A}^{E} I_{i,global} = 62{,}420{,}00\ mm^4\ \ or\ 6.242 \times 10^{-5}\ m^4$$

Calculate increased eccentricity:

$$e_{Fire} = e_o + \frac{d}{2} - Centroid_{top} = 67 + \frac{300}{2} - 93 = 124\ mm$$

Tendon Relaxation

The tendon temperature can conservatively be assumed to be equal to the cavity surface temperature. As either $t_{f,residual}$ or $t_{w,residual}$ are less than a_{heated} (40mm), therefore the cavity surface and tendon temperature can be calculated.

$$x = t_{f,residual} = t_{w,residual} = 19.8mm$$

$$T_{cavitysurface} = \theta = T_i + (T_p - T_i)\left(1 - \frac{x}{a_{heated}}\right)^2$$

$$\theta = 20 + (300 - 20)\left(1 - \frac{19.8}{40}\right)^2 = 91°C$$

Tendon original length:

$$L_o = \frac{E_{Tendon} n A_{tendon} L}{F_{PT} + E_{Tendon} n A_{tendon}}$$

$$= \frac{200 \times 10^6 \times 2 \times 99 \times 10^{-6} \times 4.36}{232 + 200 \times 10^6 \times 2 \times 99 \times 10^{-6}} = 4.334m$$

The post tensioning force must now be calculated iteratively. The initial value for the post-tensioning force is taken as the ambient post-tensioning force.

$$F_{PT,Fire}^{i=0} = \varepsilon_{mech,0} E_{cold} A_{PT} = 232kN$$

Therefore:

$$\varepsilon_{mech,0} = 0.00586$$

The thermal strain on the tendon can be calculated using the Eurocode 2 part 1-2 thermal strain relationship.

$$\varepsilon_{thermal} = -2.016E^{-4} + \mathrm{E}^{-5}\theta + 0.4E^{-8}\theta^2$$

$$\varepsilon_{thermal} = -2.016E^{-4} + \mathrm{E}^{-5}\,91 + 0.4E^{-8}\,91^2 = 0.000746$$

The deflection of the beam including end rotations are calculated for the current iteration.The bowing deflection is solved iteratively within the current iteration for the post-tensioning force.

$$D_{Load} = \frac{Pa(3L^2 - 4a^2)}{24EI} = 0.0718$$

$$D_{PT} = \frac{M_{PT} L^2}{8EI} = -0.0845m$$

$$D_{Shear} = \frac{0.6Pa}{GA} = 0.0024m$$

$$D_{Bowing} = \frac{F_{PT} \Delta_{Total} L^2}{\pi^2 EI} = 0.0126m$$

$$\Delta_{Total} = D_{Load} + D_{PT} + D_{Shear} + D_{Bowing} = 0.02296m$$

$$\varphi_{Load} = \frac{Pa(L-a)}{2EI} = 0.0516rad$$

$$\varphi_{PT} = \frac{M_{PT,Fire}L}{2EI} = -0.0775rad$$

$$\varphi_{Bowing} = \frac{F_{PT,Fire}\Delta_{total}L}{\pi EI}\left(-\cos\left(\frac{\pi L}{4}\right)+1\right) = 0.0178rad$$

$$\varphi_{end} = \varphi_{Load} + \varphi_{PT} + \varphi_{Bowing} = -0.00804rad$$

(Negative value means the ends are rotating in at the bottom and out at the top, this can occur due to the post tensioning moment acting at the ends)

The end rotation can be converted into an effective strain on the tendon:

$$\varepsilon_{roation} = \frac{2\varphi_{end}e_{Fire}}{L_o} = -0.00046$$

The additional axial compression of the timber member can be calculated as a strain on the tendon:

$$\varepsilon_{compression} = \frac{F_{PT,fire}L}{L_o E_T A_{T,fire}} - \frac{F_{PT}L}{L_o E_{\mathrm{T}} A_T} = 0.0013$$

Now the mechanical strain remaining on the tendon can be calculated:

$$\varepsilon_{mechanical} = \varepsilon_{\mathrm{mech\ 0}} - \varepsilon_{thermal} + \varepsilon_{rotation} + \varepsilon_{compression} = 0.00336$$

Thermal reduction in tendon stiffness:

Young's modulus reduction factor taken from EC1992-1-2 table 3.3 column 6 (labelled 7) for cold worked pre-stressing tendons.

$$\frac{E_{fire,tendon}}{E_{20}} = 0.98$$

$$E_{fire,tendon} = 0.98 \times E_{20} = 0.98 \times 200GPa = 196GPa$$

The reduced tendon force for the current iteration can then be calculated as:

$$F_{PT,Fire}^{i+1} = \varepsilon_{mechanical}E_{fire}A_{PT} = 130.77kN$$

This calculation is then iterated until a stable value for the post-tensioning force and therefore moment is found.

$$F_{PT,Fire} = 144kN$$

$$M^*_{PT,Fire} = F_{PT,Fire} \times e_{Fire} = 144 \times -0.124 = -18kNm$$

Actions Summary.

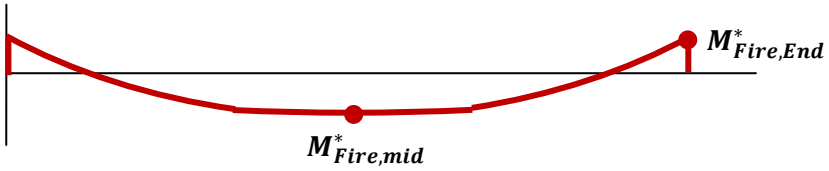

Figure B-7: Bending moment summary after 60 min duration.

Mid-span actions as found through the above iterative process

$$M^*_{fire} = 28.6\ kNm$$

$$M^*_{PT} = -18\ kNm$$

$$M^*_{Bow} = 4.7\ kNm$$

$$\boldsymbol{M^*_{Fire,mid} = M^*_{fire} + M^*_{PT} + M^*_{Bow} = 15.3\ kNm}$$

$$\boldsymbol{M^*_{Fire,end} = M^*_{PT} = -18\ kNm}$$

$$\boldsymbol{N^*_{PT} = 144\ kNm}$$

End actions

$$\boldsymbol{M^*_{PT} = -18\ kNm}$$

$$\boldsymbol{N^*_{PT} = 144\ kNm}$$

$$\boldsymbol{V^*_{fire} = 20\ kN}$$

Bending stress check at mid-span

Positive = compression

$$\sigma_{TopChordMid,fire} = \frac{N^*_{PT}}{A_{Fire,timber}} + \frac{M^*_{Fire,mid} \times Centroid_{top}}{I_{Fire,timber}} = 44{,}500\ kN/m^2$$

$$\Phi\sigma_{Cn} = 48{,}000\ kN/m^2$$

Top Fibre mid-span OK

$$\sigma_{BottomChordMid} = \frac{N^*_{PT}}{A_{Fire,timber}} + \frac{M^*_{Fire,mid} \times (-d + Centroid_{top} + Chardepth + Zero)}{I_{Fire,timber}}$$

$$= -16{,}900\ kN/m^2$$

$$\Phi\sigma_{Tn} = -48{,}000\ kN/m^2$$

Bottom fibre mid-span OK

Bending stress check at end of beam

Positive = compression

$$\sigma_{TopChordEnd,fire} = \frac{N^*_{PT}}{A_{Fire,timber}} + \frac{M^*_{Fire,PT} \times Centroid_{top}}{I_{Fire,timber}} = -4{,}900\ kN/m^2$$

$$\Phi\sigma_{Tn} = \Phi \times k_1 \times f_b = 1.0 \times 1.0 \times -48000 = -48{,}000\ kN/m^2$$

Top Fibre end OK

$$\sigma_{BottomChordMid} = \frac{N^*_{PT}}{A_{Fire,timber}} + \frac{M^*_{Fire,mid} \times (-d + Centroid_{top} + Chardepth + Zero)}{I_{Fire,timber}}$$

$$= \mathbf{66{,}960\ kN/m^2}$$

$$\boldsymbol{\Phi\sigma_{Cn} = 48{,}000\ kN/m^2}$$

Bottom fibre end **overstress**

Shear flow in web:

Using the geometric shapes and the relative dimensions provided Section 3.3.4 populate the following table and calculate the first moment of area for the appropriate portion of the charred section. For brevity on the calculation for shape B is shown here.

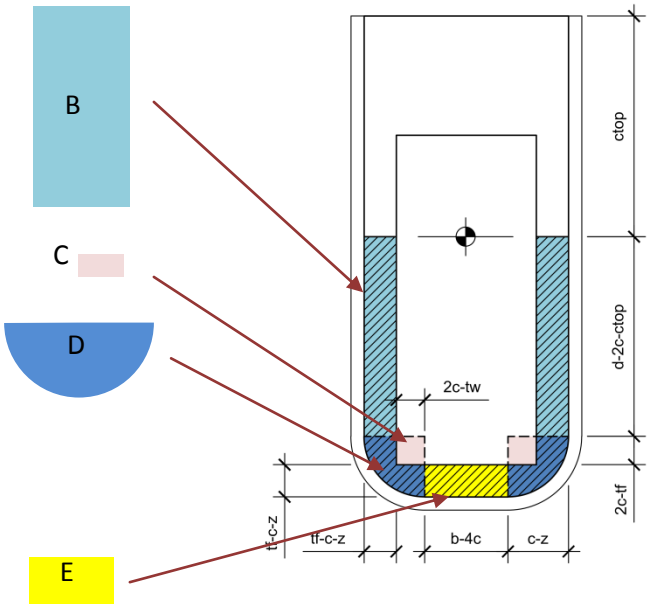

	Area (mm)	$C_{centroid}$ (mm)	First mom. of area (mm^3)
B	4792.1	60.5	289951.8
C	-1095.1	132.7	-145336.1
D	2058.4	136.4	280721.6
E	220.2	150.8	33202.9
	At = 5975.6		$Q_{Web\ Fire}$ = 458540.2

$$\boldsymbol{Area_B} = 2BD = \big(t_f - chardepth - z\big)(d - 2chardepth - Centroid_{top}\ )$$

$$= 2(63 - 43.2 - 7)(300 - 86.4 - 92.6\ ) = 3097.9\ mm^2$$

$$\boldsymbol{c_{centroid,B}} = D/2 = \frac{(d - 2chardepth - Centroid_{top}\ )}{2}$$

$$= \frac{(300 - 86.4 - 92.6\ )}{2} = 60.5mm$$

$$\boldsymbol{First\ mom.area_{centroid,B}} = Area_B \times c_{centroid,B}$$

$$= 3097.9 \times 60.5 = 187444\ mm^3$$

$$\boldsymbol{Q} = \sum_{i=b}^{E} \boldsymbol{First\ mom.area_{centroid,i}} = 356{,}032\ mm^3\ or\ 3.56 \times 10^{-4}\ m^3$$

Shear flow in web:

$$q_{web} = \frac{V_{Fire}^{*} Q}{I_{fire}} = \frac{20 \times 3.56 \times 10^{-4}}{6.242 \times 10^{-5}} = 114\ kN/m$$

$$2t_{w,fire} = 2(t_w - chardepth - z) = 63 - 43.2 - 7 = 25.6mm$$

$$\Phi q_{web,n} = \Phi k_1 f_s 2t_{w,fire} = 1.0 \times 1.0 \times 6000 \times 0.0256 = 154kN/m$$

Shear in web OK

Shear flow in corner:

Using the geometric shapes and the relative dimensions provided in section 3.3.4 populate the following table and calculate the first moment of area for the appropriate portion of the charred section. For brevity on the calculation for shape G is shown here.

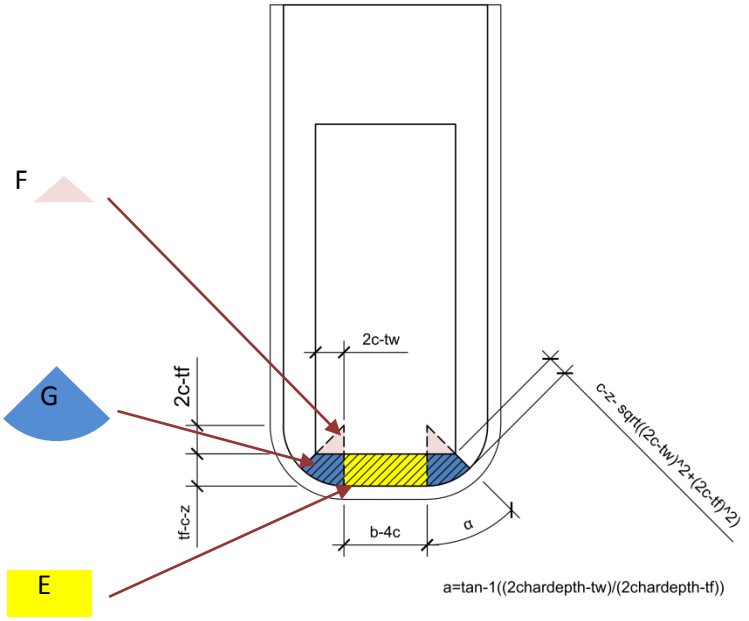

	Area (mm)	$C_{centroid}$ (mm)	First mom. of area (mm^3)
1	-547.56	136.6	-74803.6
2	1029.22	142.7	146910.6
3	220.16	150.8	33202.9
	At=701.82		$Q_{corner,Fire}$ =105310.0

Calculate angle α along which the timber is most thin

$$\alpha = \tan^{-1}\frac{2Chardepth - t_w}{2Chardepth - t_f} = \tan^{-1}\frac{86.4 - 63}{86.4 - 63} = 0.786\,rad$$

$$\boldsymbol{Area_G} = \alpha R^2 = \alpha(chardepth - zerostrength)^2$$

$$= 0.786(43.2 - 7)^2 = 1030\,mm^2$$

$$\boldsymbol{c_{centroid,B}} = d - Centroid_{top} - 2chardepth + \frac{2R\,sin\alpha}{3\alpha}$$

$$= d - Centroid_{top} - 2chardepth + \frac{2(chardepth - zerostrength)\,sin\alpha}{3\alpha}$$

$$= 300 - 92.6 - 86.4 + \frac{2(43.2 - 7)sin0.786}{3 \times 0.786} = 142.7\,mm$$

$$\boldsymbol{First\ mom.area_{centroid,B}} = Area_B \times c_{centroid,B}$$

$$= 1030 \times 142.7 = 146{,}911\ mm^3$$

$$\boldsymbol{Q} = \sum_{i=b}^{E} \boldsymbol{First\ mom.area_{centroid,i}} = 105{,}310\ mm^3\ or\ 1.05 \times 10^{-4}\ m^3$$

Shear flow in corner:

$$q_{web} = \frac{V_{Fire}^{*} Q}{I_{fire}} = \frac{20 \times 1.05 \times 10^{-4}}{6.242 \times 10^{-5}} = 33.8\ kN/m$$

$$2t_{corner,fire} = 2\left(chardepth - \sqrt{(2chardepth - t_w)^2 + \left(2chardepth - t_f\right)^2}\right)$$

$$= 2\left(43.2 - \sqrt{(86.4 - 63)^2 + (86.4 - 63)^2}\right) = 6.2\ mm$$

$$\Phi q_{web,n} = \Phi k_1 f_s 2t_{corner,fire} = 1.0 \times 1.0 \times 6000 \times 0.0062 = 37.3\ kN/m$$

Shear in corner OK

Design example conclusion

The beam is not adequate for 60 minutes fire resistance. The bottom flange in overstressed at the end of the beam due to the axial loads and bending moment from the post-tensioning. It can be found that the bottom flange becomes inadequate at 52 minutes.

Initial Setup

Char depths

$$CharDepth = CharRate \times Duration$$

$$ZeroStrengthLayer = 7mm$$

Tendon force

Calculate tendon force based on estimated cavity and tendon temperature and including the effect of increased timber compression.

Supporting Calculations

Calculate second moment of area, Centroid and Area

Use Parallel Axis theorem to calculate second moment of area using the geometric assumptions that the corner charring radius is equal to the char depth and that there is a 7mm zero strength layer.

Calculate Deflections

$$\Delta_{Total} = D_{Load} + D_{PT} + D_{Shear} + D_{Bowing}$$

D_{Load}: Deflections due to the bending induced by the external loads.

D_{Shear}: Deflections due to the shear induced by the external loads.

D_{PT}: Deflections due to the end moments due to the post-tensioning eccentricity.

D_{Bowing} : Deflection due to the axial loads acting on an initially deflected member.

Actions

Shear Action

Calculate shear flow action in the web at the centroid and in the thinnest part of the charred corners.

$$q = \frac{VQ}{I}$$

Moment action

$$M_{midspan} = M^*_{Load} + M^*_{PT} + M^*_{BOW}$$

M^*_{Load} : Moment due to external loads

M^*_{PT}: Moment due to post-tensioning eccentricity

M^*_{BOW}: Moment due to axial load due to post-tensioning

Axial Action

$$N^*_{Fire} = F_{PT,cold}$$

Axial loads due to due full post-tensioning stress to be conservative

Capacities

Shear Capacity

Calculate shear flow capacity by calculating the remaining thickness of timber.

$$\Phi q_{web,n} = \Phi k_1 f_s 2 t_{w,fire}$$
$$\Phi q_{web,n} = \Phi k_1 f_s 2 t_{corner,fire}$$

Compressive and Tensile Capacity

Calculate compressive and tensile stress capacity from the characteristic bending strength.

$$\Phi \sigma_{Cn} = \Phi k_1 k_{24} f_b$$
$$\Phi \sigma_{Tn} = -\Phi k_1 k_{24} f_b$$

Structural Checks

Shear stress check

Check the beams adequacy in shear for the required fire duration.

$$q^*_{web} \leq \Phi q_{web,n}$$

$$q^*_{corner} \leq \Phi q_{corner,n}$$

Combined bending and compression check

Check the beams adequacy in bending and compression for the required fire duration. Check compression and tensile stresses in top and bottom extreme fibres mid span and at the end of the member.

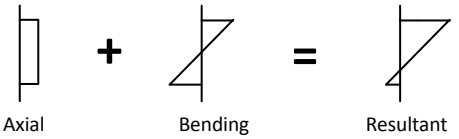

Axial Bending Resultant

$$\sigma_{TopChordEnd} \leq \Phi \sigma_{Cn} \qquad \sigma_{TopChordMid} \leq \Phi \sigma_{Cn}$$
$$\sigma_{BottomChordEnd} \leq \Phi \sigma_{Tn} \qquad \sigma_{BottomChordMid} \leq \Phi \sigma_{Tn}$$